이학박사학위논문

세포 내 칼슘 항상성 조절 메커니즘에 관한 연구

Studies on the regulatory mechanism of intracellular calcium homeostasis

2022년 8월

서울대학교 대학원

(협) 유전공학전공

유 희 석

세포 내 칼슘 항상성 조절 메커니즘에 관한 연구

Studies on the regulatory mechanism of intracellular calcium homeostasis

지도교수 정 종 경
이 논문을 이학박사 학위논문으로 제출함
2022년 6월

서울대학교 대학원
(협) 유전공학전공
유 희 석

유희석의 이학박사 학위논문을 인준함
2022년 6월

위 원 장 _____ (인)

부위원장 _____ (인)

위 원 _____ (인)

위 원 _____ (인)

위 원 _____ (인)

Studies on the regulatory mechanism of intracellular calcium homeostasis

Professor Jongkyeong Chung

Submitting a Ph.D. Dissertation of
Biological Sciences

June, 2022

Graduate School of Biological Sciences
Seoul National University
Interdisciplinary Graduate Program in Genetic Engineering

Heesuk Yoo

Confirming the Ph.D. Dissertation written by
Heesuk Yoo
June, 2022

Chair _____(Seal)

Vice Chair _____(Seal)

Examiner _____(Seal)

Examiner _____(Seal)

Examiner _____(Seal)

Abstract

Studies on the regulatory mechanism of intracellular calcium homeostasis

Heesuk Yoo

Interdisciplinary Graduate Program in Genetic Engineering

The graduate School

Seoul National University

Calcium is a remarkable multifunctional signaling ion that is involved in a wide range of biological activities, including cell birth, development, function, and eventual death. The calcium signal is precisely regulated. Spatial and temporal encoding of signals ensures that these calcium-dependent processes are activated at the appropriate time and place within cells. Thus, it is critical to maintain proper calcium homeostasis at all times. Cells use a variety of transporters and channels to control intracellular

calcium concentrations. Therefore, understanding and elucidating the mechanism of calcium channel activities that regulate calcium homeostasis are important.

In part I, I proposed a novel mechanism that regulates calcium homeostasis in the pathogenesis of Parkinson's disease (PD). Even though it is known that disruptions of intracellular calcium homeostasis play a role in the pathogenesis of PD, the molecular mechanisms behind this are unknown. I discovered that the loss of PTEN-induced kinase 1 (PINK1) or Parkin causes dysregulation of inositol 1,4,5-trisphosphate receptor (IP_3R) activity, which increases ER calcium release significantly. This phenomenon was observed in both mammalian cells and *Drosophila*. In addition, I identified that CDGSH iron sulfur domain 1 (CISD1) functions downstream of Parkin to directly control IP_3R. In PINK1 and Parkin deficient mammalian cells and flies, suppressing CISD1 restores enhanced ER calcium release, demonstrating the PINK1-Parkin pathway is an evolutionarily conserved regulatory mechanism of intracellular calcium homeostasis. Interestingly, in PINK1 and Parkin null flies, CISD knockdown rescued PD-related phenotypes such as increased apoptotic responses in the muscle, impaired locomotor activity and dopaminergic neuronal degeneration by modulating IP_3R activity. Since it has previously been demonstrated that CISD1 and the anti-diabetic drug pioglitazone, which is used to treat type 2 diabetes (T2D),

interact, I investigated pioglitazone as a potential treatment for PD. Similar to CISD knockdown, pioglitazone treatment reduced ER calcium release by blocking direct interaction between CISD and IP_3R in both mammalian cells and *Drosophila*. Furthermore, feeding of the pioglitazone rescued the PD-related phenotypes in PINK1 and Parkin null flies. Based on these results, I believe that the regulation of ER calcium release by PINK1 and Parkin via CISD1 and IP_3R is a potential target for treating PD pathogenesis.

In part II, I attempted to identify a new factor regulating intracellular calcium homeostasis among factors related to metabolic activity. Using a genetic screen to identify factors that regulate calcium channel activity, I discovered that fumarate, an intermediate metabolite of the TCA cycle, inhibits SERCA, which imports calcium into the ER. I showed that calcium flux alterations in the ER, cytosol, and mitochondria occur when the knockdown of the enzymes that produce or degrade fumarate, or when the membrane permeable fumarate called dimethyl fumarate (DMF) was treated. In both mammalian cells and *Drosophila*, these results were observed. When the level of fumarate was increased, I discovered that a post-translational modifications (PTM) known as succination was induced on the 876 cysteine residue of SERCA, causing the inhibition of SERCA, and therefore, the ER failed to uptake calcium. In hyperglycemia, it is known that higher pyruvate levels activate the TCA cycle, resulting in increased

fumarate production. Similarly, when a high sugar diet (HSD) was fed to induce hyperglycemia in *Drosophila*, I observed tachycardia according to SERCA C876 succination. However, even in the HSD situation, SERCA C876S knock-in flies did not show any changes with cardiac functions. Based on these results, I propose fumarate as a new regulator of intracellular calcium homeostasis. I believe that my study will be able to provide a new insight into the relationship between metabolites and intracellular calcium homeostasis.

Keywords: CISD, IP_3R, PINK1-Parkin pathway, Parkinson's disease, pioglitazone, fumarate, SERCA, hyperglycemia, tachycardia

***Student number*:** 2015-20498

Table of Contents

List of Figures

List of Tables

Introduction

Intracellular calcium homeostasis

Calcium (Ca^{2+}) has an impact on almost every aspect of cellular physiology. It is becoming clear that changes in cellular calcium dynamics play a role in the regulation of normal and pathological signal transduction that regulates cell growth and survival (Taylor and Tovey, 2010). They are involved in a variety of physiological functions such as cell growth, cell migration, gene transcription, neuronal excitability, and muscular contraction (Clapham, 2007; Orrenius et al., 2003). Therefore, it is critical to maintain intracellular calcium homeostasis. The flow of calcium into and out of cells and organelles must be properly regulated to maintain calcium homeostasis. As high cellular calcium concentrations can cause cell death over time, the calcium transport and buffering systems are designed to precisely control the fluxes and concentrations of calcium in the nanomolar range within the cell (Schober et al., 2019). Intracellular calcium homeostasis is a strongly integrated process including a variety of hormonally controlled feedback loops and the complex systems of calcium channels or transporters (Carreras-Sureda et al., 2018; van Goor et al., 2017). Therefore, it is very important to understand how calcium channels or transporters work and to study their novel regulatory mechanisms.

ER calcium channels

Cells store most of the intracellular calcium in the sarco-/endoplasmic reticulum (SR/ER) reservoir **(Fig. 1)**. Calcium is released from the SR/ER into the intracellular organelles in response to various stimulations. And also, SR/ER reuptakes calcium to maintain intracellular calcium homeostasis (Clapham, 2007; Raffaello et al., 2016b). There are two major routes for SR/ER calcium release. The first is ubiquitously expressed inositol 1,4,5-triphosphate receptors (IP_3Rs), and the second is ryanodine receptors (RyRs), which are found mostly in excitable cells. IP_3R belongs to a voltage-independent class of calcium channels, whereas RyR is inextricably linked to voltage-operated channels (Taylor and Tovey, 2010; Thillaiappan et al., 2019). In general, IP_3Rs are more prevalent than RyRs, with almost all animal cells expressing at least one of the three IP_3R subtypes (Carreras-Sureda *et al.*, 2018). The activation of IP_3R is totally dependent on inositol 1,4,5-triphosphate (IP_3). Extracellular stimuli can cause calcium release from intracellular reservoirs by activating particular cell surface receptors and trigger the signal transduction pathway, which includes phospholipase C (PLC) activation (Thillaiappan *et al.*, 2019). Furthermore, the phospholipase-dependent catalysis of phosphatidylinositol 1,4-bisphosphate produces IP_3, a diffusive messenger that binds to IP_3Rs

and activates them. The structure of IP_3R is similar to that of the square mushroom. The majority of the stalk is buried in the ER membrane, while the cap extends ~13 nm into the cytosol with a diameter of ~25 nm (Fan et al., 2015; Paknejad and Hite, 2018). The IP_3 binding site is located at the N-terminus of IP_3R, and the transmembrane region is placed at the C-terminus of IP_3R (Hamada et al., 2017). In mammals, there are three IP_3R subtypes. By associating with diverse molecules, each IP_3R type serves a specific role as a signaling hub, which defines cell signaling and functions (Saleem et al., 2013). The most well-known inhibitors of IP_3Rs are 2-aminoethoxydiphenyl borinate (2-APB) and Xestospongin C (Zhang et al., 2020). RyR channels can be triggered by the binding of ryanodine, and also calcium binds itself to activate the channels, which is called calcium-induced calcium release (CICR). However, when ryanodine is at a high concentration, the role of RyR channels is rather blocked (Essin and Gollasch, 2009).

Next, SR/ER calcium uptake pump is known as sarco/endoplasmic reticulum calcium ATPases, or SERCA. SERCA, a member of the P-type ATPase superfamily of primary active transporters, is primarily responsible for the removal of cytosolic calcium into the lumen of the ER (Apell, 2003; Vandecaetsbeek et al., 2011). As an ER calcium uptake pump, SERCA keeps the cytosolic calcium levels low, allowing signaling pathways or physiological processes to function. In the case of SERCA, the hydrolysis of

ATP is linked to the movement of two calcium ions across the ER membrane and against a concentration gradient (Vandecaetsbeek *et al.*, 2011; Xu and Van Remmen, 2021). Although a proton gradient is not maintained across the ER membrane, SERCA counter-transports two to three protons out of it (Toyoshima et al., 2000; Toyoshima and Nomura, 2002). Through alternative splicing, the SERCA family of three genes produces various isoforms. Among the isoforms, SERCA2 is best known for encoding ubiquitously expressed isoform and plays a housekeeping function in intracellular calcium homeostasis. SERCA is composed of three cytosolic domains (A, N, and P), one short luminal loop, and ten transmembrane α-helices (M1-M10) (Chami et al., 2001). Four transmembrane α-helices (M2-M5) make the formation of the three cytosolic domains. Calcium binding and release occurs in the actuator (A) domain, the ATP-binding cavity is mediated by the nucleotide-binding (N) domain, and the phosphorylation (P) domain generates the high-energy phosphorylation intermediate products (Britzolaki et al., 2020; Chami *et al.*, 2001). The overall shape, transmembrane topology, and tertiary structure of SERCA isoforms are all predicted to be highly conserved. The highly conserved nature of SERCAs explains why the plat-derived sesquiterpene thapsigargin inhibits all isoforms (Tadini-Buoninsegni et al., 2018). Phospholamban, a 52 amino acid integral membrane protein, and Sarcolipin, a 31 amino acid integral

membrane protein, were previously thought to be the only known regulators of SERCA (Glaves et al., 2019; Gorski et al., 2015).

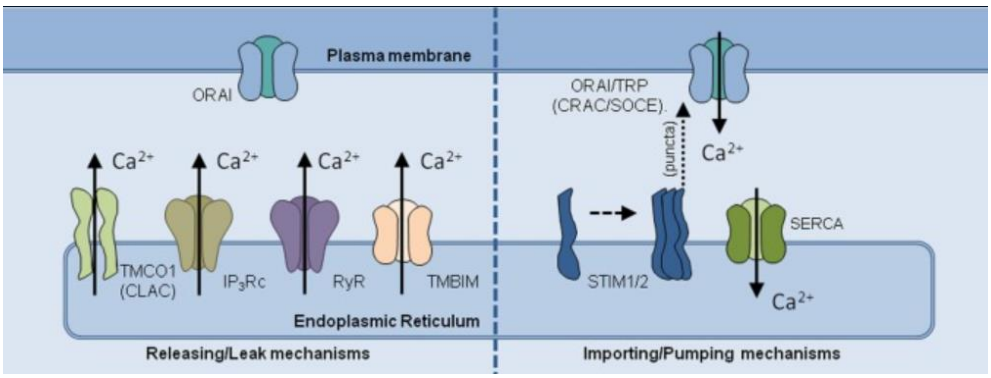

Figure 1. Calcium channels in the ER that regulate calcium homeostasis (image adopted from the ref. (Carreras-Sureda *et al.*, 2018)).

In the left panel, calcium channels that release or leak from the ER are mentioned. It is suggested that TMCO1 is activated by high ER calcium levels, or it is speculated to pH-dependent calcium leak channels. In addition, IP_3R and RyRs are involved in calcium signaling in cells and are tightly controlled by various agonists from the plasma membrane to enhance calcium signaling. In the right panel, a broad family of proteins known as SERCA is responsible for calcium importing or pumping pathways. SERCA pumps consume ATP as they import calcium into the cell against the electrochemical gradient. SERCA activity is linked to SOCE mechanisms that detect ER calcium depletion and interact with plasma membrane CRAC channels to open and induce calcium (Carreras-Sureda *et al.*, 2018).

Mitochondrial calcium channels and MAM

Mitochondria, the organelle responsible for intracellular energy production and cell death signaling, also serve as a calcium reservoir within the cell (Contreras et al., 2010). The mitochondria-associated ER membrane (MAM) is formed by the endoplasmic reticulum making intimate contact with mitochondria. Rapid mitochondrial calcium uptake necessitates the presence of an ER-mitochondria junction that offers microdomains of high calcium content when calcium is released from the ER (Contreras *et al.*, 2010; Rowland and Voeltz, 2012). Various proteins in the MAM play important roles in regulating the movement of calcium from the ER to the mitochondria. Calcium from the ER is transported to the outer mitochondrial membrane (OMM) via the voltage-dependent anion channel (VDAC), and then moves to the mitochondria via the mitochondrial calcium uniporter (MCU) on the inner mitochondrial membrane (IMM) (Yuan et al., 2022). Glucose-regulated protein 75 (GRP75), the molecular chaperone, is located in the MAM and connects the ER to the mitochondria through their respective interactions with IP_3R and VDAC (Szabadkai et al., 2006; Yuan *et al.*, 2022). ER-mitochondrial tethering is also mediated by mitofusin2 (Mfn2) in the ER and mitochondrial membranes (de Brito and Scorrano, 2008). Calcium ions can diffuse OMM due to the electrochemical gradients because OMM is permeable to the various small molecules with less than

5,000 daltons, such as calcium ions. The beta barrel channel protein voltage-dependent anion channel 1 (VDAC1) forms a large pore in the OMM, and it allows calcium ions to enter efficiently (Camara et al., 2017). Whereas, the IMM is ionically impermeable, mitochondrial calcium transport is carried out by a variety of transporters located across the IMM. Due to the mitochondrial membrane potential, mitochondria maintain the basal calcium ion concentration of ~0.1 μM (Mammucari et al., 2018). When calcium is released from the ER as a result of the various stimuli or signaling pathways, MCU, a highly selective and ruthenium red-sensitive transporter quickly uptakes it. MICU1 was the first mitochondrial uniporter complex component to be identified (Perocchi et al., 2010). The gene encoding MCU was found a year later (Baughman et al., 2011; De Stefani et al., 2011). After that, MICU2, MCUb, EMRE, and SLC25A23 were suggested as other subunits that consist a complex with MCU and MICU1 (Hoffman et al., 2014; Plovanich et al., 2013; Raffaello et al., 2013) **(Fig. 2)**.

Mitochondrial calcium is involved in a variety of intracellular processes ranging from energy production to apoptosis. A sufficient level of mitochondrial calcium contributes to enhanced ATP synthesis by activating several enzymes involved in the TCA cycle (Modesti et al., 2021; Rossi et al., 2019). However, in pathological situations in which calcium cannot be maintained in an adequate amount, mitochondrial calcium overload causes

an increase in reactive oxygen species (ROS) production and the opening of the mitochondrial permeability transition pore (mPTP) (Kent et al., 2021). Apoptotic or necrotic cell death occurs when the mPTP is temporarily or permanently opened. Like ER, mitochondria act as a calcium buffer in cellular calcium signaling by releasing or absorbing calcium from the cytosol (Contreras *et al.*, 2010). As a result, mitochondrial calcium uptake should be tightly regulated in order to maintain intracellular calcium homeostasis.

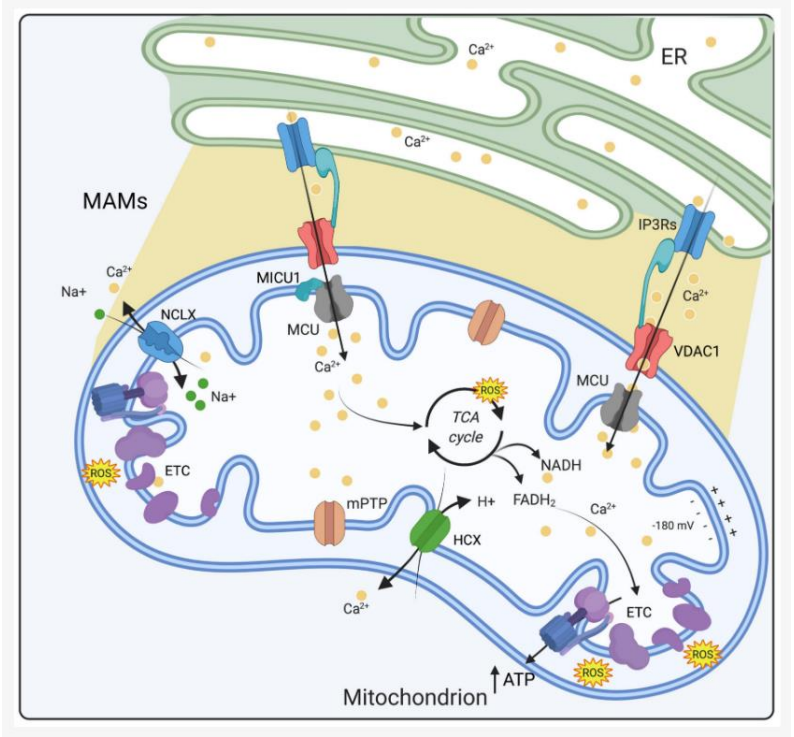

Figure 2. Calcium channels in the mitochondria and their interaction with the ER through MAM (image adopted from the ref. (Modesti *et al.*, 2021)).

Influx and efflux mechanisms play a key role in maintaining mitochondrial calcium homeostasis. MCU and a strong electronegative potential allow calcium to enter the mitochondrial matrix, while NCLX and HCX exchangers are responsible for calcium extrusion. Calcium promotes the activity of 3 Krebs cycle dehydrogenases and ATP generation within the matrix (Modesti *et al.*, 2021).

Roles of calcium in PD pathogenesis

Since calcium homeostasis is essential for cellular functions and survival, abnormal calcium dynamics play an important role in aging and neurodegeneration. Parkinson's disease (PD) is characterized by a malfunction in cellular quality control mechanisms, neuroinflammation, oxidative stress, and defective calcium homeostasis (Jiang et al., 2019). Defective calcium homeostasis, in particular, plays a critical role in the progression of PD. PD is the world's second most prevalent neurological disease. Its causes are poorly understood, and there is no effective treatment to slow the disease's progression (Mhyre et al., 2012). It is well known that the core motor symptoms of PD are caused by the selective degeneration of dopaminergic neurons in the substantia nigra. Dopaminergic (DA) neurons generate action potentials, which are accompanied by the intracellular calcium signaling that is caused by the various calcium channels of the plasma membrane or the ER (Drui et al., 2014; Khaliq and Bean, 2010). When neurons lose control of their calcium homeostasis, they become more susceptible to the stresses associated with PD, such as ER stress, oxidative stress, mitochondrial dysfunction, and so on (Scorziello et al., 2020). It has been reported that the cytosolic calcium levels of DA neurons are consistently altered in aging or PD circumstances, and neuronal activities become increasingly reliant on the various calcium channels (Giguère et al.,

2018; Guzman et al., 2018; Surmeier et al., 2017).

Several PD-associated proteins, such as PTEN-induced kinase 1 (PINK1), Parkin, leucine-rich repeat kinase 2 (LRRK2), and alpha-synuclein, have also been implicated in the cellular calcium homeostasis (Cherra et al., 2013; Huang et al., 2017; Kostic et al., 2015; Matteucci et al., 2018; Rcom-H'cheo-Gauthier et al., 2014; Sandebring et al., 2009). The first evidence for their involvement in calcium handling came from the finding that when the PINK1 mutant is expressed, it causes PD phenotypes such as mitochondrial shape modifications, reduction of ATP levels, or the loss of the membrane potential. PD phenotypes were partially rescued by the treatment of cyclosporine A, a drug that desensitizes the mitochondrial permeability transition pore opening, and fully rescued by the inhibitor of MCU, ruthenium red (Marongiu et al., 2009). These findings suggest that excessive mitochondrial calcium uptake plays a role in the mechanisms of mitochondrial dysfunction in PD. Previous studies suggested that PINK1 regulated calcium efflux from the mitochondria via the mitochondrial Na^+/Ca^{2+} exchanger, causing calcium accumulation in the mitochondria and resulting in mitochondrial calcium overload (Gandhi et al., 2009) **(Fig. 3A)**. Lately, PINK1 was discovered to directly phosphorylate the mitochondrial inner membrane protein leucine zipper-EF-hand-containing transmembrane protein (LETM1), which has been proposed to mediate mitochondrial

proton dependent calcium exchange (Huang *et al.*, 2017; Jiang et al., 2009; Jiang et al., 2013; Shao et al., 2016). Knockdown of LETM1 decelerated the rate of the mitochondrial calcium release and uptake, resulting in metabolic signaling defects, and sensitization to cell death, particularly in neurons. LETM1 phosphorylation by PINK1 appeared to be critical for its activity on mitochondrial calcium regulation and neuronal survival. In addition, it was proposed that PINK1 ablation enhances the sensitivity to calcium-induced mitochondrial permeability transition, which is responsible for increased cell death susceptibility and consequent dopaminergic neuronal loss. Furthermore, the PINK1-Parkin pathway has been implicated in regulating mitochondrial calcium influx through the MCU complex **(Fig. 3B)**. Parkin ubiquitylates MICU1, which is rapidly degraded by the proteasome system, in basal conditions. In this way, Parkin indirectly influences MICU2 levels in this way, as MICU2 stability is dependent on MICU1 stability. It was also discovered that inhibiting the MCU pore subunit can rescue dopaminergic neuronal degeneration in the PINK1 knockout zebrafish model (Soman et al., 2017). Altogether, these findings indicate that defects in the cellular calcium homeostasis could have an important role in the early onset and/or progression of neurodegenerative diseases.

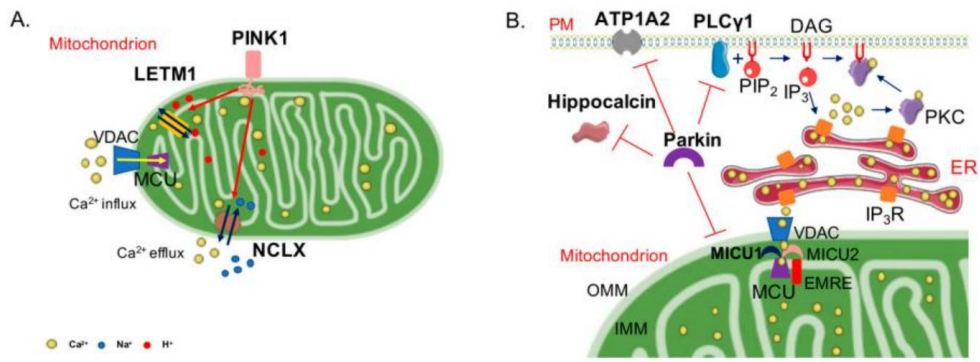

Figure 3. The PINK1-Parkin pathway and mitochondrial calcium (image adopted from the ref. (Barazzuol et al., 2020)).

PINK1 is involved in the processing of calcium in mitochondria **(A)**. The depletion of PINK1 causes mitochondrial calcium excess. The mechanisms behind this PINK1 activity are unknown, but it has been suggested that PINK1-dependent regulation of mitochondrial calcium influx by modulation of calcium influx or efflux via modification of the NCLX. PINK1 also increases the activity of the LETM1. The role of Parkin in calcium homeostasis is better understood **(B)**. It controls the turnover of MICU1, as well as the stability of MICU2, which is dependent on MICU1. Parkin also interacts with and ubiquitylate phospholipase PLC1γ, responsible for the generation of the second messenger IP_3 and DAG. Parkin deficiency causes an increase in intracellular calcium levels that is PLC-dependent, presumably due to excessive PLC1γ activation (Barazzuol *et al.*, 2020).

CDGSH iron sulfur domain 1, CISD1

The CDGSH iron sulfur domain 1 (CISD1, also known as mitoNEET) proteins play critical roles in a variety of processes associated with normal metabolism and disease. CISD1 proteins regulate apoptosis and autophagy, and are involved in iron, Fe-S, and reactive oxygen species homeostasis in the cell (Colca et al., 2004; Wiley et al., 2007). CISD1 is a homodimeric protein with a transmembrane domain and a 39 amino acid sequence called the CDGSH iron-sulfur (Fe-S) domain, harboring its unique 3Cys:1His [2Fe-2S] cluster coordination through evolution (Kwak et al., 2020; Lin et al., 2007; Nechushtai et al., 2020) **(Fig. 4)**. The exposure of the coordinating His lability was shown to interact with the [2Fe-2S] clusters of CISD1 proteins. CISD1 is found on the outer mitochondrial membrane, or it is also found in the contact site between the mitochondrial outer membrane and the ER membrane, known as the MAM. As the MAM is a key place where the ER and mitochondria interact to exchange signals and regulate appropriate cellular functions, such as calcium signaling, it is possible that CISD1 located in the MAM regulates calcium homeostasis. CISD1 has been found to play a functional role in maintaining mitochondrial labile iron (mLI), Fe, and mROS homeostasis, as well as having the ability to influence calcium levels through regulating iron and ROS (Rouzier et al., 2017; Shen et al., 2017). During autophagy, CISD1 interacts with Bcl-2, which is

controlled by the presence or absence of its [2Fe-2S] clusters, and autophagy is assumed to be linked to the Bcl2-CISD1-regulated ER calcium stores. (Chang et al., 2012; Wang et al., 2014). CISD1 is thought to maintain iron homeostasis in the mitochondria (Golinelli-Cohen et al., 2016), and CISD1-depleted mice have dysregulated functions, as shown by increased ROS generation and the reduced ability to synthesize ATP (Tamir et al., 2015a).

These diverse effects of CISD1 in cells suggest that it may play a role in the pathogenesis of various diseases, including PD, cancer, and diabetes. CISD1 proteins have been found to play a key role in cancer, regulating cancer cell proliferation and survival as well as promoting cancer cell metastasis and tumor growth (Mittler et al., 2019). A previous study found that increased ROS downregulates diverse components of the Wnt/β-catenin signaling pathway, suggesting that phloretin anticancer activity could be mediated by producing ROS to influence Wnt/β-catenin signaling, which is regulated by CISD1 (Kim et al., 2020). CISD1 is also suggested to enhance mitochondrial iron and ROS metabolism, supporting cancer cell viability through HIF1 stabilization and apoptosis suppression. Inhibition of CISD1 in breast cancer cells activates cellular stress pathways connected to HIF1 stabilization and mTOR inactivation, and increased iron uptake into cells and mitochondria produces a metabolic shift that increases oxygenic

glycolysis (Holt et al., 2016). CISD1 proteins also have been found to play a role in the pathogenesis of diseases involving mitochondrial malfunction, such as diabetes (Tamir et al., 2015b). Overexpression of CISD1 in adipose tissues results in sustained insulin sensitivity, whereas decreased CISD1 expression results in increased oxidative stress and glucose intolerance (Kusminski et al., 2012). When the level of CISD1 protein decreases, mitochondrial defects cause the decreased insulin production by the pancreas in type 1 diabetes (Danielpur et al., 2016). The differential role of CISD1 in pancreatic α- and β-cells indicates an essential mechanism by which impaired mitochondrial function affects β-cells insulin secretion and α-cell glucagon production, preserving insulin sensitivity under metabolic stresses (Kusminski et al., 2016).

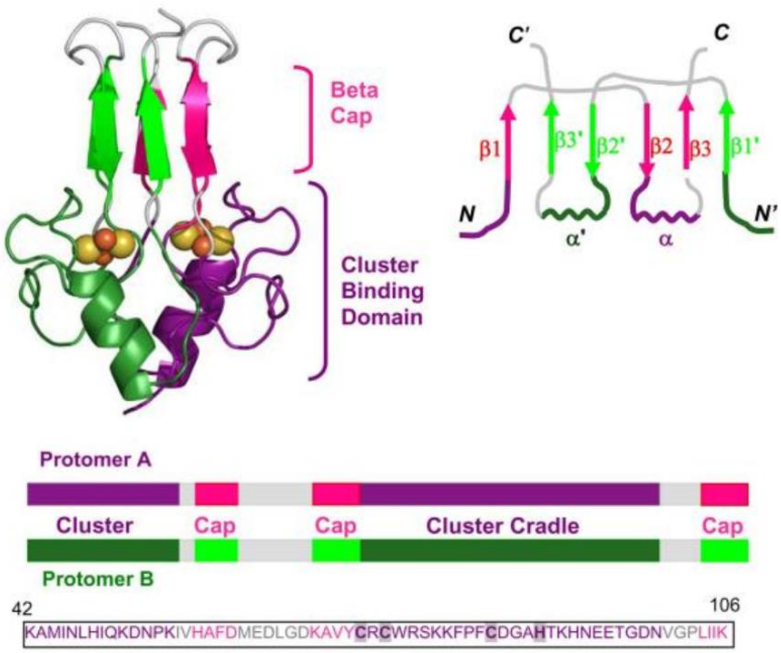

Figure 4. Structural organization and domain topology of CISD1 (image adopted from the ref. (Paddock et al., 2007)).

The two domains of CISD1 dimer are highlighted in a ribbon graphic. A six stranded β-sandwich forms the intertwined β-cap domain and a larger cluster-binding domain carries two 2Fe–2S clusters. The strand swap between protomers is depicted in a topology diagram that highlights the arrangement of the secondary structural units (Paddock *et al.*, 2007).

CISD1 as a potential drug target

As mentioned above, it can be seen that various diseases are related to the expression of CISD1. It was discovered that interrupting the lability of CISD1 clusters has a crucial function in the development of cancer or many other mitochondria-associated diseases (Nechushtai *et al.*, 2020). As a result, CISD1 proteins are novel and extremely promising therapeutic targets. In a previous study, the mitochondrial protein CISD1 was discovered to be cross-linked to the anti-diabetic drug thiazolidinedione (TZD), which is used to treat type 2 diabetes (T2D). TZD is known as a direct activator of the peroxisome proliferator activated receptor-γ (PPAR-γ) (Colca *et al.*, 2004). Treatment with TZD improves insulin action and sensitivity in all tissues. TZD has also been shown to stabilize the [2Fe-2S] clusters of CISD proteins, preventing their loss or transfer to apo-acceptor proteins. So that, TZD binding inhibits cluster mobilization from the mitochondria to the cytosol, as well as impaired mitochondrial iron and ROS balances (Tamir *et al.*, 2015a). In fact, this stabilization of the [2Fe-2S] reduced cancer cell proliferation and tumor growth (Tamir *et al.*, 2015a). Many studies are still being conducted to determine the possibility of the various small compounds that interact with CISD1 may potentially modify the reduction or oxidation state of the [2Fe-2S] clusters. Among them, pioglitazone, one of the TZD drugs that is used as a treatment for type 2

diabetes, has been shown to bind to CISD (Colca *et al.*, 2004). Takahashi then designed and synthesized a pioglitazone derivative that interacts with CISD1, particularly without interacting with PPAR-γ, which pioglitazone was supposed to target, and named it TT01001. For using CISD1 proteins as powerful therapeutic drug targets for many different human diseases, much better understanding and more efficient delivery techniques may be necessary.

Generation and degradation of fumarate in the TCA cycle

Disturbances in mitochondrial activity have been linked to a variety of rare developmental problems and may also be linked to a number of prevalent aging diseases, including PD and dementia (Moon and Paek, 2015). There has also been increasing evidence linking mitochondrial dysfunction with tumorigenesis (Hsu et al., 2016). In the mitochondrial matrix, the TCA cycle oxidizes acetyl coenzyme A obtained from carbohydrates, ketone bodies, fatty acids, and amino acids to create reduced nicotinamide adenine dinucleotide (NADH) and reduced flavin adenine dinucleotide ($FADH_2$) for ATP synthesis in the respiratory chain (Rustin et al., 1997). The TCA cycle is catalyzed by succinate dehydrogenase (SDH) and fumarate hydratase (FH). SDHA, -B, -C, and -D are the four subunits of the electron transporter chain (ETC) that catalyze the conversion of succinate to fumarate. FH transforms fumarate to malate and is not engaged in the ETC (Welter et al., 1989). The two enzymes, SDH and FH, are ubiquitously expressed and play an important role in the generation of ATP via the mitochondrial respiratory chain. Heterozygous germline mutations in two TCA enzymes have recently been found to predispose individuals to tumors. FH mutations are related to leiomyomatosis and renal cell cancer, while SDH mutations are linked to paraganglioma (PGL) and

phaeochromocytoma predisposition (PCC) (Baysal et al., 2000; Benn et al., 2003; Kiuru et al., 2001; Tomlinson et al., 2002). There are currently few data to explain the pathways involved in this neoplasia propensity caused by TCA cycle abnormalities (Cockman et al., 2000; Eng et al., 2003; Ernster and Dallner, 1995; Rustin et al., 2002).

Various effects of protein succination

Succination, S-oxidation, S-glutathionylation, and S-nitrosylation are all post-translational modifications (PTMs) of cysteine residues that alter protein function or turnover in response to a changing intracellular redox environment (Lin et al., 2012). Succination is a chemical modification of cysteine in proteins, resulting in S-(2-succino) cysteine (2SC), by the Krebs cycle intermediate fumarate **(Fig. 5)**. Succination affects a wide range of proteins, including enzymes, adipokines, cytoskeletal proteins, and ER chaperones with functional cysteine residues (Merkley et al., 2014). Uncouplers, which discharge the mitochondrial membrane potential and relieve the electron transport chain, suppress succination of adipocyte proteins in diabetes as a result of nutritional excess-induced mitochondrial stress (Thomas et al., 2012). Therefore, 2SC has recently been considered as a biomarker for mitochondrial stress or dysfunction in chronic diseases like obesity, diabetes, and cancer. According to recent research, succination also acts as a mechanistic link between mitochondrial dysfunction, oxidative stress and ER stress, and the progression of cells to apoptosis (Merkley *et al.*, 2014).

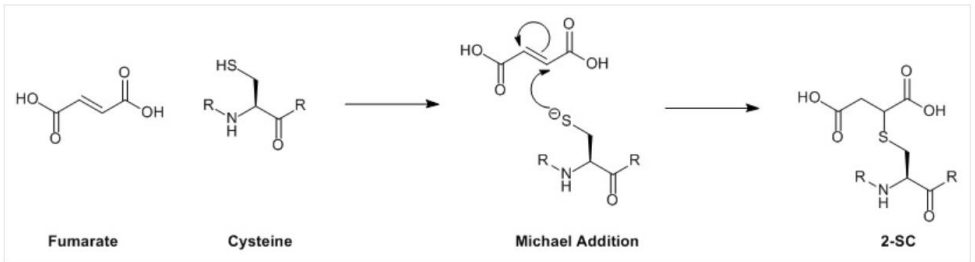

Figure 5. Fumarate and succinocysteine modification (image adopted from the ref. (Merkley *et al.*, 2014)).

Protein succination is a post-translational modification that occurs when the tricarboxylic acid cycle intermediate fumarate reacts with cysteines in proteins to generate S-(2-succino) cysteine (2SC). Cysteine is most commonly found as a thiolate and can act as a reactive nucleophile. At physiological pH, a michael addition reaction between fumarate and the free thiol groups of protein cysteine forms cysteine succination non-enzymatically. The thioether bond in 2SC is thought to be acid hydrolysis resistant and irreversible. Because fumarate is a weak electrophile, its ability to modify thiols is pH-dependent (Merkley *et al.*, 2014).

Several roles of fumarate-induced succination

Psoriasis is a chronic inflammatory skin condition caused by skin-directed T lymphocytes that results in scaly plaques. Fumaric acid esters have been used as a therapeutic for psoriasis for many years (Mrowietz et al., 2007; Mrowietz et al., 1998; Prinz, 2003). After years, dimethyl fumarate (DMF) was approved as an oral first-line medication for people with multiple sclerosis (MS) in 2013. It has high effectiveness, as well as neuroprotective and immunomodulatory properties and a favorable benefit-risk profile. Prior to its release on the market, however, the effects of DMF on the immune systems of MS patients were unknown. MS is a central nervous system (CNS) chronic inflammatory disorder in which infiltrating autoreactive immune cells destroy myelin, resulting in a chronic demyelinating and neurodegenerative disease (Browne et al., 2014; Compston and Coles, 2008).

Although the therapeutic mechanism of DMF remains uncertain, it can covalently bind to cysteine residues of proteins via protein succination. The most well-known role of DMF is to activate the transcription factor nuclear factor erythroid-derived 2 (Nrf2), resulting in neuroprotection **(Fig 6)**. Neurons, astrocytes, microglia, and immune cells all express Nrf2 as a redox sensor (Moi et al., 1994; Mrowietz *et al.*, 2007). The treatment of

DMF causes Keap1 to separate from Nrf2, so that Nrf2 is activated and enhanced transcription of anti-oxidant target genes (Linker et al., 2011). DMF could thus have neuroprotective and cell survival properties. The DMF treatment of MS mice animal models results in an increase in free Nrf2 in neuronal and glial cells, which improved illness scores. When using Nrf2 knockout mice, this impact is nearly completely eliminated (Linker *et al.*, 2011). And also, cysteines of several proteins involved in the nuclear factor (NF)-κB pathway, including IB kinase β(IKKβ), have been reported to interact with DMF. DMF blocked the nuclear translocation of p65 and p52 in the NF-κB pathway, and DMF also inhibits IL-2 secretion by blocking cysteine residues in PKC-θ (Blewett et al., 2016; Gillard et al., 2015). In addition, previous study showed that DMF succinates and inactivates the catalytic cysteine of the glycolytic enzyme GAPDH in vitro and in vivo. As a result, DMF inhibits aerobic glycolysis in activated myeloid and lymphoid cells, resulting in anti-inflammatory actions (Kornberg et al., 2018).

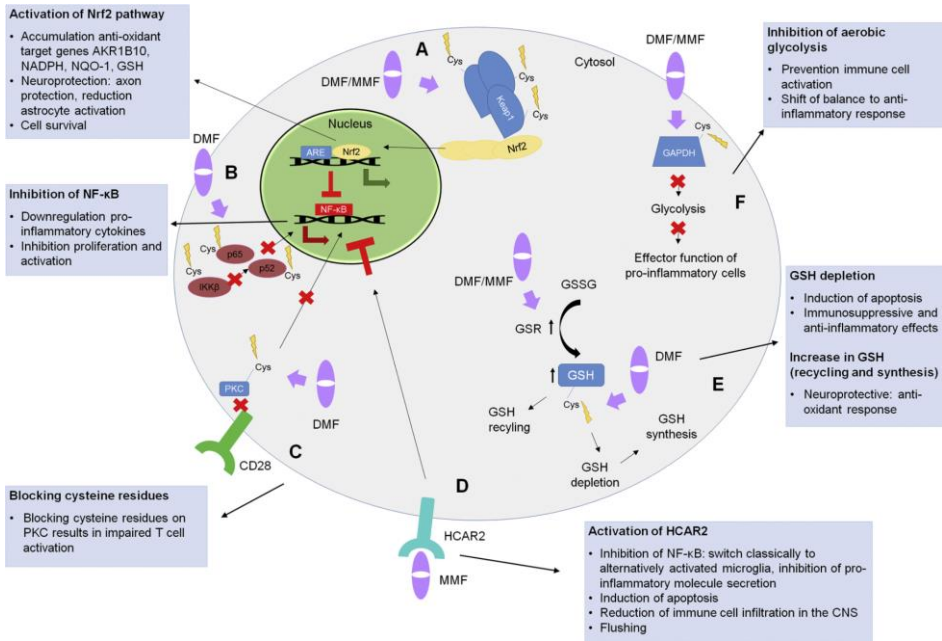

Figure 6. Dimethyl fumarate controls a number of molecular pathways through cysteine modification (image adopted from the ref. (Montes Diaz et al., 2018)).

Dimethyl fumarate (DMF) treatment reacts with Keap1 cysteine residues, causing Keap1 to dissociate from Nrf2, resulting in Nrf2 activation. DMF also modifies NF-κB or PKC-θ cysteine residues to inhibit NF-κB. Furthermore, DMF activates HCAR2, as well as induces transient GHS depletion or inhibition of aerobic glycolysis via interaction with cysteine resides of each (Montes Diaz *et al.*, 2018).

Specific Aims

Aim 1. – To identify the role of intracellular calcium in the pathogenesis of PD

- **Investigate the mechanism of intracellular calcium homeostasis regulated by the PINK1-Parkin pathway**
- **Identify the mechanism of calcium channel regulation by CISD1**
- **Identify the pathological mechanism of PD regulated by CISD1 in animal models**
- **Provide a new insight into the treatment of PD**

Aim 2. – To discover a new factor that regulates the activity of calcium channel

- **Identify ER or mitochondrial factors regulating intracellular calcium homeostasis**
- **Determine the regulatory mechanism of the factor**
- **Investigate the physiological role of the factor in animal models**

Materials and Methods

Plasmid constructs and chemical reagents

Wild-type CISD1 (NM_018464.5) was cloned into a pcDNA3.1 zeo (+) C-terminal Myc-tagged vector. CISD1 mutants (K55/68R double mutant and C74A mutant) were generated using a site-directed point mutagenesis method. The N-terminal GST-tagged human Parkin WT and C431S mutant were cloned into a pEBG vector. The C-terminal Myc-tagged human PINK1 WT and 3KD (K219A/D362A/D384A) mutant were cloned into a pcDNA3.1 zeo (+) vector. The N-terminus HA-tagged human ubiquitin was cloned into a pRK5 vector. I obtained bovine IP_3R1 cloned into a pGFP-N1 vector from Dr. Sang Ki Park (Postech, Korea)(Park et al., 2015). CISD1 siRNA was purchased from Bioneer (Daejeon, Korea). Cells were treated with antimycin A (Sigma), oligomycin (Sigma), carbobenzoxy-Leu-Leu-leucinal (MG132, Calbiochem), or cycloheximide (CHX, Sigma). Commercially available pioglitazone (Actos®) was used to treat mammalian cells and to feed *Drosophila*.

Cell culture and transfection

PINK1 WT and KO MEF, Parkin WT and KO MEF, HEK293, and HEK293T cells were used. HEK293 and HEK293T cells were cultured in DMEM (Welgene, Korea) supplemented with 10% fetal bovine serum (Invitrogen) at 37°C in a humidified atmosphere composed of 5% CO_2.

HEK293T cells were transfected using a polyethyleneimine reagent (Sigma). HEK293 and MEF cells were transfected using Lipofectamine 3000 (Invitrogen) as instructed by the manufacturer. For siRNA transfection, we used Lipofectamine RNAiMAX (Invitrogen). I used Lipofectamine 2000 (Invitrogen) for co-transfection of both siRNA and plasmid DNA.

Generation of CISD1 KO cells

The CRISPR genome editing technique was used for the generation of CISD1 mutant MEF cells. To generate CISD1 KO MEF cells, the guide RNA sequence (GCACAGCGGAGTTGGAGCTG) was cloned into the PX459 vector (Addgene, #62988). I generated CISD1 KO cells using the previously reported method (Ran et al., 2013). The plasmid was transfected into MEF cells. 48 hr after transfection, transfected cells were selected by 10 μg/ml puromycin for 3 days, and then single colonies were transferred onto 96-well plates with one colony in each well. The CISD1 KO clones were screened by immunoblot analysis with rabbit anti-CISD1 antibody (Proteintech).

Antibodies

For immunoblot analysis, the following antibodies were used; rabbit anti-HA (Cell Signaling), rabbit anti-GST (Cell Signaling), mouse anti-GFP

(Santacruz), mouse anti-tubulin (DSHB), and rabbit anti-CISD1 (Proteintech). Peroxidase-conjugated secondary antibodies were purchased from Jackson Laboratory. For immunoprecipitation and immunoblot analysis, we used mouse anti-Myc antibody (MBL).

Immunoprecipitation and immunoblotting

For immunoprecipitation, cells were lysed using a lysis buffer A (20 mM Tris pH 7.5, 100 mM NaCl, 1 mM EDTA, 2 mM EGTA, 50 mM β-glycerophosphate, 50 mM NaF, 1 mM sodium vanadate, 2 mM DTT, 1 mM PMSF, 10 μg/ml leupeptin, 1 μg/ml pepstatin A, and 1% Triton X-100) and were subjected to immunoprecipitation and immunoblotting according to standard procedures. Cell lysates were centrifuged at 13,000 rpm, 4°C for 20 min, and were incubated overnight after the addition of primary antibodies. Lysates were then incubated with protein A/G agarose beads for 2 hr at 4°C, washed 4 times in detergent-free lysis buffer A, and eluted with 2× Laemmli buffer at 95°C. Lysates were subjected to SDS-PAGE analysis followed by immunoblotting according to standard procedures. The blots were developed and viewed under LAS-4000 (Fujifilm, Japan). Image J software was used to quantify the protein band intensity.

Measurement of calcium in mammalian cells

Parkin WT or KO MEF, PINK1 WT or KO MEF, HEK293 cells were cultured on 12 mm L-poly-lysine coated coverslips embedded in a 24 well plate, and transfected with ER calcium indicator G-CEPIA1er (472±15 nm excitation/520±17.5 nm emission; Addgene, #105012), cytosol calcium indicator RCaMP1h (543±20 nm excitation/580±20 nm emission; Addgene, #105014), and mitochondrial calcium indicator 4mitD3 (458 nm excitation/470- to 500- nm and 530- to 560- nm emission; provided by Kyu-Sang Park, Yonsei University Wonju Medical School, Wonju, Republic of Korea), using Lipofectamine 3000. After 48 hr of transfection, I monitored the live cells expressing G-CEPIA1er, RCaMP1h, or 4mitD3 using LSM710 laser scanning confocal microscopy (Carl Zeiss, Germany). The cells were placed in a 37°C heated chamber and perfused with KRB buffer (140 mM NaCl, 3.6 mM KCl, 0.5 mM NaH_2PO_4, 0.5 mM $MgSO_4$, 1.5 mM $CaCl_2$, 10 mM HEPES, 2 mM $NaHCO_3$, 5.5 mM glucose, and pH 7.4-titrated with NaOH). After 2~3 min of baseline recording, a single pulse of 100 μM ATP was delivered to liberate calcium stores for 3 min and then washed out. Peak amplitudes of calcium responses to 100 μM ATP were normalized to the basal fluorescence (F_0) before stimulation. The area-under-the-curve (AUC) of the bar graph was calculated by multiplying the changes in fluorescence over the basal ($\Delta F/F_0$) by the time (S). Calcium transients were continuously recorded and analyzed on Zen software (Carl Zeiss, Germany).

Measurement of the influx and efflux of ER calcium

For this assay, I used a modified KRB buffer (140 mM NaCl, 5 mM KCl, 0.4 mM KH_2PO_4, 1 mM $MgSO_4$, 5.5 mM glucose, 20 mM HEPES, and pH 7.4-titrated with NaOH). To reconstitute G-CEPIA1er with high efficiency, the luminal calcium of the ER had to be reduced by incubating cells for 1 hr at 4°C in modified KRB buffer supplemented with 10 μM calcium ionophore ionomycin and 600 μM EGTA. Cells were washed with modified KRB buffer supplemented with 2% bovine serum albumin after incubation and then transferred to the perfusion chamber. After 2~3 min of baseline recording in the modified KRB supplemented with 100 μM EGTA, the influx of ER calcium was estimated by G-CEPIA1er in the same solution without EGTA and containing 1 mM calcium. After that, the modified KRB with 1 μM ATP was perfused to estimate the efflux of ER calcium. Peak amplitudes of calcium responses to solution changes were normalized to the basal fluorescence (F_0) before stimulations. The ER calcium release rate of the bar graph was calculated by dividing the changes in fluorescence over the maximum ($\Delta F/F_{max}$) by the time (S).

***Drosophila* strains and genetics**

Drosophila lines used in the experiments were *hs*-GAL4 (2077;

Bloomington *Drosophila* Stock Center), *mef2*-GAL4 (27390; Bloomington *Drosophila* Stock Center), *PINK1*^{B9} (34749; Bloomington *Drosophila* Stock Center), *park*^{1} (34747; Bloomington *Drosophila* Stock Center), UAS-CISD RNAi (3392; Vienna *Drosophila* Resource Center), UAS-Itpr (30742; Bloomington *Drosophila* Stock Center), UAS-Itpr RNAi (6484; Vienna *Drosophila* Resource Center), and UAS-GCaMP5G (42037; Bloomington *Drosophila* Stock Center). UAS-D1ER was provided with generosity from Dr. Xun Huang and UAS-CISD WT-HA was generated by microinjecting pUAST-CISD-HA into *w*^{1118} embryos. The RNAi lines for Parkin substrate genes used in Fig. 13 are described in Table 1. All *Drosophila* stocks were maintained at 25°C on the standard cornmeal-yeast-agar medium.

Generation of SERCA C876S knock-in *Drosophila* using the CRISPR/Cas9 system

Following guide-RNAs were used for SERCA C876S knock-in *Drosophila* generation:

5’ CTTCGGGCGGTGGCGACGAGTTCA and

3’ AAACTGAACTCGTCGCCACCGCCC.

Guide RNAs were ligated into pU6 chi-RNA vector and injected with pBS-Hsp70-Cas9 into *w*^{1118} embryos

Measurement of calcium in *Drosophila*

D1ER was expressed in the muscle by *mef2*-GAL4 and UAS-D1ER for ER calcium measurement in *Drosophila* larval muscle. GCaMP5G was also expressed by *mef2*-GAL4 and UAS-GCaMP5G for cytosolic calcium measurement. And also, MTRP was expressed by *mef2*-GAL4 and UAS-MTRP for mitochondrial calcium. I dissected wandering third larvae as described previously with some modifications (Choi et al., 2017). Larvae were dissected in a perfusion buffer (2 mM $CaCl_2$, 4 mM $MgCl_2$, 2 mM KCl, 2 mM NaCl, 5 mM HEPES, 35.5 mM sucrose, 7 mM L-glutamic acid, and pH 7.3-titrated with NaOH) on a stereomicroscope. After dissection of larval muscle, I transferred to a confocal microscope and the larvae were perfused with the same buffer. Peak amplitudes of calcium responses to 10 mM caffeine were normalized to the basal fluorescence (F_0) before stimulation. The area-under-the-curve (AUC) of the bar graph was calculated by multiplying the changes in fluorescence over the basal ($\Delta F/F_0$) by the time (S). Fluorescence images were acquired by using an IX-73 inverted microscope platform (Olympus, Japan) with a camera (Prime-BSI CMOS camera, Teledyne Photometrics) attachment and an illuminator (pe-340Fura, CoolLED, UK). The ratio fluorescence responses of D1ER (440±10.5 nm excitation/480±15 nm and 535±15 nm emission), GCaMP5G (480±10 nm excitation/510±10 nm emission), or MTRP (435 nm

excitation/535 nm emission) were analyzed using Metafluor 6.3 software (Molecular Devices).

Quantification of *Drosophila* thorax and wing abnormality

The percentage of 3-day-old male flies with a defective thorax and upturned or downturned wings was measured out of ten flies to quantify the abnormalities of the thorax and wing. To quantify, ten independent experiments were performed. Finally, the percentage of normal phenotype was calculated out of 100 flies.

Immunohistochemistry of *Drosophila* thorax

To observe the adult fly thorax, the fly head was removed from 3-day-old mal flies and the remaining body was fixed with 4% paraformaldehyde (PFA) for 1 hr and washed out 3 times in 0.1% PBST (0.1% Triton X-100 in 1× PBS) buffer for 10 min, then it was dissected to get the thorax. The fly thoraces were permeabilized with 0.5% PBST for 5 min and washed out 3 times in 0.1% PBST. After that, the thoraces were incubated with 3% bovine serum albumin in 0.1% PBST for 30 min at room temperature. Streptavidin (1:200, Alexa Fluor 488 streptavidin, Invitrogen) and phalloidin (1:200, phalloidin-tetramethylrhodamine B isothiocyanate, Merck) were applied for overnight at 4°C to stain mitochondria and thorax

muscle actin filament, respectively. On the next day, the thoraces were washed out 3 times in 0.1% PBST and mounted on a slide glass with SlowFade mounting solution (S36936, Invitrogen). To quantify the percentage of flies having mitochondrial abnormalities, we defined the flies having the mitochondria over length 5 μM and width 3 μM as the flies having abnormal mitochondria. Ten 3-day-old male flies were counted for the percentages, and ten independent experiments were performed for quantification.

TUNEL assay in *Drosophila*

Collected thoraces according to the method described above were incubated with 0.1 M sodium citrate in 0.1% PBST for 30 min at 65°C, and cell death was detected using *in situ* cell death detection kit (Roche Applied Science). After the TUNEL reaction, the thoraces were stained by Hoechst (1:200, Hoechst 33258, Invitrogen) to detect the nucleus for 15 min at room temperature. To quantify the percentage of flies showing apoptosis, we defined the flies having more than ten TUNEL dots as the fly with apoptosis(Ham et al., 2021). For the percentages, ten 3-day-old male flies were counted, and ten independent experiments were performed for the data quantification.

Climbing assay in *Drosophila*

To conduct the climbing assay, ten 3-day-old male flies were transferred into 18-cm-long vials and incubated for 30 min at room temperature for the acclimatization period. After all flies were moved completely down to the bottom by gently tapping, we measured the time of their climbing at the 15-cm finish line when more than five flies had arrived. Tree trials were performed for each group, and ten independent experiments were performed. The average climbing time was calculated for each genotype.

DA neuron staining in *Drosophila*

30-day-old male flies were fixed with 4% paraformaldehyde (PFA) for 3 hr and washed out 3 times in 0.1% PBST (0.1% Triton X-100 in 1× PBS) for 10 min. Next, the brains were dissected and permeabilized with 0.5% PBST (0.5% Triton X-100 in 1× PBS) for 5 min, and washed out 3 times in 0.1% PBST. After 30 min of incubation with 3% bovine serum albumin in 0.1% PBST at room temperature, DA neurons were stained with anti-tyrosine hydroxylase (TH) mouse antibody (1:200, Immunostar) at 4°C for 48 hr. DA neurons were observed by LSM710 laser scanning confocal microscopy (Carl Zeiss, Germany) via Z-stack analysis. We counted the number of DA neurons of ten flies from each genotype.

Heart beat measurement

Adult flies were dissected in a modified hemolymph-like 3 (HL3) solution (70 mM NaCl, 5 mM KCl, 20 mM $MgCl_2$, 10 mM $NaHCO_3$, 1 mM $CaCl_2$, 5 mM trehalose, 115 mM sucrose, 25 mM N,N-Bis-(2-hydroxyethyl)-2-aminoethane sulfonic acid (BES), and pH 7.1-titrated with NaOH) Since the *Drosophila* heart and aorta are on the dorsal side, the flies were pinned upside down flat after being slit along the mid-ventral longitudinal axis. Internal organs and the gastrointestinal tract were removed with caution to avoid damaging the trachea or heart. Because the anterior end of the heart tube is attached to the connective tissue surrounding the brain, the brain was left intact. Fresh saline was applied to the exposed heart, and the basal heart contraction rate was counted for a minute. The heart beat was then measured in beats per minute for 1 minute (BPM). BPM measurements of all individual flies were recorded by video.

Fly food recipes

Bloomington standard cornmeal food was used to raise all flies from the embryo stage (Na et al., 2013a). Adults were transferred to LSD or HSD food after eclosion, which was made based on Bloomington semi-defined medium, with sugar concentration adjusted. 100 ml food contains agar (1 g),

yeast (8 g), yeast extract (2 g), peptone (2 g), $MgSO_4$ (200 µl of 1 M solution), $CaCl_2$ (340 µl of 1 M solution), propionic acid (600 µl), mold inhibitor (1000 µl), and sucrose (5.13g = 0.15 M for LSD, 34.2 g = 1.0 M for HSD).

Statistical analysis

A blind manner was used in all experiments and analyses. Image areas were randomly selected during observing samples. For computing *P* values, one-way ANOVA (Dunnett's multiple comparison test and Tukey's multiple comparison test), two-way ANOVA (Sidak's multiple comparison test and Tukey's multiple comparison test), and multiple t-tests were used. **** represents $p < 0.0001$, *** represents $p < 0.001$, ** represents $p < 0.01$, * represents $p < 0.05$, and NS represents not significant. All data were presented as mean ± SD. All tests were examined via GraphPad Prism v.8 (GraphPad Software) for the statistics.

Results and Discussion

Part I

Regulation of IP_3R-mediated ER calcium release by PINK1 and Parkin through CISD1

PINK1 and Parkin regulates ER calcium flux by regulating IP_3R activity

First of all, I set up the calcium imaging systems with the perfusion tools to see the correlation between the PINK1-Parkin pathway and intracellular calcium homeostasis. For confirmation, I measured the calcium flux of the ER, the largest intracellular calcium reservoir. I used G-CEPIA1er as an ER-specific calcium indicator to monitor ER calcium flux in Parkin KO mouse embryonic fibroblast (MEF) cells (Suzuki et al., 2014). In addition, I treated ATP to cause IP_3 to bind to IP_3R to release calcium from the ER (Bezprozvanny and Ehrlich, 1993). Surprisingly, when treated with ATP, it was confirmed that there was a difference between Parkin KO MEF cells compared to wild-type (WT). In the graph, after ATP treatment, ER calcium of the Parkin KO MEF line was significantly lower than the WT line, indicating that Parkin KO MEF cells showed highly increased ER calcium release compared to WT **(Fig. 7A)**. Exogenous expression of Parkin WT, but not an inactive mutant of Parkin (C431S, indicated as CS), suppressed this increase. These data suggest that the activity of the E3 ligase Parkin appears to control ER calcium efflux. Alterations in cytosol calcium were also measured to confirm the modifications of the cytosol calcium in response to changes in ER calcium efflux. RCaMP1h was used as a cytosol calcium indicator (Akerboom et al., 2013). In the graph, after ATP treatment,

the cytosol calcium of the Parkin KO MEF line was significantly higher than the WT line. This graph means that Parkin KO MEF cells had higher cytosolic calcium levels as a result of increased ER calcium release as compared to WT, which was suppressed by the expression of Parkin WT but not by Parkin CS **(Fig. 7B)**.

I proceeded to test whether PINK1, functionally upstream of Parkin, regulates the ER calcium release. In comparison to PINK1 WT cells, PINK1 KO MEF cells, like Parkin KO MEF cells, demonstrated increased ER calcium release and higher cytosol calcium levels, which were subsequently reduced by PINK1 WT expression **(Fig. 8A)**. The expression of the PINK1 kinase-dead mutant (3KD; K219A/D362A/D384A), on the other hand, was unable to rescue the ER and cytosol calcium abnormalities **(Fig. 8B)**. From these results, it was found that the calcium flux was changed according to the activity of PINK1 kinase. I also investigated whether PINK1 is required for Parkin to regulate ER calcium release. Exogenous Parkin WT expression suppressed ER calcium release in PINK1 WT MEF cells, but Parkin CS had no effect **(Fig. 9A and 9B)**. Surprisingly, neither Parkin WT nor Parkin CS expression altered the increased ER calcium release and cytosol calcium levels in PINK1 KO MEF cells, indicating that intact PINK1 and Parkin signaling functions are required to control ER calcium release **(Fig. 10A and 10B)**.

I planned to measure the activity of ER-localized calcium influx and efflux channels in Parkin KO MEF cells to figure out how Parkin regulates ER calcium release. It is well known that SERCA transports calcium from the cytosol into the ER, whereas IP_3R releases ER calcium in reaction to IP_3. As demonstrated by the above results, it was assumed that the activity of these ER-localized calcium channels was altered by the abnormality of calcium homeostasis in PINK1 or Parkin KO MEF cells. Thus, I used G-CEPIA1er as an ER calcium indicator to test the effect of the functional loss of Parkin on ER calcium influx or efflux. Cells were first treated with EGTA to chelate intracellular calcium before measuring SERCA and IP_3R activities, respectively. After that, I used calcium chloride to stimulate ER calcium influx, followed by an ATP treatment to induce ER calcium efflux. To summarize this experiment, in the graph, the activity of SERCA is represented by the reaction when the calcium chloride was treated, while the activity of IP_3R is represented by the reaction when the ATP was treated. I discovered that Parkin KO MEF cells released significantly more ER calcium than WT cells, despite the fact that there were no significant differences in ER calcium uptake between Parkin WT and KO MEF cells **(Fig. 11A)**. PINK1 KO MEF cells also showed unchanged calcium uptake and increased ER calcium release compared to WT MEF cells **(Fig. 11B)**. Parkin KO MEF cells and PINK1 KO MEF cells demonstrated the same

pattern in the SERCA and IP_3R activity measurement experiments as they did in the ER and cytosol calcium change experiment for ATP induction. Overall, these results imply that the loss of PINK1 and Parkin selectively increase IP_3R activity.

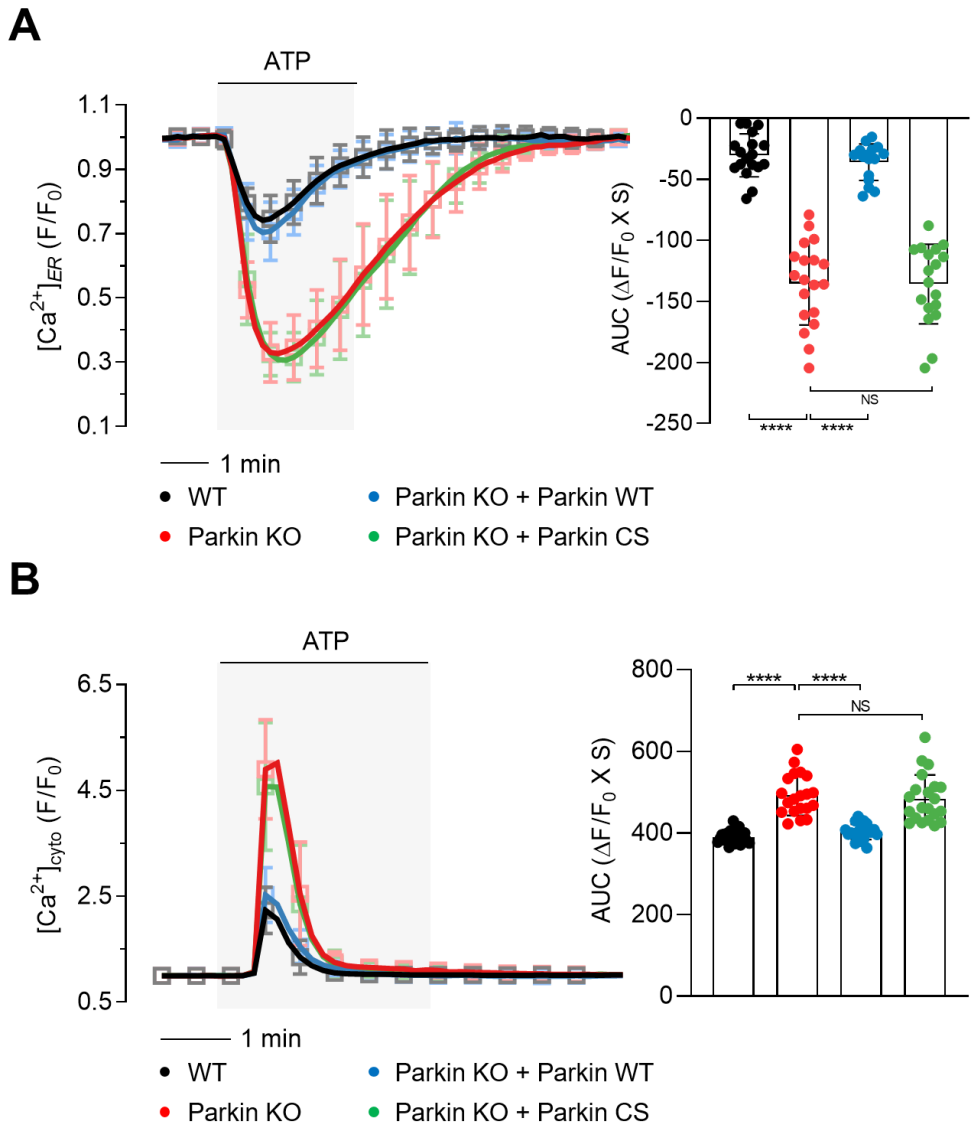

Figure 7. Defects in calcium homeostasis in Parkin KO cells.

Measurement of ER **(A)** and cytosolic **(B)** modulation in WT (black) and Parkin KO (red) MEF cells. Similarly, Parkin KO MEF cells expressing exogenous Parkin WT (blue) or CS mutant (green) were investigated. 100

μM ATP was delivered to initiate IP_3R-mediated calcium release. The right side bar graphs indicate the area-under-the-curve (AUC) of calcium release during ATP treatment, which was used to quantify the normalized calcium traces. $n > 100$ cells.

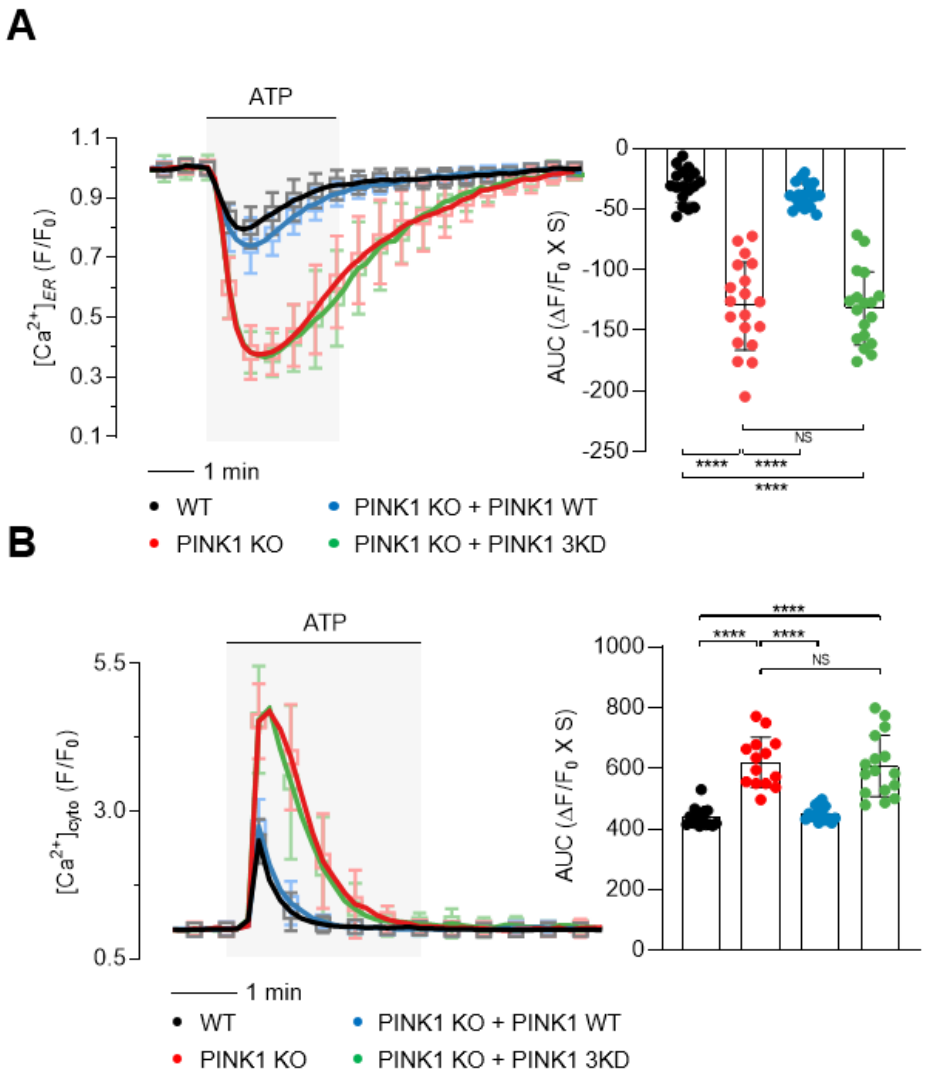

Figure 8. Defects in calcium homeostasis in PINK1 KO cells.

Measurement of ER **(A)** and cytosolic **(B)** modulation in WT (black) and PINK1 KO (red) MEF cells. Similarly, PINK1 KO MEF cells expressing exogenous PINK1 WT (blue) or 3KD (K219A/D362A/D384A) mutant

(green) were investigated. 100 μM ATP was delivered to initiate IP_3R-mediated calcium release. The right side bar graphs indicate the area-under-the-curve (AUC) of calcium release during ATP treatment, which was used to quantify the normalized calcium traces. $n > 100$ cells.

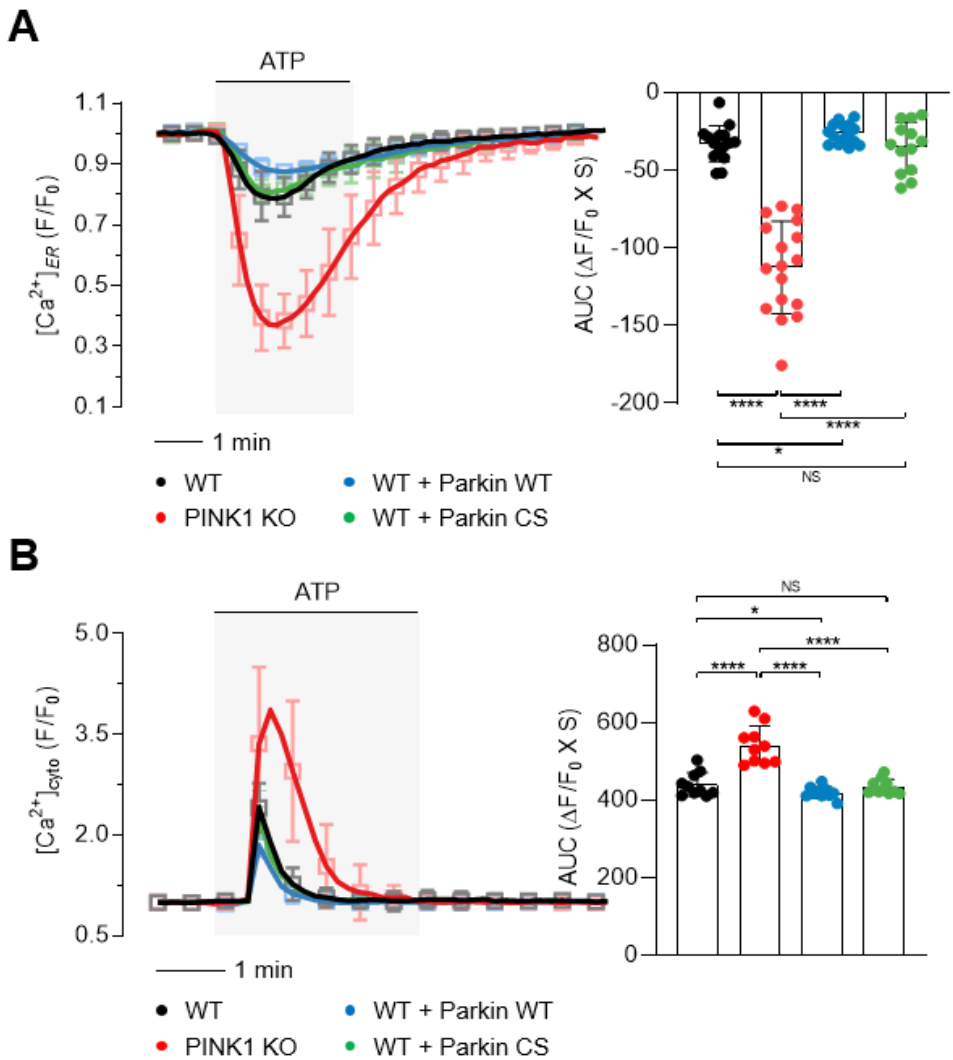

Figure 9. PINK1 is required for Parkin to regulate ER calcium release.

Measurement of ER **(A)** and cytosolic **(B)** modulation in WT (black) and PINK1 KO (red) MEF cells. Similarly, PINK1 WT MEF cells expressing exogenous Parkin WT (blue) or CS mutant (green) were investigated. The

right side bar graphs indicate the area-under-the-curve (AUC) of calcium release during ATP treatment, which was used to quantify the normalized calcium traces. $n > 80$ cells.

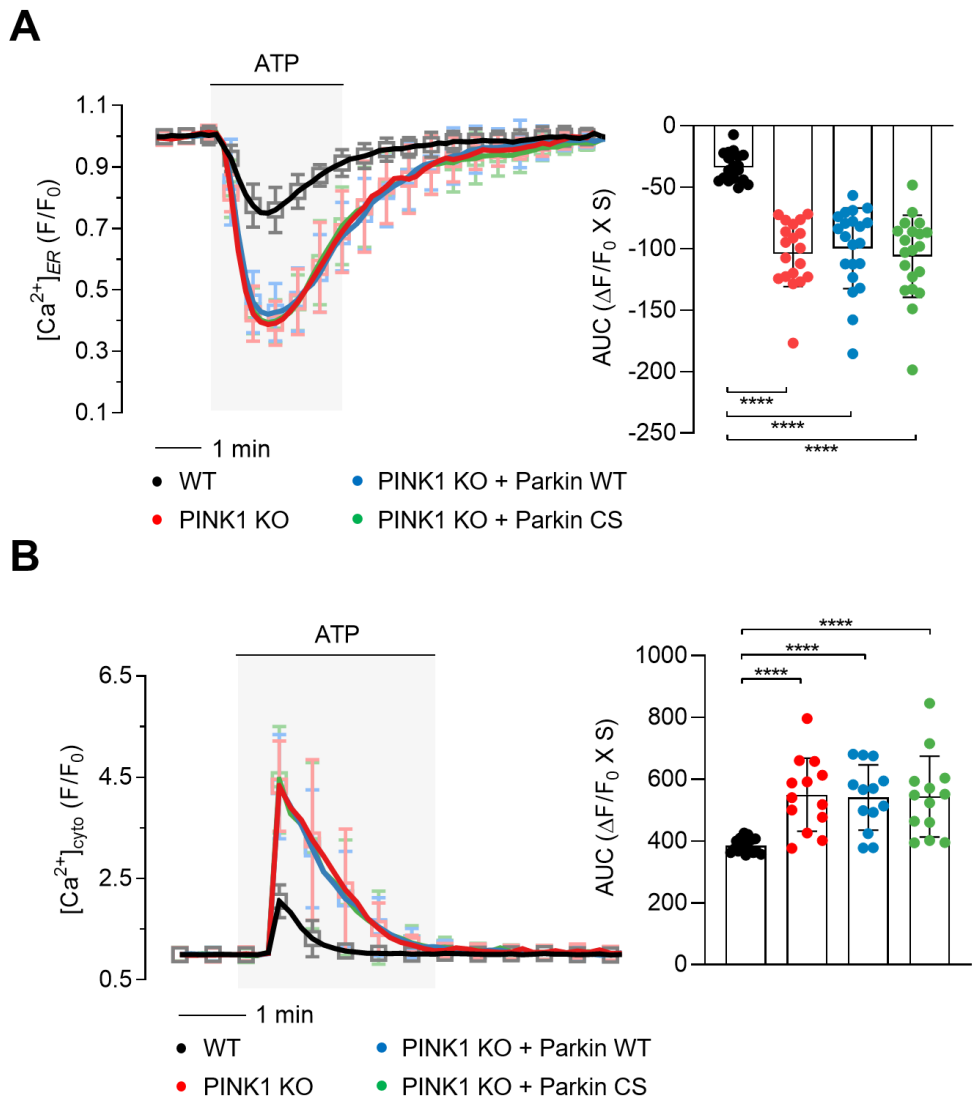

Figure 10. The PINK1-Parkin pathway modulates ER calcium release.

Measurement of ER **(A)** and cytosolic **(B)** modulation in WT (black) and PINK1 KO (red) MEF cells. Similarly, PINK1 KO MEF cells expressing exogenous Parkin WT (blue) or CS mutant (green) were investigated. The

right side bar graphs indicate the area-under-the-curve (AUC) of calcium release during ATP treatment, which was used to quantify the normalized calcium traces. $n > 100$ cells.

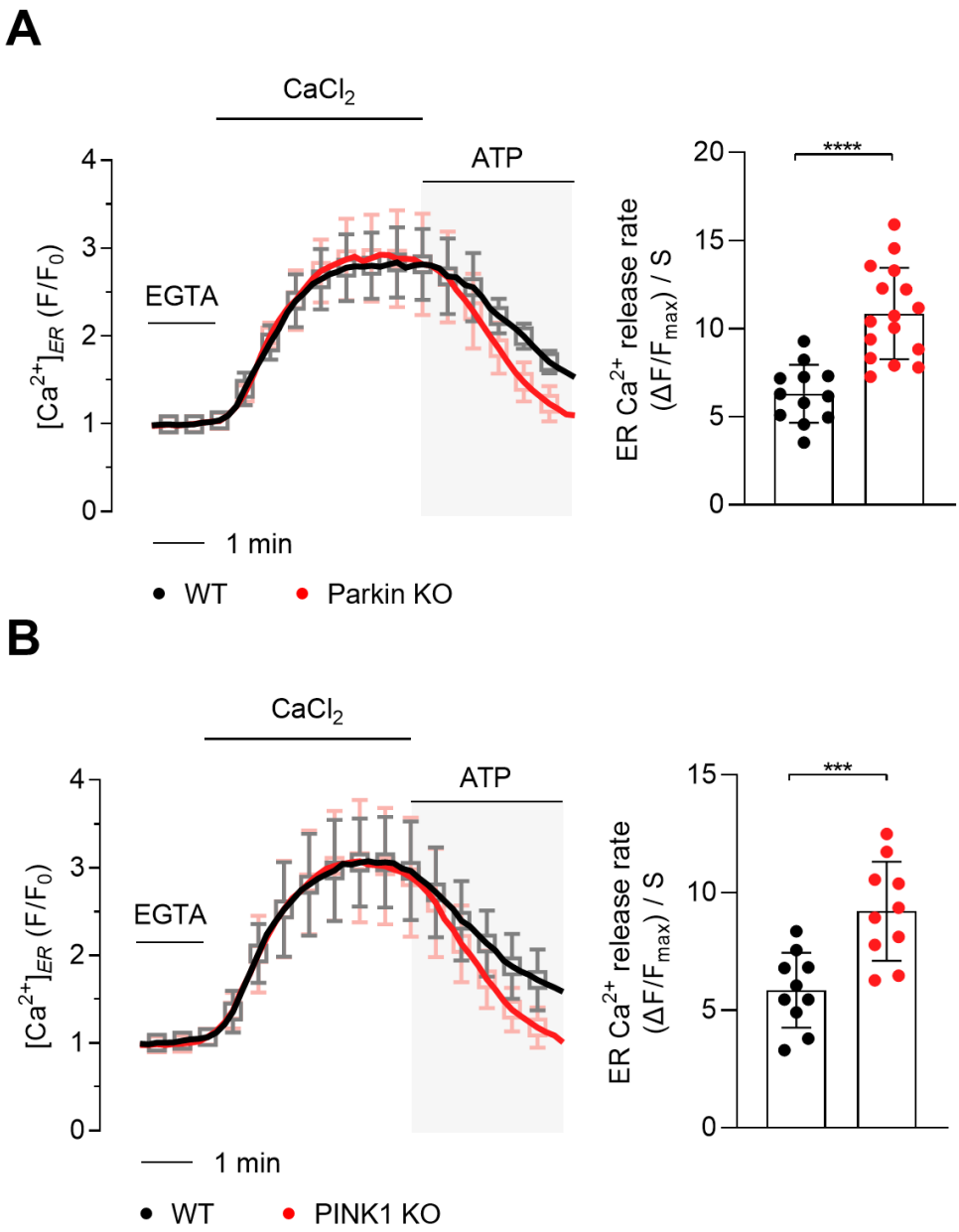

Figure 11. PINK1 and Parkin modulates intracellular calcium levels through regulating the activity of IP_3R.

Measurement of IP_3R activity. Following the depletion of intracellular calcium stores, cells were perfused in a modified KRB buffer, as described in the Methods section. The influx of ER calcium was then estimated using 1 mM $CaCl_2$. After reaching a steady-state, 1 M ATP was introduced to evoke ER calcium release to estimate the efflux of ER calcium. Measurement of ER calcium release in WT (black) and Parkin KO (red) MEF cells **(A)**. The bar graphs indicate the maximum rate of calcium release during ATP treatment. $n > 50$ cells. Measurement of ER calcium release in WT (black) and PINK1 KO (red) MEF cells **(B)**. $n > 50$ cells.

Parkin regulates IP_3R activity through CISD1

I performed a small-scale fly genetic screen to see how PINK1 and Parkin modulate IP_3R activity. Before that, I set up the calcium imaging systems that can be used in *Drosophila* in vivo systems **(Fig. 12)**. After expressing various organelle calcium indicators in muscle using *mef2*-GAL4, which results in muscle-specific expression in *Drosophila*, the muscles were dissected and calcium was induced using perfusion systems. Then, using a confocal microscope, I targeted specific areas of the muscle and obtained calcium imaging data. Next, I listed the 32 candidate proteins that are known substrates of Parkin and also localized to ER or mitochondrial membranes **(Table. 1)**. In order to investigate the causes of the ER calcium changes, the proteins on the list were knocked out one by one in the PINK1 and Parkin fly mutants. Although the release of ER calcium is increased in PINK1 or Parkin null flies, I tried to find the protein that rescues it through the screen using the *Drosophila* calcium imaging system. I obtained flies expressing D1ER (Bi et al., 2014), an ER calcium indicator, and crossed them with PINK1 or Parkin null flies, in addition to flies expressing candidate RNAi to measure ER calcium levels. The primary screen was performed with $PINK1^{B9}$, PINK1 null flies, and secondary with $park^{1}$, Parkin null flies **(Fig. 13)**. Among the 32 candidate lines, 14RNAi lines under the *mef2*-GAL4 driver were lethal, so their ER calcium levels could

not be measured **(Table. 2)**.

I successfully discovered that knocking down CISD, the *Drosophila* homolog of human CISD1, rescued the increased ER calcium release in PINK1 and Parkin null flies by the genetic calcium imaging screen **(Fig. 14A, 14B, 15A, and 16A)**. I also confirmed whether this result is repeated in the mammalian cell systems. The increased ER calcium release was similarly observed in PINK1 or Parkin KO MEF cells. But it was rescued by the expression of CISD1 siRNA **(Fig. 17A and 18A)**. Furthermore, in PINK1 or Parkin KO *Drosophila* or cells, cytosol calcium is dramatically increased. With the respective knockdown of CISD and CISD1, all of these phenomena were rescued **(Fig. 15B, 16B, 17B, and 18B)**.

I used the clustered regularly interspaced short palindromic repeats (CRISPR)-Cas9 system to generate CISD1 KO MEF cells **(Fig. 19)** and analyzed ER calcium channel activity to confirm if CISD1 knockdown rescues ER calcium release levels by modulating IP_3R activity in PINK1 and Parkin KO MEF cells. First, when looking at the response to ATP, ER calcium release was decreased in CISD KO MEF cells compared to WT cells **(Fig. 20A)**. Also, CISD1 KO MEF cells exhibited decreased cytosol calcium levels in response to ATP compared to WT cells **(Fig. 20B)**. Next, I confirmed the ER calcium channel activity. As expected, CISD1 KO MEF cells released significantly less ER calcium than WT cells, despite the fact

that there were no significant differences in ER calcium uptake between WT and KO MEF cells **(Fig. 21)**. It implies that the IP_3R activity is reduced in CISD1 KO MEF cells. These results strongly support that CISD1 activates IP_3R calcium channel activity.

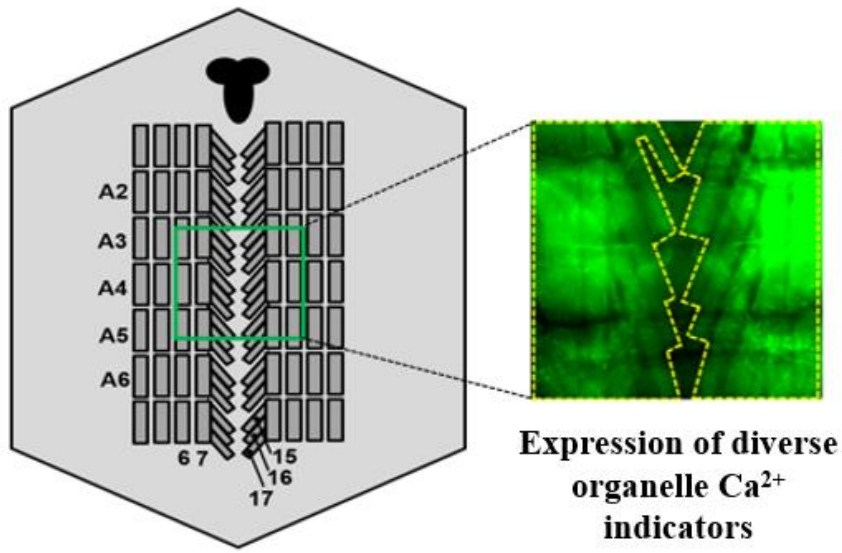

Figure 12. Schematic representation of the muscle region of *Drosophila* larva to measure in vivo calcium levels.

D1ER was expressed in larval muscle in *mef2*>D1ER. Fluorescence intensity was recorded from a well-focused region of body wall muscles 6, 7, 15, 16, and 17 of abdomen segments A2–A6. The central nervous system is marked with solid black. For simplicity, not all muscles and segments are shown. Fluorescence intensity from D1ER expressed in muscle was measured upon stimulation with 10 mM caffeine.

Gene	Flybase	Human homolog gene	RNAi#
CISD	CG1458	CISD1, 2	V33925
porin	CG6647	VDAC1, 2, 3	v330138
Eip55E	CG5345	CTH	v103779
eIF2B-beta	CG2677	EIF2B2	v25426
Aats-ala	CG13391	AARS	v39776
Sply	CG8946	SGPL1	v103485
rdhB	CG7077	DHRS11	v102434
AdSS	CG17273	ADSS, ADSSL1	v29520
Tom70	CG6756	TOMM70A	v18112
CG17333	CG17333	PGLS	v100734
Vps4	CG6842	VPS4A, B	v105977
Syx5	CG4214	STX5	v108928
Mpcp	CG4994	SLC25A3	v101316
Vps35	CG5625	VPS35	v22180
eIF-2alpha	CG9946	EIF2S1	v7798
CG11396	CG11396	TRAPPC12	v103546
sesB	CG16944	SLC25A4, 5, 6, 31	v104576
CG13887	CG13887	BCAP29, 31	v106452
CG2064	CG2064	DHRS13	v103276
CG8839	CG8839	FAAH2	v104479
Vha26	CG1088	ATP6V1E1, 2	v102378
Cyp4p1	CG10842	CYP4V2, F2, 3, 8, 11, 12, 22 A11, 22, X1	v3331
Idh	CG7176	IDH1,2	v100554
ALiX	CG12876	PDCD6IP	v32047
Pp2B-14D	CG9842	PPP3CA	v46873
CG4199	CG4199	AIFM3	v26424
Cat	CG6871	CAT	v103591
Pdh	CG4899	HPGD	v104428
Vha55	CG17369	ATP6V1B1, 2	v46554
CG5525	CG5525	CCT4	v106099
Vha44	CG8048	ATP6V1C1, 2	v101527
CG31694	CG31694	IFRD1, 2	v21398

Table 1. List of genes encoding the proteins that are located in the ER or mitochondrial membrane among the substrates of Parkin.

All RNAi lines for candidate genes were obtained from the Vienna *Drosophila* Stock Center (VDRC) and the lines were denoted as vstock#.

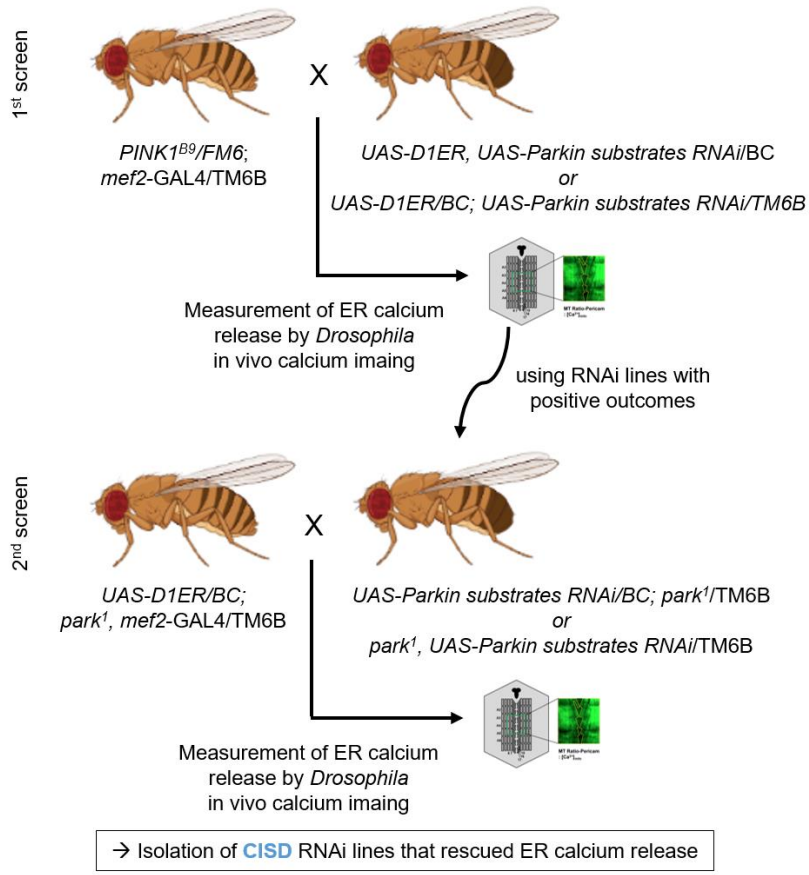

Figure 13. Genetic scheme to screen new genes that alleviate defective ER calcium release of PINK1 and Parkin null mutants.

To measure ER calcium release in *Drosophila* larval muscle, *mef2*-GAL4 and UAS-D1ER were used to express D1ER, an ER calcium indicator. After dissection of the third instar larvae, fluorescence images of larval muscle were acquired by confocal microscope with a perfusion system.

Gene	Flybase	Human homolog gene	RNAi#	Lethality
CISD	CG1458	CISD1, 2	V33925	-
porin	CG6647	VDAC1, 2, 3	v330138	-
Eip55E	CG5345	CTH	v103779	-
eIF2B-beta	CG2677	EIF2B2	v25426	-
Aats-ala	CG13391	AARS	v39776	O
Sply	CG8946	SGPL1	v103485	O
rdhB	CG7077	DHRS11	v102434	O
AdSS	CG17273	ADSS, ADSSL1	v29520	O
Tom70	CG6756	TOMM70A	v18112	-
CG17333	CG17333	PGLS	v100734	-
Vps4	CG6842	VPS4A, B	v105977	O
Syx5	CG4214	STX5	v108928	O
Mpcp	CG4994	SLC25A3	v101316	O
Vps35	CG5625	VPS35	v22180	-
eIF-2alpha	CG9946	EIF2S1	v7798	-
CG11396	CG11396	TRAPPC12	v103546	O
sesB	CG16944	SLC25A4, 5, 6, 31	v104576	-
CG13887	CG13887	BCAP29, 31	v106452	O
CG2064	CG2064	DHRS13	v103276	-
CG8839	CG8839	FAAH2	v104479	-
Vha26	CG1088	ATP6V1E1, 2	v102378	O
Cyp4p1	CG10842	CYP4V2, F2, 3, 8, 11, 12, 22 A11, 22, X1	v3331	-
Idh	CG7176	IDH1,2	v100554	-
ALiX	CG12876	PDCD6IP	v32047	-
Pp2B-14D	CG9842	PPP3CA	v46873	O
CG4199	CG4199	AIFM3	v26424	-
Cat	CG6871	CAT	v103591	O
Pdh	CG4899	HPGD	v104428	O
Vha55	CG17369	ATP6V1B1, 2	v46554	-
CG5525	CG5525	CCT4	v106099	O
Vha44	CG8048	ATP6V1C1, 2	v101527	-
CG31694	CG31694	IFRD1, 2	v21398	-

Table 2. List of the fly genes used for the genetic screen.

List of the genes screened for the regulators of ER calcium mobilization. When these candidate RNAi were expressed by *mef2*-GAL4 that induces gene expression in the muscle of *Drosophila*, 14 RNAi showed lethal phenotypes. Therefore, I used the remaining 18 candidate gene RNAi lines to perform calcium imaging experiments.

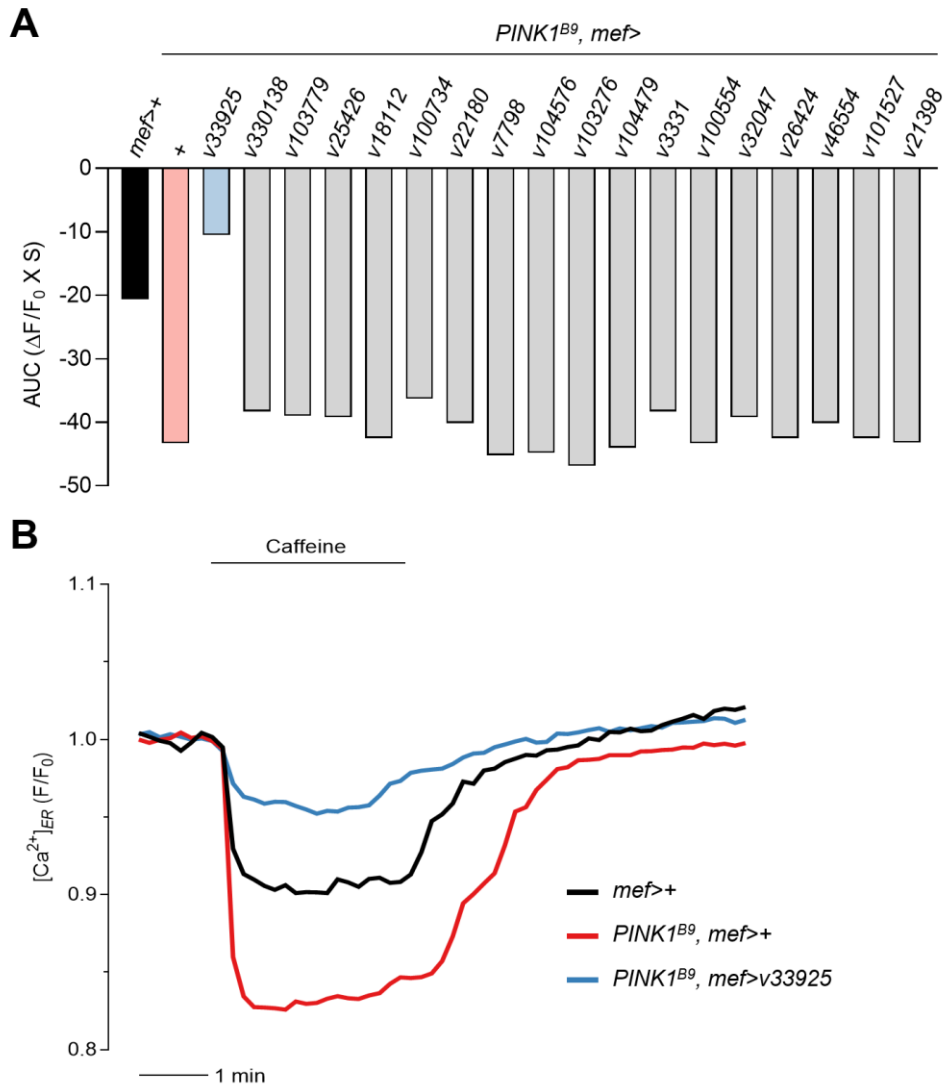

Figure14. Results of the genetic screen for the regulators of ER calcium release.

List of the genes screened for the regulators of ER calcium mobilization. When these candidate RNAi were expressed by *mef2*-GAL4 that induces gene expression in the muscle of *Drosophila*, 14 RNAi showed lethal phenotypes. I therefore conducted calcium imaging experiments with the remaining 18 candidate gene RNAi lines. The bar graphs indicate the quantification of the normalized calcium trace of all RNAi candidates using AUC of calcium release during ATP treatment **(A)**. Measurement of ER **(B)** calcium modulation in WT (*mef*>+, black), PINK1 null mutant flies (*PINK1*^{B9}, *mef*>+, red), and PINK1 null mutant expressing v33925 (*PINK1*^{B9}, *mef*>v33925, blue).

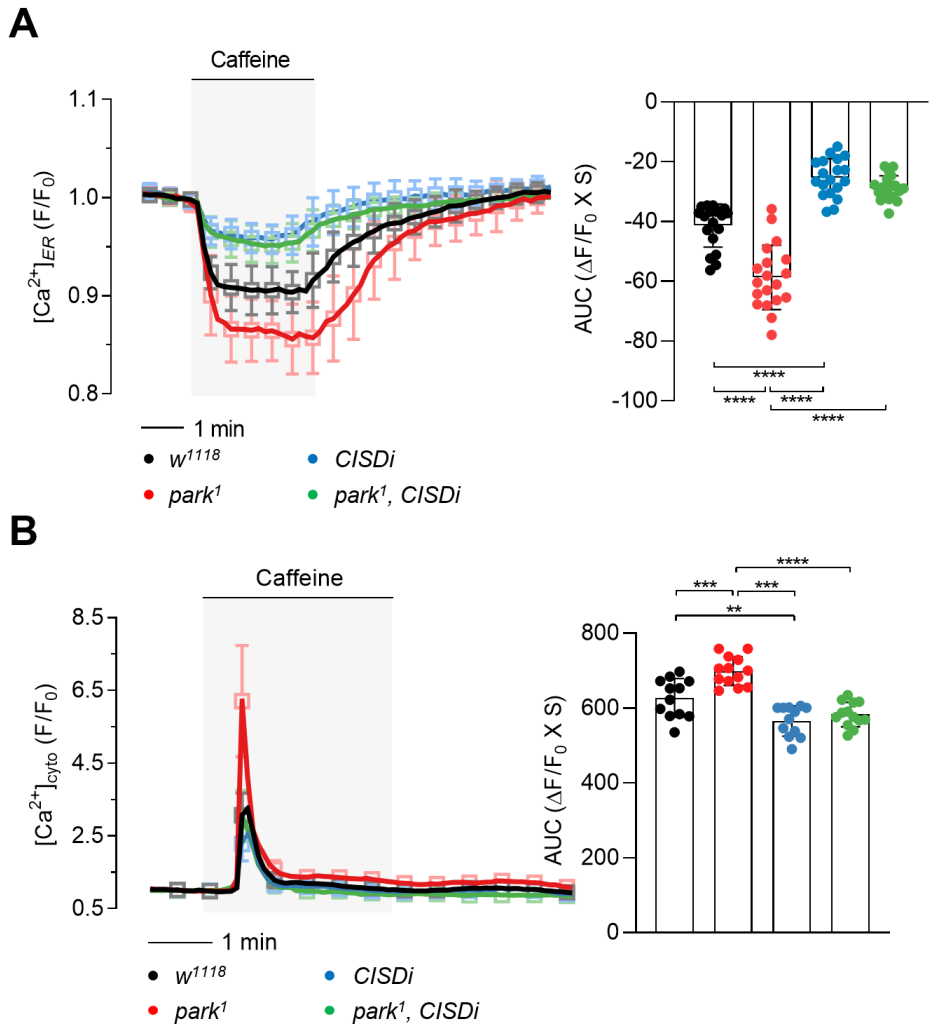

Figure 15. CISD knockdown rescues the abnormal calcium flux in Parkin-deficient flies.

Measurement of ER **(A)** and cytosolic **(B)** modulation in WT (w^{1118}, black) and Parkin null mutant flies ($park^{1}$) (red). Similar experiments were also

conducted in CISD knockdown flies (*CISDi*) (blue) and Parkin null flies expressing CISD RNAi (*park*^{1}, *CISDi*) (green). The right side bar graphs indicate the quantification of the normalized calcium traces using AUC of calcium release during caffeine treatment. $n > 12$ flies.

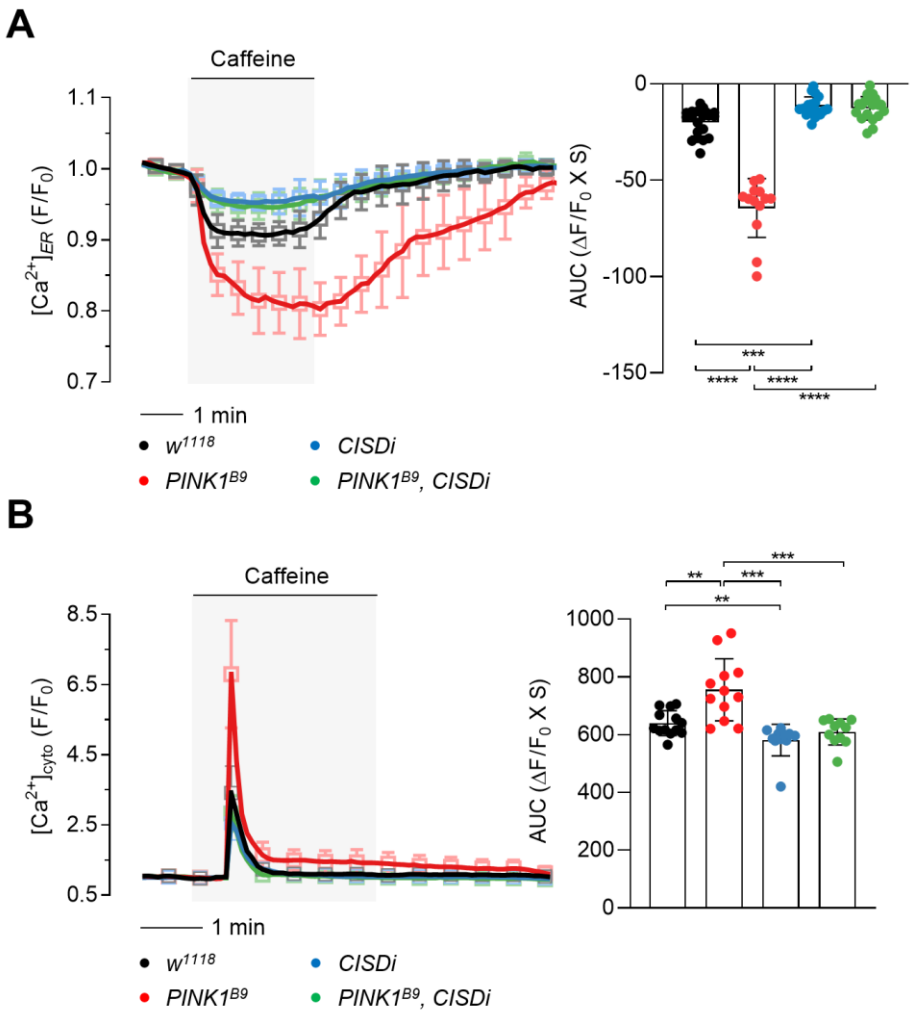

Figure 16. CISD knockdown rescues the abnormal calcium flux in PINK1-deficient flies.

Measurement of ER **(A)** and cytosolic **(B)** modulation in WT (w^{1118}, black) and PINK1 null mutant flies ($PINK1^{B9}$) (red). Similar experiments were also

conducted in CISD knockdown flies (*CISDi*) (blue) and PINK1 null flies expressing CISD RNAi (*PINK1*^{B9}, *CISDi*) (green). The right side bar graphs indicate the quantification of the normalized calcium traces using AUC of calcium release during caffeine treatment. $n > 11$ flies.

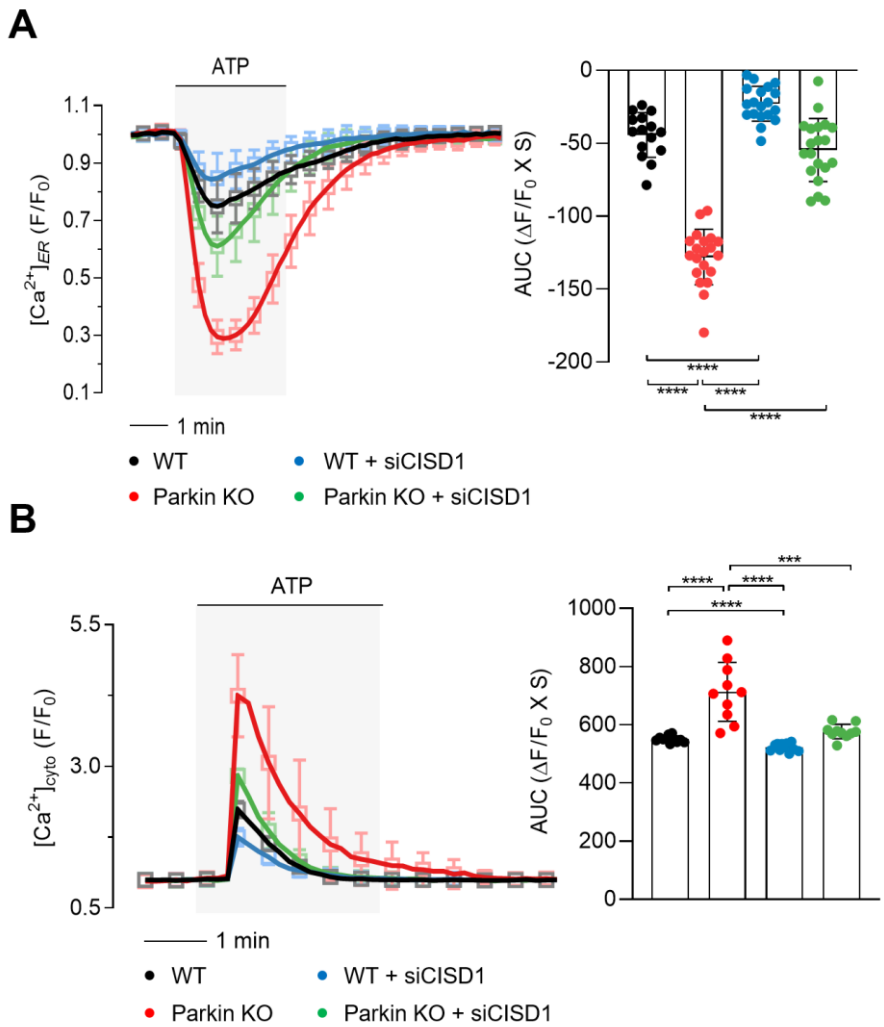

Figure 17. CISD1 knockdown rescues the abnormal calcium flux in Parkin KO MEF cells.

Measurement of ER **(A)** and cytosolic **(B)** modulation in WT (black) and Parkin KO (red) MEF cells. Similar experiments were also conducted for

WT (blue) and Parkin KO (green) MEF cells expressing siCISD1. The right side bar graphs indicate the quantification of the normalized calcium traces using AUC of calcium release during ATP treatment. $n > 100$ cells.

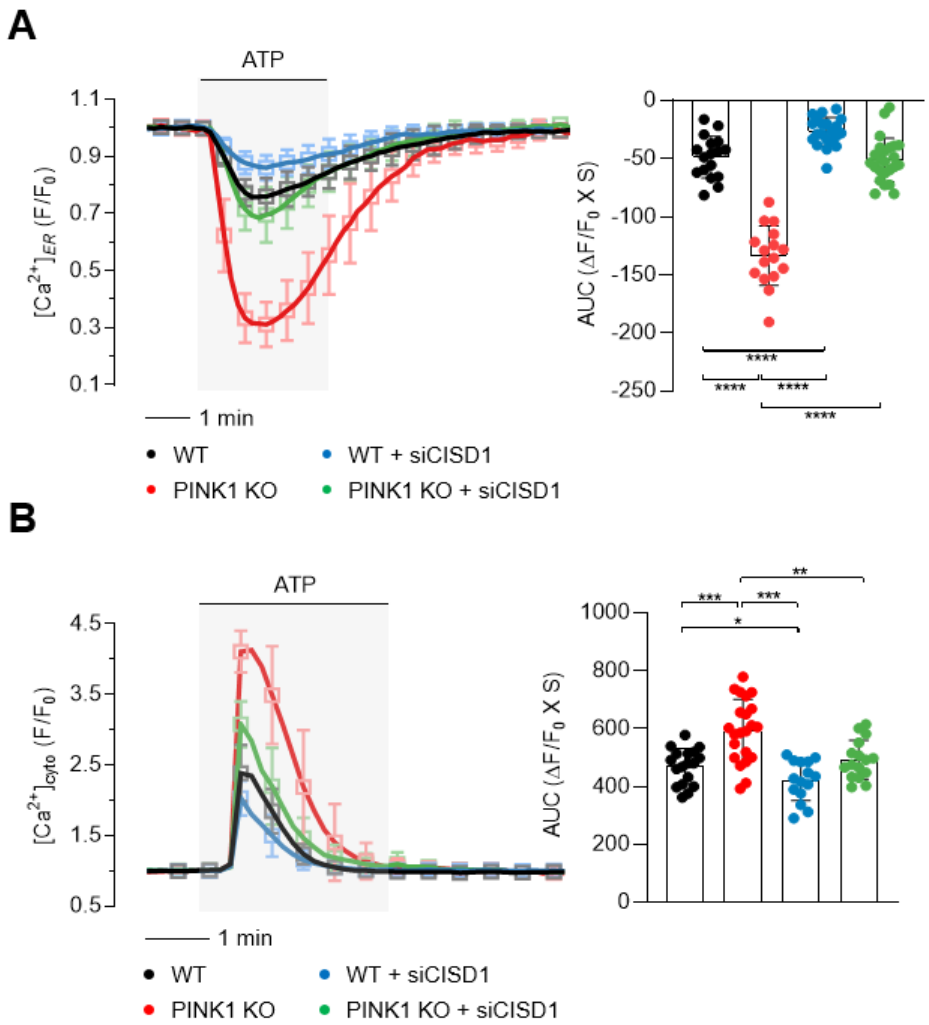

Figure 18. CISD1 knockdown rescues the abnormal calcium flux in PINK1 KO MEF cells.

Measurement of ER **(A)** and cytosolic **(B)** calcium modulation in WT (black) and PINK1 KO (red) MEF cells. Similar experiments were also

conducted for WT (blue) and PINK1 KO (green) MEF cells expressing siCISD1. The right side bar graphs indicate the quantification of the normalized calcium traces using AUC of calcium release during ATP treatment. $n > 100$ cells.

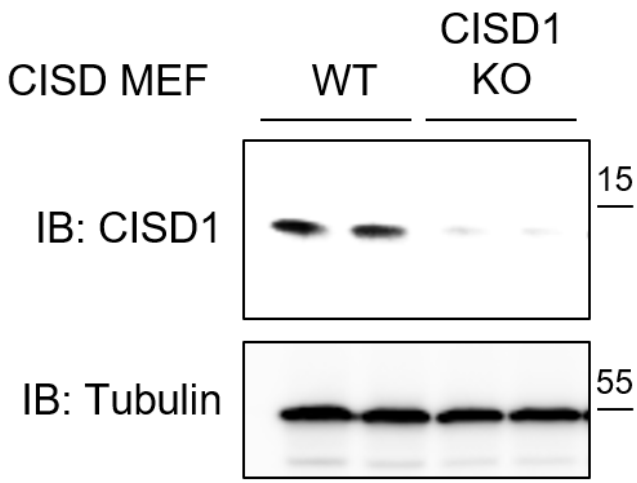

Figure 19. CISD1 KO MEF cells were generated using the CRISPR-Cas9 system.

Immunoblot analysis of endogenous CISD1 in WT and PINK1 KO MEF cells. Clustered regularly interspaced short palindromic repeats (CRISPR)-Cas9 system was used to generate CISD1 KO MEF cells.

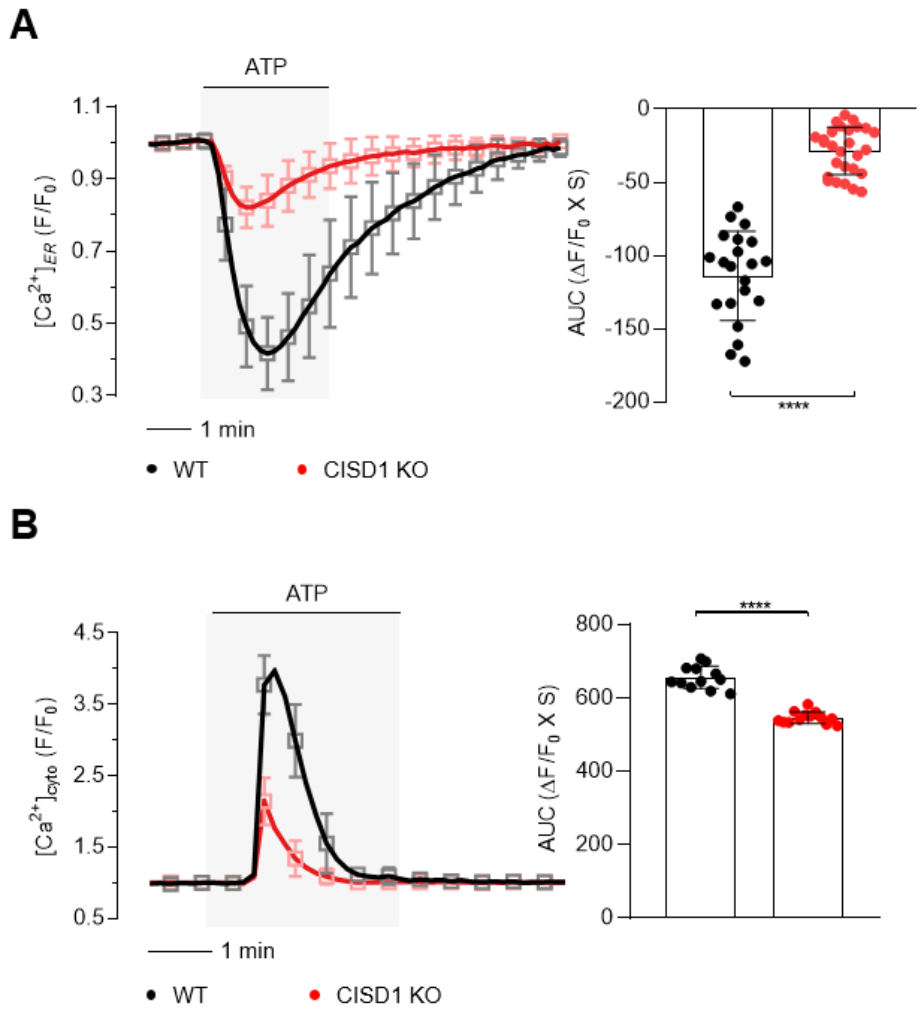

Figure 20. CISD1 KO MEF cells show abnormal calcium flux.

Measurement of ER **(A)** and cytosolic **(B)** calcium modulation in WT (black) and CISD1 KO (red) MEF cells. The right side bar graphs indicate

the quantification of the normalized calcium traces using AUC of calcium release during ATP treatment. $n > 100$ cells.

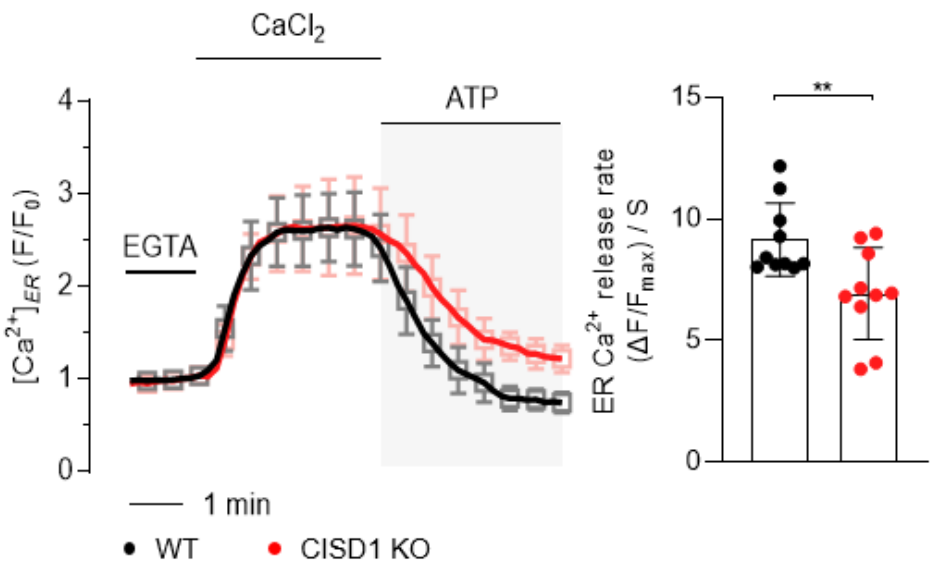

Figure 21. IP$_3$R activity is reduced in CISD1 KO MEF cells.

Measurement of ER calcium release through IP$_3$R in WT (black) and CISD1 KO (red) MEF cells. The bar graphs indicate the maximum rate of calcium release during ATP treatment. n > 50 cells.

CISD1 is a substrate of the E3 ligase Parkin

Through the previous experiments, I figured out that IP_3R activity was regulated by the PINK1-Parkin pathway, and it was confirmed that CISD1, known as a downstream substrate of Parkin, regulated IP_3R activity. I performed a ubiquitination assay for CISD1 with Parkin WT and the CS mutant to confirm whether the CISD1 protein is a direct target of Parkin. The combination of antimycin and oligomycin causes mitochondrial membrane potential loss and stimulates Parkin activity. So, I treated cells with antimycin and oligomycin, and CISD1 was ubiquitinated by Parkin WT, as expected **(Fig. 22)**. The catalytically inactivated Parkin CS mutant, on the other hand, did not ubiquitinate CISD1 **(Fig. 22)**.

As I discovered that CISD1 was ubiquitinated by Parkin, I searched for the sites of CISD1 that were ubiquitinated by Parkin. It can be noted that CISD1 has well-conserved lysine residues among a variety of species **(Fig. 23)**. Among them, I discovered that the CISD1 K55/68R double mutant is hardly ubiquitinated by Parkin **(Fig. 24)**. Cycloheximide, an inhibitor of protein biosynthesis due to its prevention in translational elongation, is used to compare protein stability in eukaryotic cells. It is commonly used in cell biology to figure out the half-life of a given protein. So, I treated cycloheximide (CHX) to Parkin-transfected cells and observed the varied

protein stability of CISD1 WT and the K55/68R double mutant to see the effect of CISD1 ubiquitination by Parkin. In contrast to CISD1 WT protein levels, the CISD1 K55/68R double mutant protein levels were strongly stabilized **(Fig. 25)**. Next, I attempted to look at the changes in CISD1 protein levels at the endogenous levels rather than the exogenously expressed protein levels. So, after grinding *Drosophila PINK1*^{B9} and *Park*^{1}, proteins were extracted respectively, CISD1 protein levels were measured, and it was also confirmed in the mammalian cells. Endogenous CISD1 protein levels were elevated in PINK1 and Parkin null flies, as well as in PINK1 and Parkin KO MEF cells **(Fig. 26)**. These findings indicate that Parkin ubiquitinates CISD1 and enhances its protein degradation.

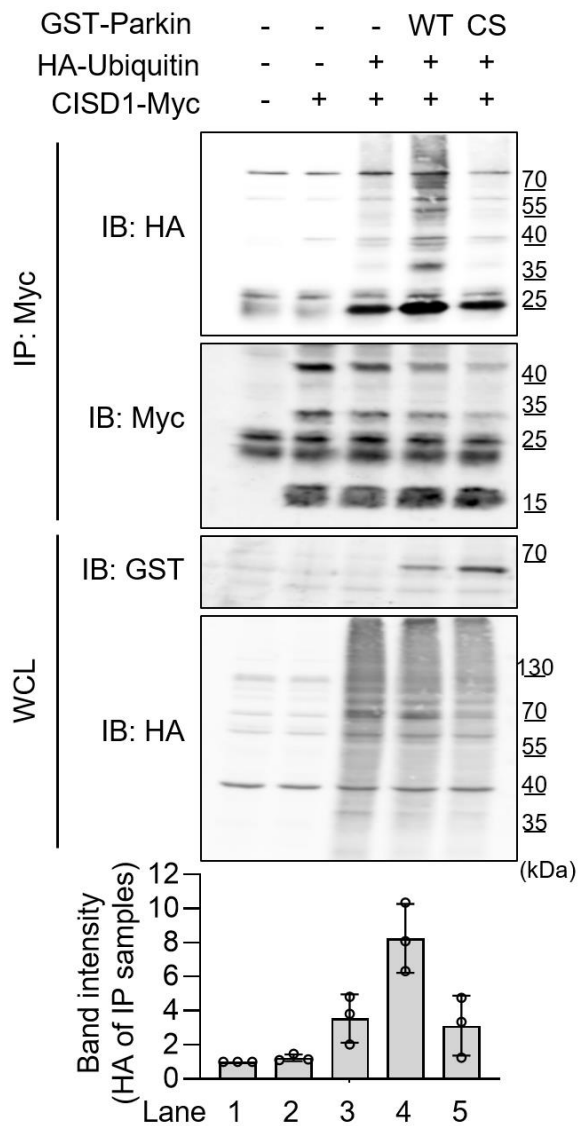

Figure 22. Parkin WT, but not Parkin CS, ubiquitinates CISD1.

Ubiquitination levels of CISD1 in HEK293T cells expressing Parkin WT or C431S (CS). The cells were treated with 20 μM MG132 for 4 hr and lysed

for anti-Myc immunoprecipitation to compare the level of CISD1 ubiquitination by immunoblot analyses. The immunoblot band intensity for ubiquitinated CISD1 was quantified in three different experiments (bar graphs in bottom).

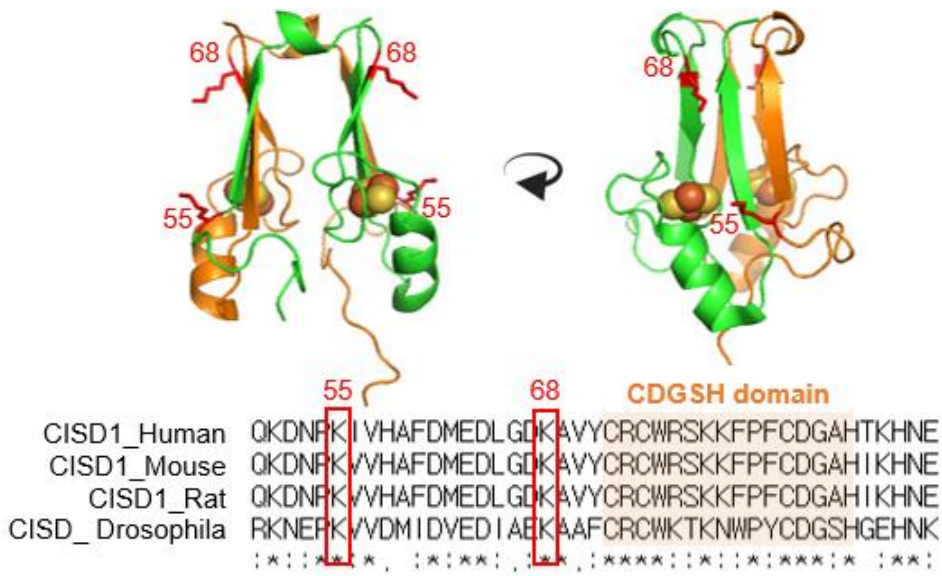

Figure 23. CISD1 has conserved lysine residues across many species.

Aligned CISD1 protein sequences of human (Q9NZ45.1), mouse (NP_598768.1), rat (B0K020.1), and *Drosophila* (Q9VAM6.1) with indication of the conserved lysine residues in red boxes. Three-dimensional human CISD1 protein structures, RCSB PDB-2QD0, show K55 and K68 ubiquitination sites.

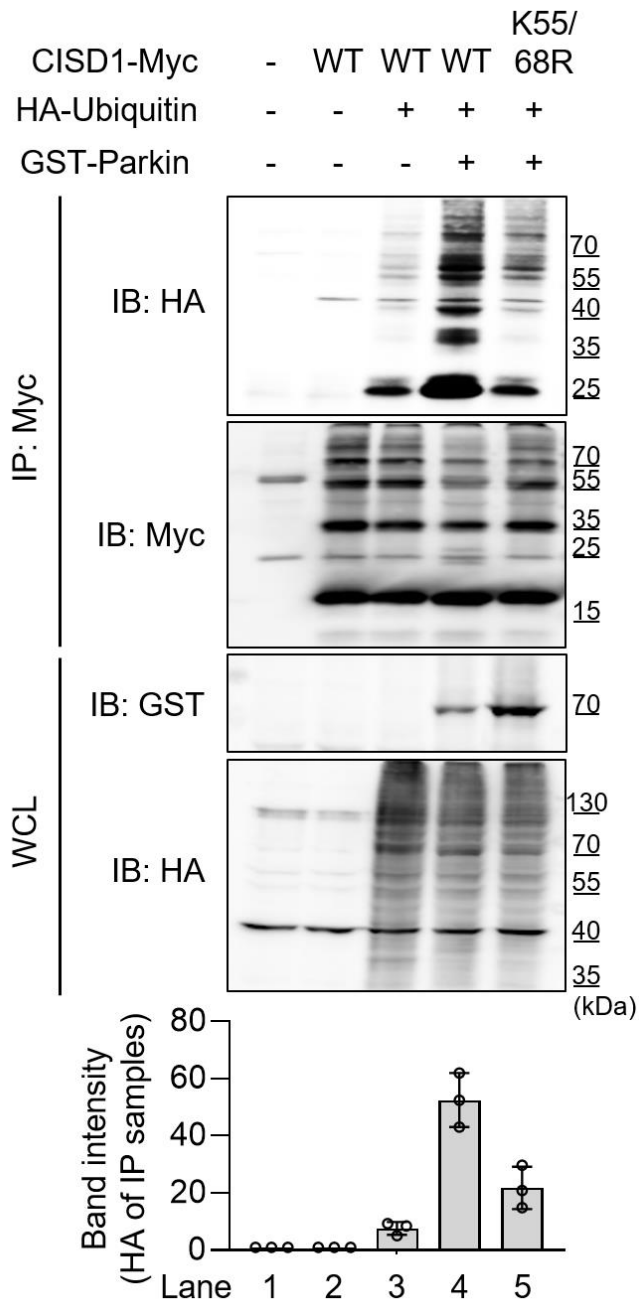

Figure 24. Parkin ubiquitinates CISD1 K55/68 sites.

Ubiquitination levels of CISD1 WT and K55R/K68R (K55/68R) double mutant in HEK293T cells expressing Parkin WT. The cells were treated with 20 μM MG132 for 4 hr and lysed for anti-Myc immunoprecipitation to compare the level of CISD1 ubiquitination by immunoblot analyses. The immunoblot band intensity for ubiquitinated CISD1 was quantified in three different experiments (bar graphs in bottom).

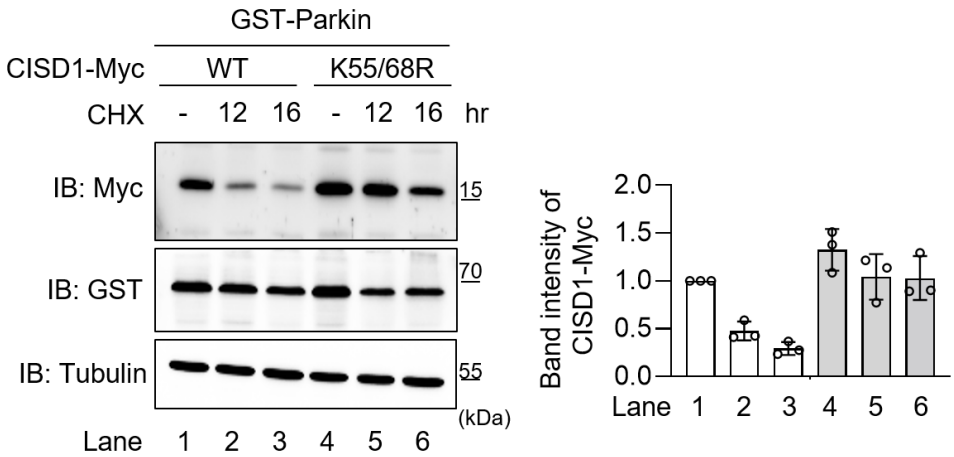

Figure 25. CISD1 K55/68R are highly stabilized compared to CISD1 WT.

In HEK293T cells, immunoblot analyses of the CISD1 protein suggested that Parkin-dependent K55 and K68 ubiquitination had reduced its stability. The cells were treated with 100 µg/µl cycloheximide (CHX) for 12 or 16 hr and analyzed the level of CISD1 protein. The immunoblot band intensity for ubiquitinated CISD1 was quantified in three different experiments (bar graphs in bottom).

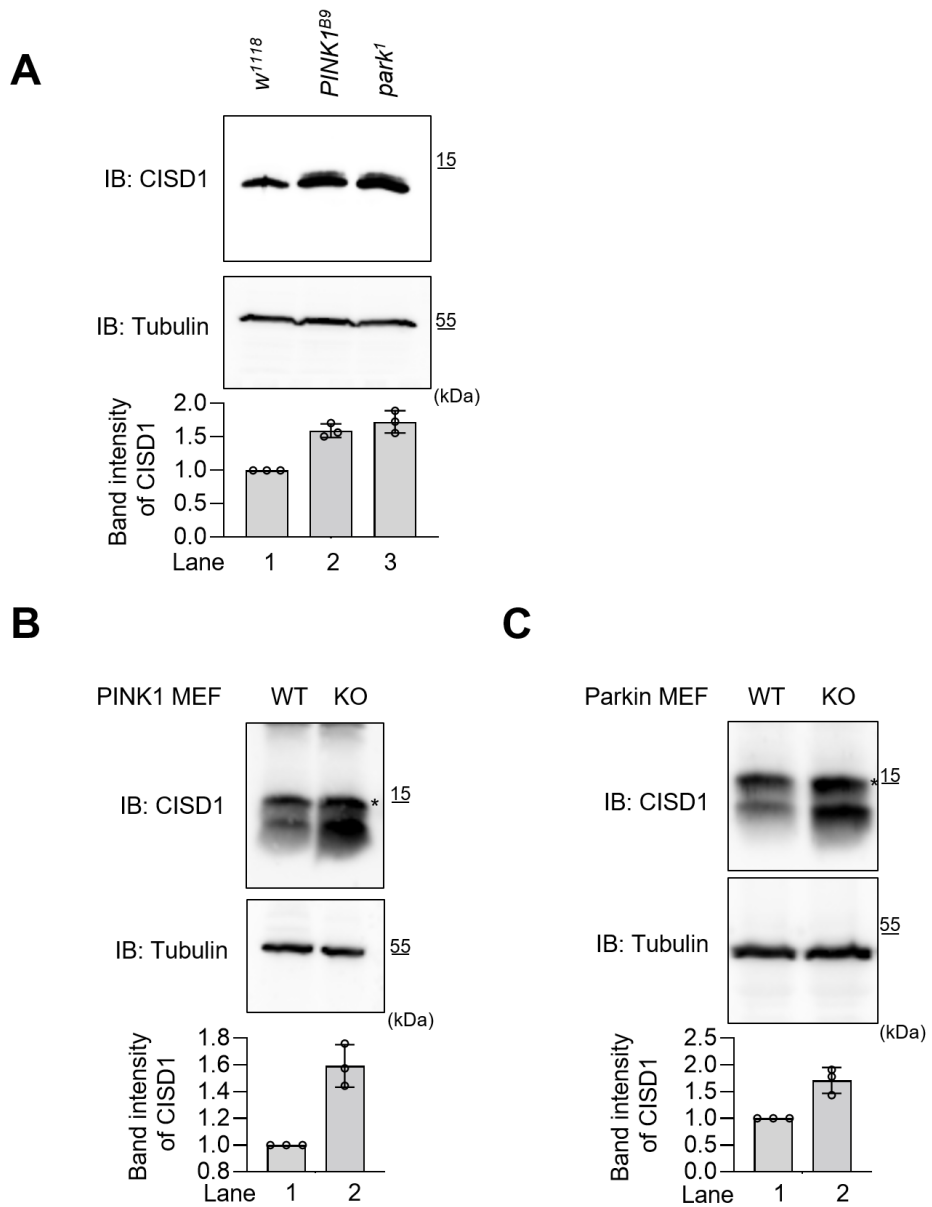

Figure 26. Endogenous CISD1 protein levels are elevated in PINK1- and Parkin-deficient flies and MEF cells.

Immunoblot analysis of endogenous CISD1 in WT (w^{1118}), PINK1 null ($PINK1^{B9}$), and Parkin null ($park^{1}$) flies **(A)**. Immunoblot analysis of endogenous CISD1 in WT and PINK1 KO MEF cells **(B)** and WT and Parkin KO MEF cells **(C)**. Three independent experiments were conducted and the immunoblot band intensity for CISD1 were quantitated (bar graphs in bottom).

CISD knockdown rescues PINK1 and Parkin deficient phenotypes by regulating IP_3R activity

Our previous studies have shown that PINK1- and Parkin-deficient flies exhibit crushed thoracic, upturned or downturned abnormal wings, abnormal mitochondrial morphology, and increased thoracic apoptotic signals (Ham *et al.*, 2021; Park et al., 2006). In addition, PINK1 or Parkin null flies show a decreased climbing ability and loss of DA neurons in protocerebral posterior medial 1/2 (PPM1/2) and posterior protocerebrum lateral 1 (PPL1) (Cha et al., 2005; Ham *et al.*, 2021; Park *et al.*, 2006). Knowing that these phenotypes are problematic, as in Parkinson's disease, I knocked down the target genes in the PINK1 or Parkin null flies and observed how the phenotypes changed. Excitingly, these phenotypes of PINK1 and Parkin null flies – including crushed thoraces, abnormal wing postures, abnormal mitochondrial morphology in thoraces, increased apoptotic responses in the muscle, impaired climbing ability, and reduced numbers of DA neurons in the PPM1/2 and PPL1 regions of the adult brain – were fully rescued with CISD knockdown **(Fig. 27, 28, 29, and 30)**. To summarize, these results indicate that inhibiting CISD rescues PD-associated pathogenesis caused by PINK1 or Parkin deficiency. If that's the case, I investigated to see if the PD phenotypes reemerge when CISD WT is

overexpressed in CISD knockdown-rescued flies. Simultaneous expression of CISD WT blocked the rescue effects of CISD knockdown in PINK1 and Parkin null flies **(Fig. 31, 32, 33, and 34)**.

Next, since I found that CISD regulates the IP_3R activity, I wondered if the rescuing effects of CISD knockdown are really due to reduced IP_3R activity. So, I observed PD-related phenotypes in PINK1 or Parkin null flies co-expressing CISD RNAi and exogenous *Drosophila* IP_3R, *itpr*. If the phenotypes were rescued by decreasing IP_3R activity with CISD RNAi, it was expected that the phenotype would deteriorate again if *itpr* was co-expressed. Surprisingly, whereas CISD knockdown totally rescued PD-related phenotypes in PINK1 and Parkin null flies, simultaneous expression of *itpr* resulted in reappearance of PD-related phenotypes **(Fig. 27, 28, 29, and 30)**. It indicates that the rescuing effects of CISD knockdown were strongly diminished.

Since I discovered the relationship between the PINK1-Parkin pathway and the activity of IP_3R, I investigated to see if PD-related phenotypes of PINK1 and Parkin null flies could be rescued simply by reducing IP_3R activity. Therefore, PD-related phenotypes were examined by expressing IP_3R RNAi in PINK1 and Parkin null flies. Expectedly, IP_3R knockdown strongly rescued all PD-related phenotypes of PINK1 and Parkin null flies including crushed thorax, abnormal wing postures,

abnormal mitochondrial morphology, increased apoptotic signals, defective climbing ability, and reduced number of DA neurons **(Fig. 35, 36, 37, and 38)**. Overall, I propose that CISD deficiency reduces IP_3R activity, which restores intracellular calcium homeostasis and rescues the PD-related pathogenesis in PINK1 and Parkin null flies.

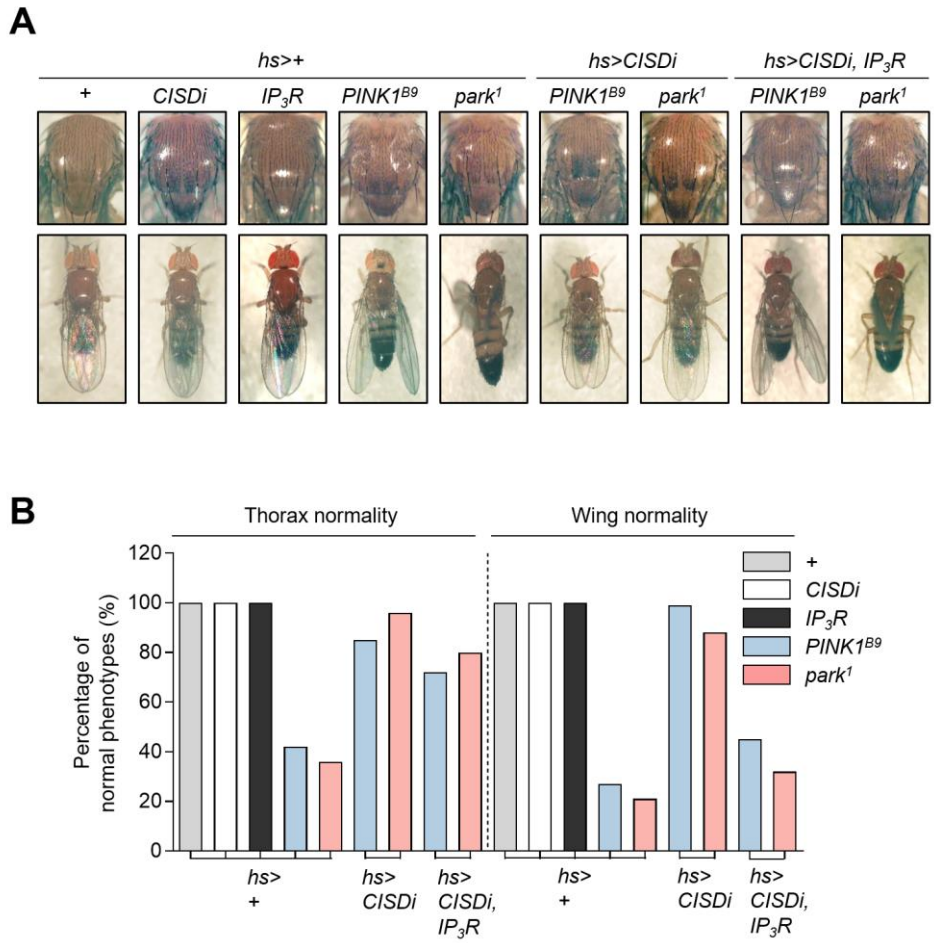

Figure 27. CISD knockdown rescues the abnormal thoracic and wing phenotypes of PINK1 and Parkin null flies by regulating IP$_3$R.

Images of *Drosophila* thoracic (top panels) and wing posture (bottom panels) phenotypes **(A)** and percentages of the flies having normal phenotypes **(B)**. *hs>IP$_3$R* and *hs>CISDi* indicate heat shock-induced overexpression of the *Drosophila* IP$_3$R gene, *itpr*, and the RNAi for *Drosophila CISD*, respectively.

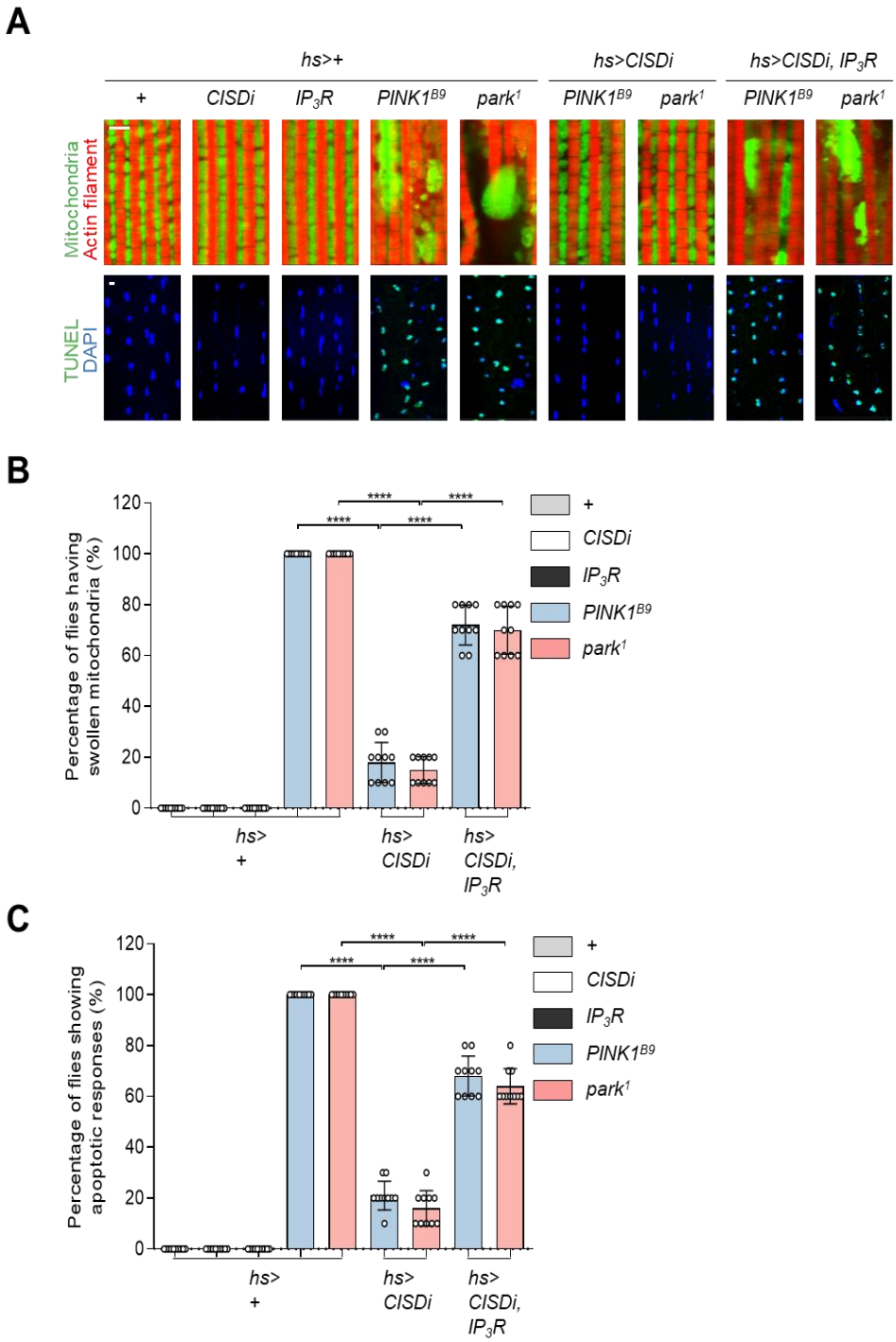
A
hs>+
hs>CISDi
hs>CISDi, IP3R
+
CISDi
IP3R
PINK1B9
park1
PINK1B9
park1
PINK1B9
park1
Mitochondria
Actin filament
TUNEL
DAPI
B
Percentage of flies having swollen mitochondria (%)
120
100
80
60
40
20
0
****
****
****
****
+
CISDi
IP3R
PINK1B9
park1
hs> +
hs> CISDi
hs> CISDi, IP3R
C
Percentage of flies showing apoptotic responses (%)
120
100
80
60
40
20
0
****
****
****
****
+
CISDi
IP3R
PINK1B9
park1
hs> +
hs> CISDi
hs> CISDi, IP3R

Figure 28. CISD knockdown rescues aberrant mitochondrial morphology and increased apoptosis of PINK1 and Parkin null flies by regulating IP_3R.

Immunofluorescence images **(A)** of the adult flight muscles (top). Green (mitochondria) and red (actin filament). *n* = 10. Scale bar, 5 μm. TUNEL assays of the adult flight muscles (bottom). Green (TUNEL) and blue (DAPI). *n* = 10. Scale bar, 5 μm. Quantification of the percentage of flies having swollen mitochondria. *n* = 10 **(B)**. Quantification of the percentage of flies showing apoptotic responses. *n* = 10 **(C)**. *hs>IP$_3$R* and *hs>CISDi* indicate heat shock-induced overexpression of the *Drosophila* IP_3R gene, *itpr*, and the RNAi for *Drosophila CISD*, respectively.

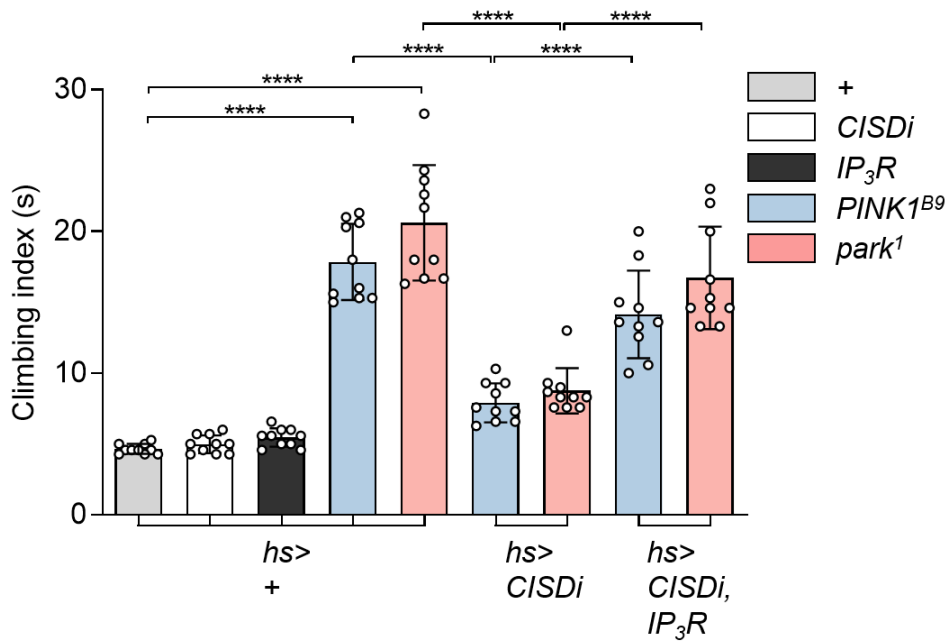

Figure 29. CISD knockdown rescues impaired climbing ability of PINK1 and Parkin null flies by regulating IP$_3$R.

Measurement of the climbing ability in the adult flies with indicated genotypes. *n* = 10. *hs>IP$_3$R* and *hs>CISDi* indicate heat shock-induced overexpression of the *Drosophila* IP$_3$R gene, *itpr*, and the RNAi for *Drosophila CISD*, respectively.

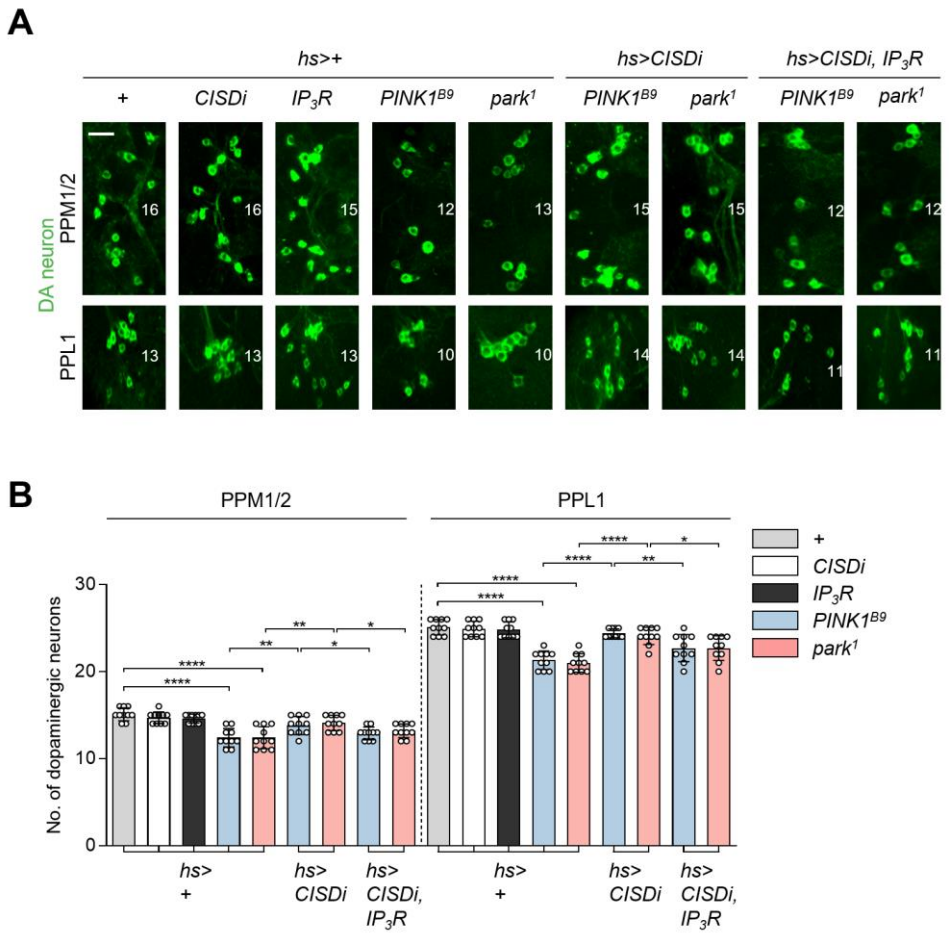

Figure 30. CISD knockdown rescues reduced number of DA neurons of PINK1 and Parkin null flies by regulating IP$_3$R.

Immunofluorescence images **(A)** and number **(B)** of DA neurons in PPM1/2 (top), and PPL1 (bottom) regions of adult fly brains with indicated genotypes. Green (DA neuron). *n* = 10. Scale bar, 20 μm. *hs>IP$_3$R* and *hs>CISDi* indicate heat shock-induced overexpression of the *Drosophila* IP$_3$R gene, *itpr*, and the RNAi for *Drosophila CISD*, respectively.

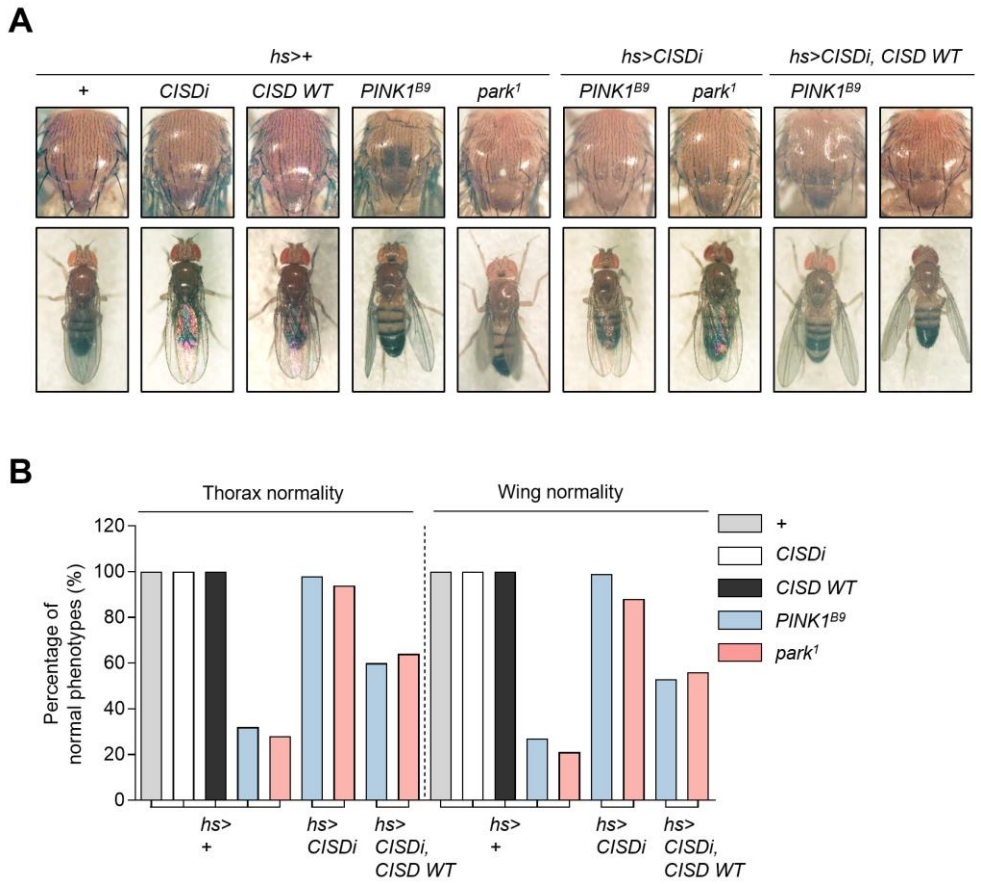

Figure 31. Rescuing effects of CISD knockdown on the abnormal thoracic and wing phenotypes are blocked by simultaneous expression of CISD WT.

Images of *Drosophila* thoracic (top panels) and wing posture (bottom panels) phenotypes **(A)** and percentages of the flies having normal phenotypes **(B)**.

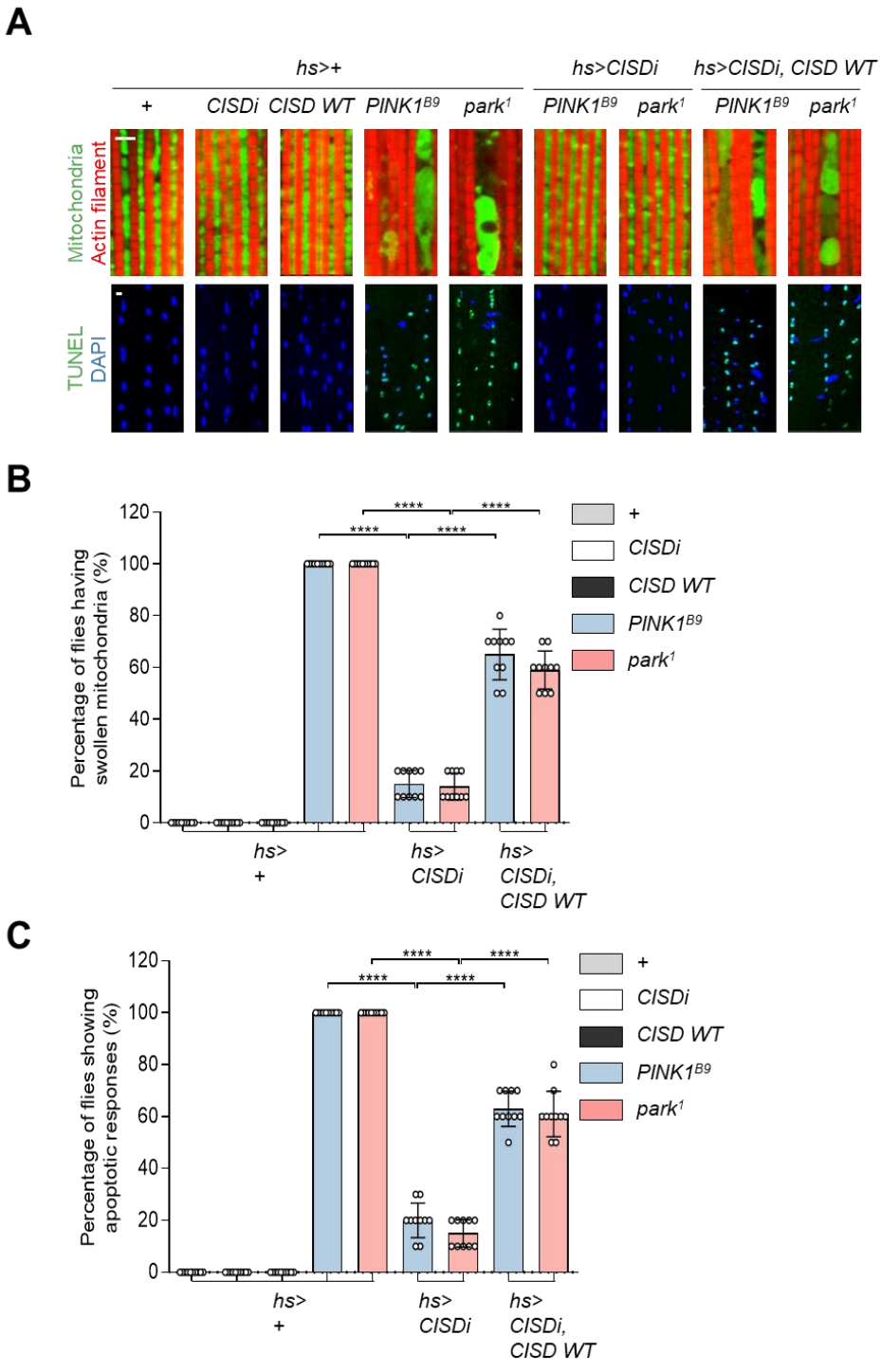
A
hs>+
hs>CISDi
hs>CISDi, CISD WT
+
CISDi
CISD WT
PINK1B9
park1
PINK1B9
park1
PINK1B9
park1
Mitochondria
Actin filament
TUNEL
DAPI
B
Percentage of flies having swollen mitochondria (%)
120
100
80
60
40
20
0
****
****
****
****
+
CISDi
CISD WT
PINK1B9
park1
hs> +
hs> CISDi
hs> CISDi, CISD WT
C
Percentage of flies showing apoptotic responses (%)
120
100
80
60
40
20
0
****
****
****
****
+
CISDi
CISD WT
PINK1B9
park1
hs> +
hs> CISDi
hs> CISDi, CISD WT

Figure 32. Rescuing effects of CISD knockdown on the aberrant mitochondrial morphology and increased apoptosis are blocked by simultaneous expression of CISD WT.

Immunofluorescence images **(A)** of the adult flight muscles (top). Green (mitochondria) and red (actin filament). *n* = 10. Scale bar, 5 μm. TUNEL assays of the adult flight muscles (bottom). Green (TUNEL) and blue (DAPI). *n* = 10. Scale bar, 5 μm. Quantification of the percentage of flies having swollen mitochondria. *n* = 10 **(B)**. Quantification of the percentage of flies showing apoptotic responses. *n* = 10 **(C)**.

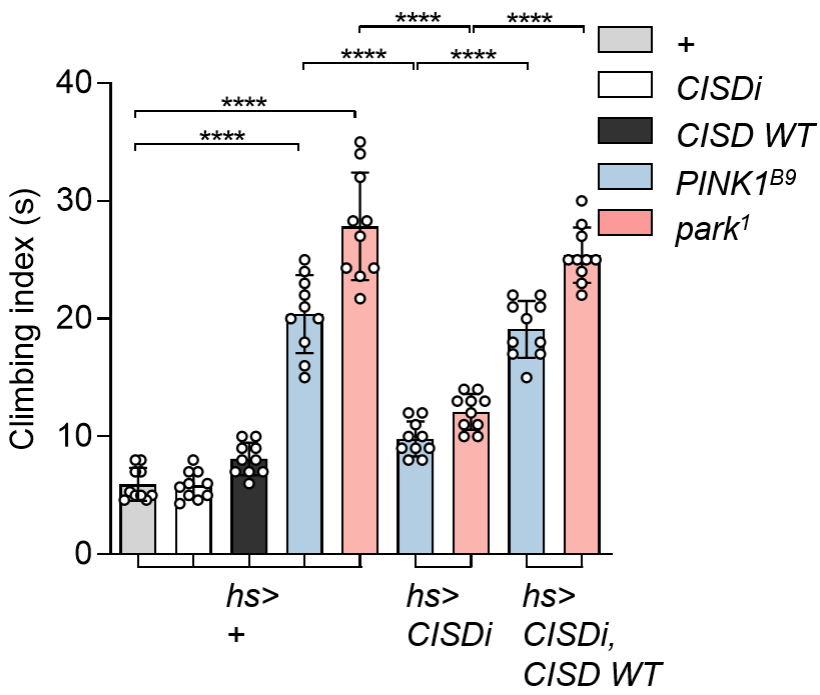

Figure 33. Rescuing effect of CISD knockdown on the impaired climbing ability is blocked by simultaneous expression of CISD WT.

Measurement of the climbing ability in the adult flies with indicated genotypes. *n* = 10.

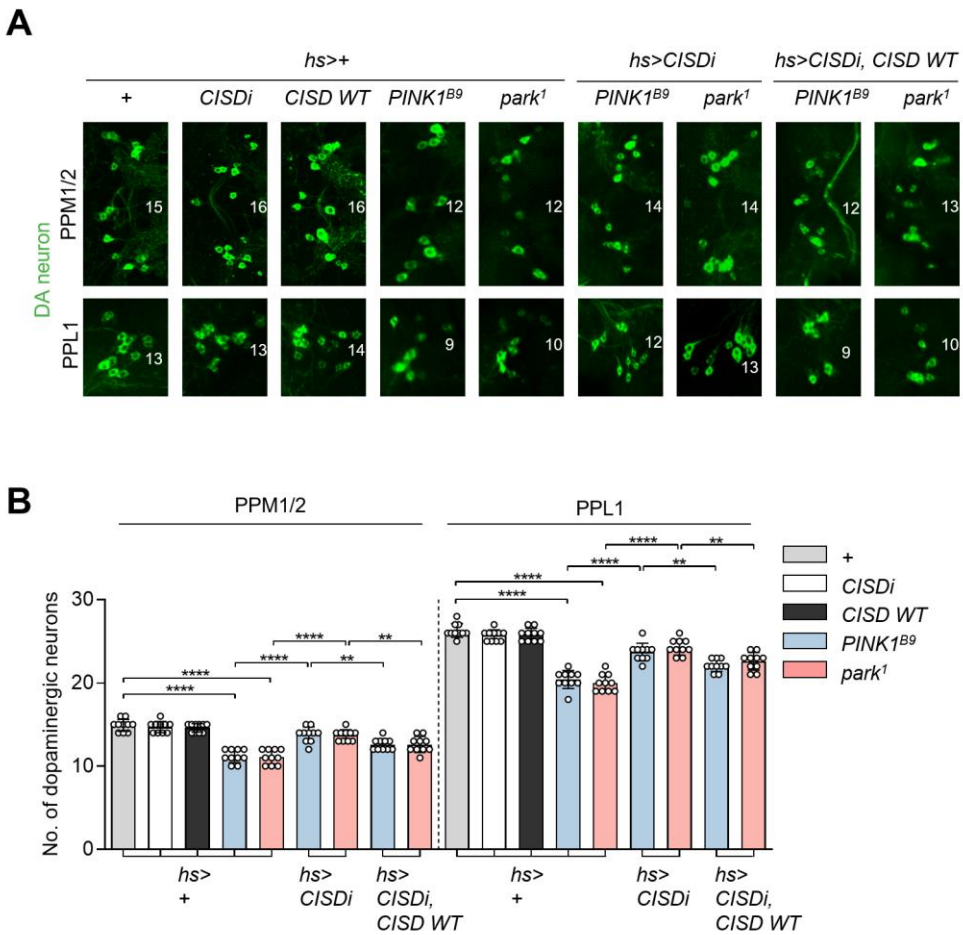

Figure 34. Rescuing effect of CISD knockdown on the reduced number of DA neurons is blocked by simultaneous expression of CISD WT.

Immunofluorescence images **(A)** and number **(B)** of DA neurons in PPM1/2 (top), and PPL1 (bottom) regions of adult fly brains with indicated genotypes. Green (DA neuron). *n* = 10. Scale bar, 20 μm.

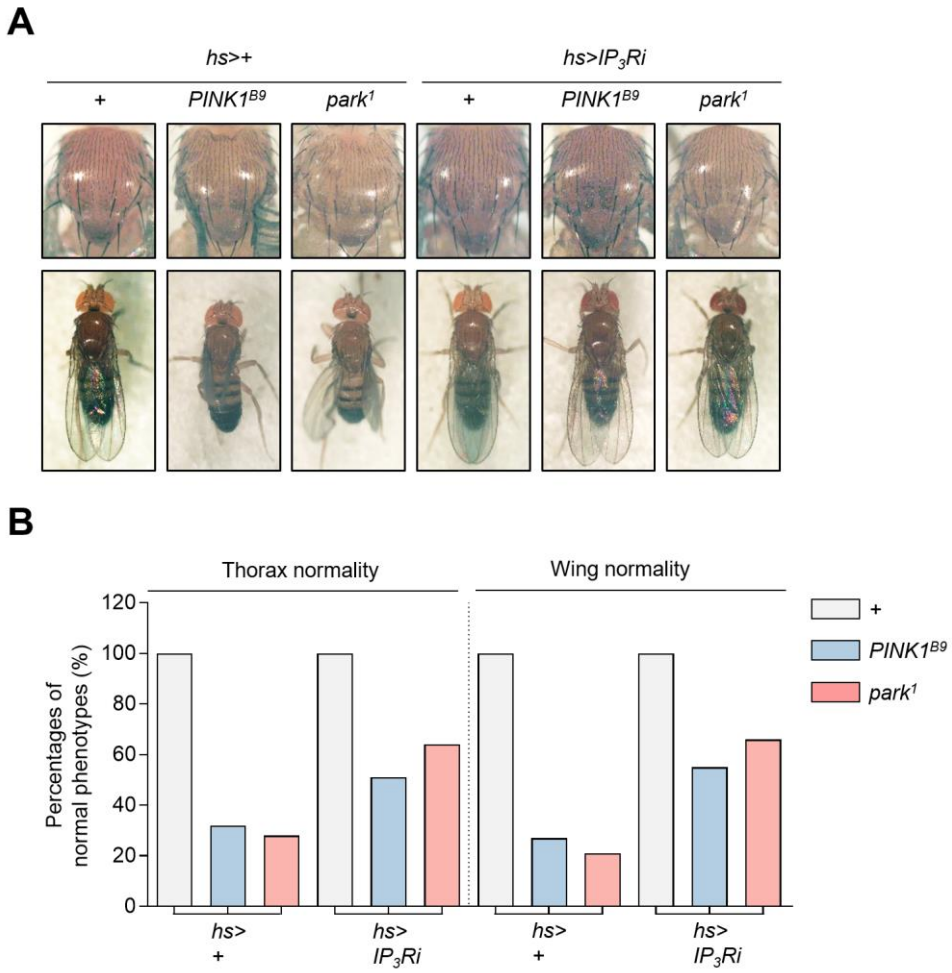

Figure 35. Knockdown of IP$_3$R rescues the abnormal thoracic and wing phenotypes of PINK1 and Parkin null flies.

Images of *Drosophila* thoracic (top panels) and wing posture (bottom panels) phenotypes **(A)** and percentages of the flies having normal phenotypes **(B)**. IP$_3$Ri indicates RNAi knockdown of the *Drosophila* IP$_3$R gene, *itpr*.

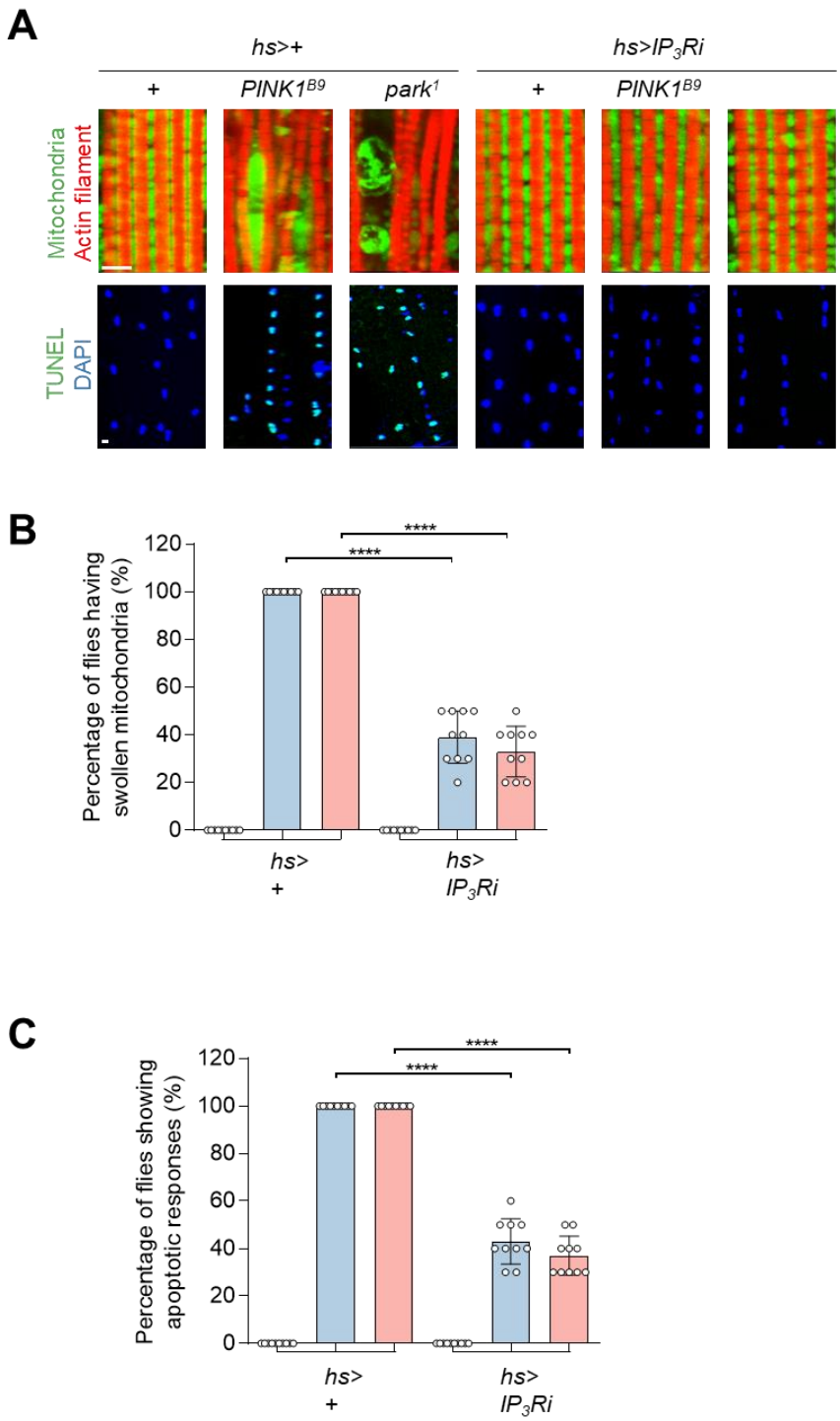
A
hs>+
hs>IP3Ri
+
PINK1B9
park1
+
PINK1B9
Mitochondria
Actin filament
TUNEL
DAPI
B
Percentage of flies having swollen mitochondria (%)
120
100
80
60
40
20
0
****
****
hs>
+
hs>
IP3Ri
C
Percentage of flies showing apoptotic responses (%)
120
100
80
60
40
20
0
****
****
hs>
+
hs>
IP3Ri

Figure 36. Knockdown of IP_3R rescues aberrant mitochondrial morphology and increased apoptosis of PINK1 and Parkin null flies.

Immunofluorescence images **(A)** of the adult flight muscles (top). Green (mitochondria) and red (actin filament). *n* = 10. Scale bar, 5 μm. TUNEL assays of the adult flight muscles (bottom). Green (TUNEL) and blue (DAPI). *n* = 10. Scale bar, 5 μm. Quantification of the percentage of flies having swollen mitochondria. *n* = 10 **(B)**. Quantification of the percentage of flies showing apoptotic responses. *n* = 10 **(C)**. IP_3Ri indicates RNAi knockdown of the *Drosophila* IP_3R gene, *itpr*.

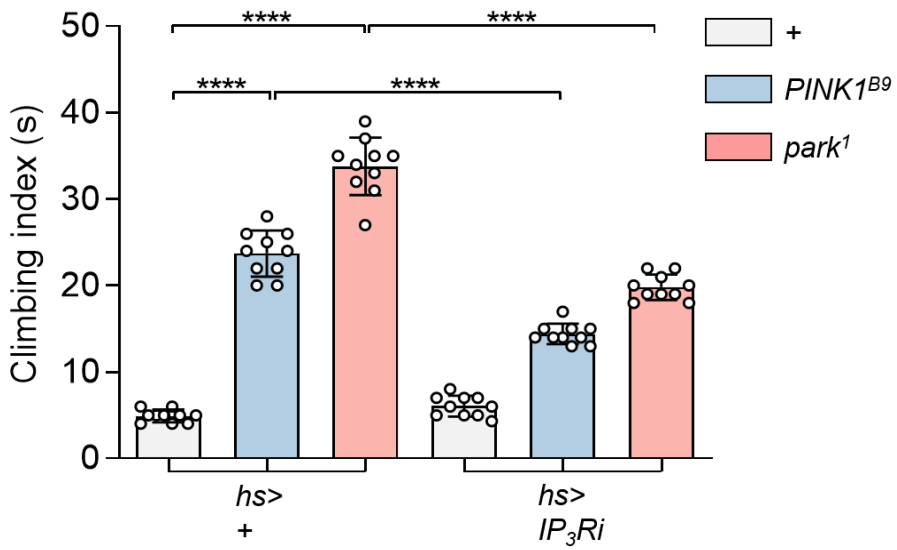

Figure 37. Knockdown of IP$_3$R rescues impaired climbing ability of PINK1 and Parkin null flies.

Measurement of the climbing ability in the adult flies with indicated genotypes. *n* = 10. IP$_3$Ri indicates RNAi knockdown of the *Drosophila* IP$_3$R gene, *itpr*.

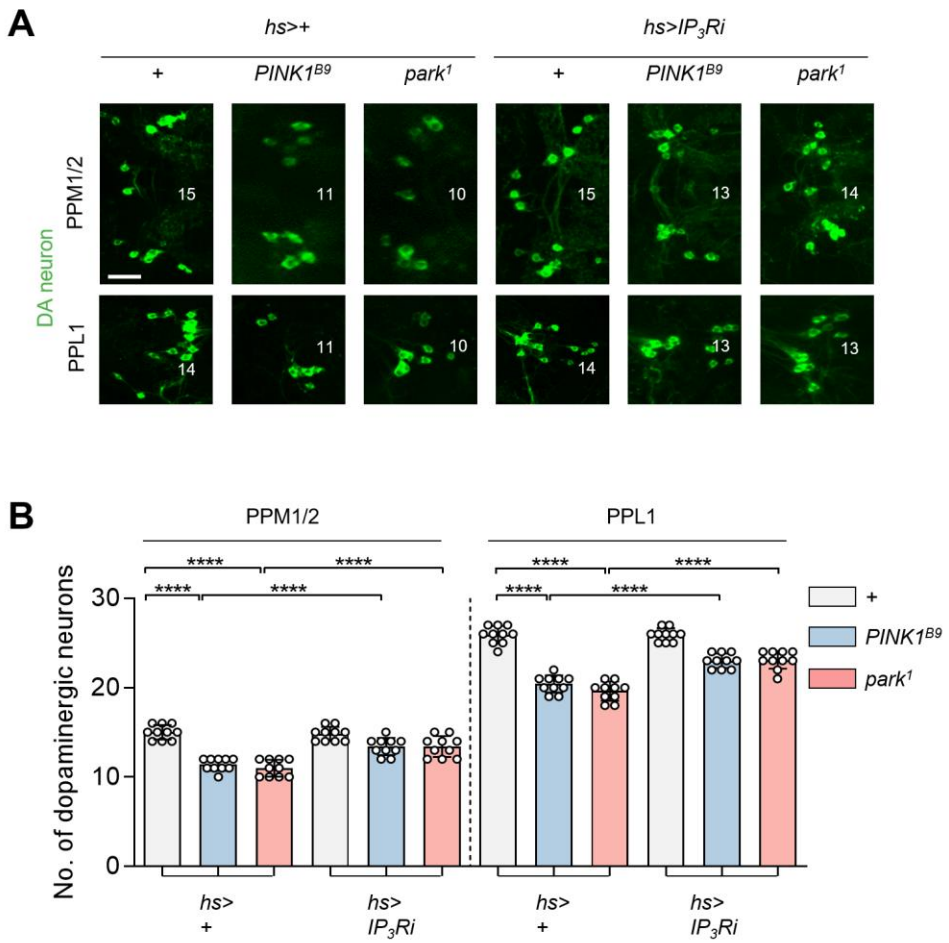

Figure 38. Knockdown of IP$_3$R rescues reduced number of DA neurons of PINK1 and Parkin null flies.

Immunofluorescence images **(A)** and number **(B)** of DA neurons in PPM1/2 (top), and PPL1 (bottom) regions of adult fly brains with indicated genotypes. Green (DA neuron). *n* = 10. Scale bar, 20 μm. IP$_3$Ri indicates RNAi knockdown of the *Drosophila* IP$_3$R gene, *itpr*.

CISD1 regulates IP_3R activity by directly interacting with IP_3R

It was confirmed that CISD regulates the IP_3R activity, and if so, I wondered how it is controlled. It has been previously reported that several proteins directly interact with IP_3R to regulate its activity, such as sigma-1 receptor, B-cell lymphoma-2 (BCL-2), and BRCA1-associated protein 1 (BAP1) (Bonneau et al., 2016; Bononi et al., 2017; Wu and Bowen, 2008). They showed physical interactions between IP_3R and such proteins, and as a result, calcium flux was altered. According to the researchers, these proteins associate in mitochondria-associated membranes (MAMs) and their interactions regulates apoptosis.

So, to see if the CISD1 protein binds to IP_3R activity, I performed co-immunoprecipitation experiments for CISD1 and IP_3R1 proteins. First, through this experiment, I found that bovine IP_3R1 directly interacts with the full length of CISD1 **(Fig. 39)**. Following that, I generated mutant forms of CISD in which each domain was deleted **(Fig. 40)**, and co-immunoprecipitation was performed to determine which part of CISD is required for interaction with IP_3R1. As a result, the D1 construct, which lacks the CDGSH domain, was not able to interact with IP_3R1 **(Fig. 39)**. This suggests that the CDGSH domain of CISD1 is responsible for the interaction between CISD1 and IP_3R1. Next, I generated several mutations in the CDGSH domain to find the key amino acid residue of CISD1 that

interacts with IP_3R1. Through co-ip results using various mutants, I found that the C74A mutant form of CISD1 did not bind to IP_3R1 **(Fig. 41)**. This indicates that cysteine 74 of the CISD1 protein is critical for the CISD1-IP_3R1 interaction.

Since I discovered that cysteine 74 is a key amino acid residue of CISD1 that interacts with IP_3R, I wondered if it affects IP_3R activity. Because previous results have shown that IP_3R activity is reduced in CISD KO MEF **(Fig. 21)**, I overexpressed CISD1 WT and CISD1 C74A in CISD KO MEF cells and measured IP_3R activity. Surprisingly, expression of CISD1 WT, but not the CISD C74A mutant, rescued the decreased IP_3R activity in CISD1 KO MEF cells **(Fig. 42)**. Furthermore, when compared to WT cells, CISD KO MEF cells showed abnormal calcium flux in response to ATP. CISD1 WT expression also improved ER calcium release **(Fig. 43A)** and cytosolic calcium levels **(Fig. 43B)**, whereas CISD1 C74A expression did not. These results suggest that the direct interaction between CISD1 and IP_3R is necessary for maintaining IP_3R activity.

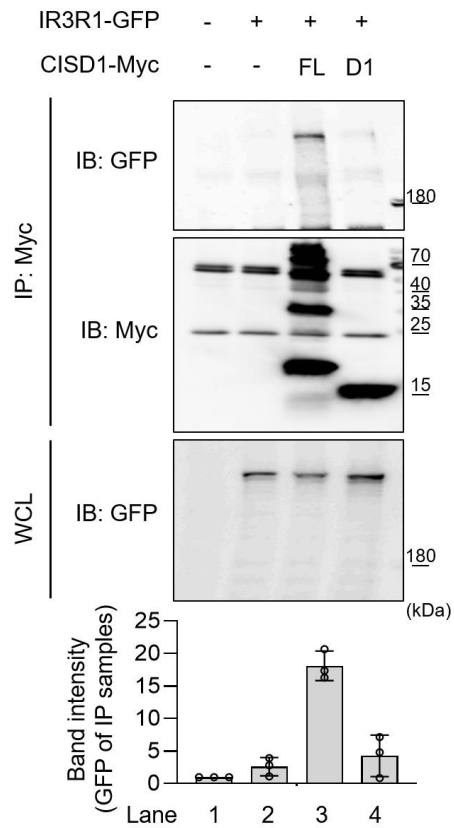

Figure 39. CDGSH domain is necessary for CISD1 to directly bind to IP_3R.

HEK293T cells were transfected as indicated and cell lysates were subjected to anti-Myc immunoprecipitation followed by immunoblot analysis. The D1 construct lacks the CDGSH domain. Three independent experiments were repeated and the band intensity for the interaction between CISD1 and IP_3R1 shown by co-immunoprecipitation experiments was displayed in bar graphs (bottom).

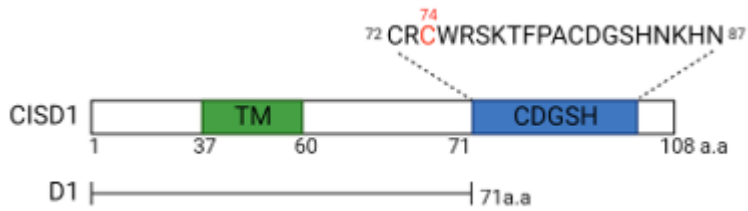

Figure 40. The domain architecture of human CISD1.

The transmembrane domain (TM) and the CDGSH domain are indicated. I generated the D1 construct which lacks the CDGSH domain. Cysteine 74 of CISD1 is marked in red.

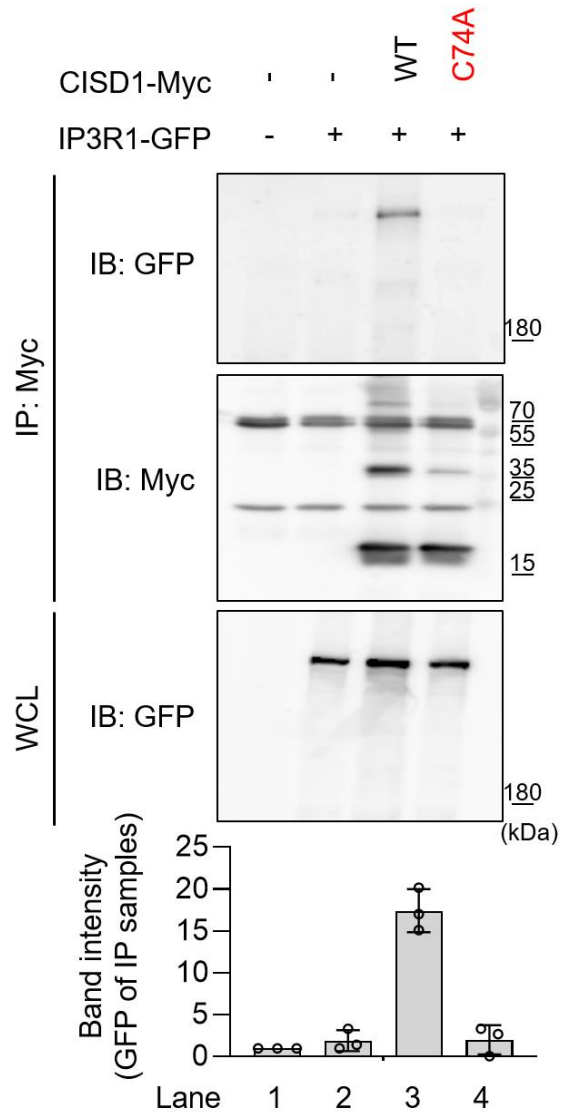

Figure 41. Cysteine 74 is a key amino acid residue of CISD1 that interacts with IP$_3$R.

HEK293T cells were transfected as indicated and cell lysates were subjected

to anti-Myc immunoprecipitation followed by immunoblot analysis. The C74A mutant form of CISD1 is marked in red. Three independent experiments were repeated and the band intensity for the interaction between CISD1 and IP_3R1 shown by co-immunoprecipitation experiments was displayed in bar graphs (bottom).

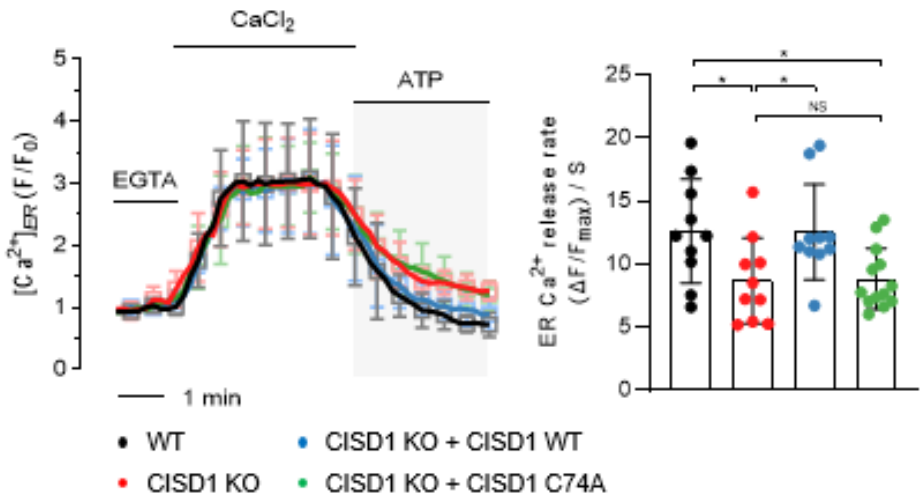

Figure 42. Decreased IP$_3$R activity in CISD1 KO MEF cells is rescued by the expression of CISD1 WT but not by CISD1 C74A mutant.

Measurement of the IP$_3$R activity of WT (black) and CISD1 KO (red) cells when transfected with exogenous CISD WT (blue) and CISD C74A mutant (green). The bar graphs indicate the maximum rate of calcium release during ATP treatment. $n > 50$ cells.

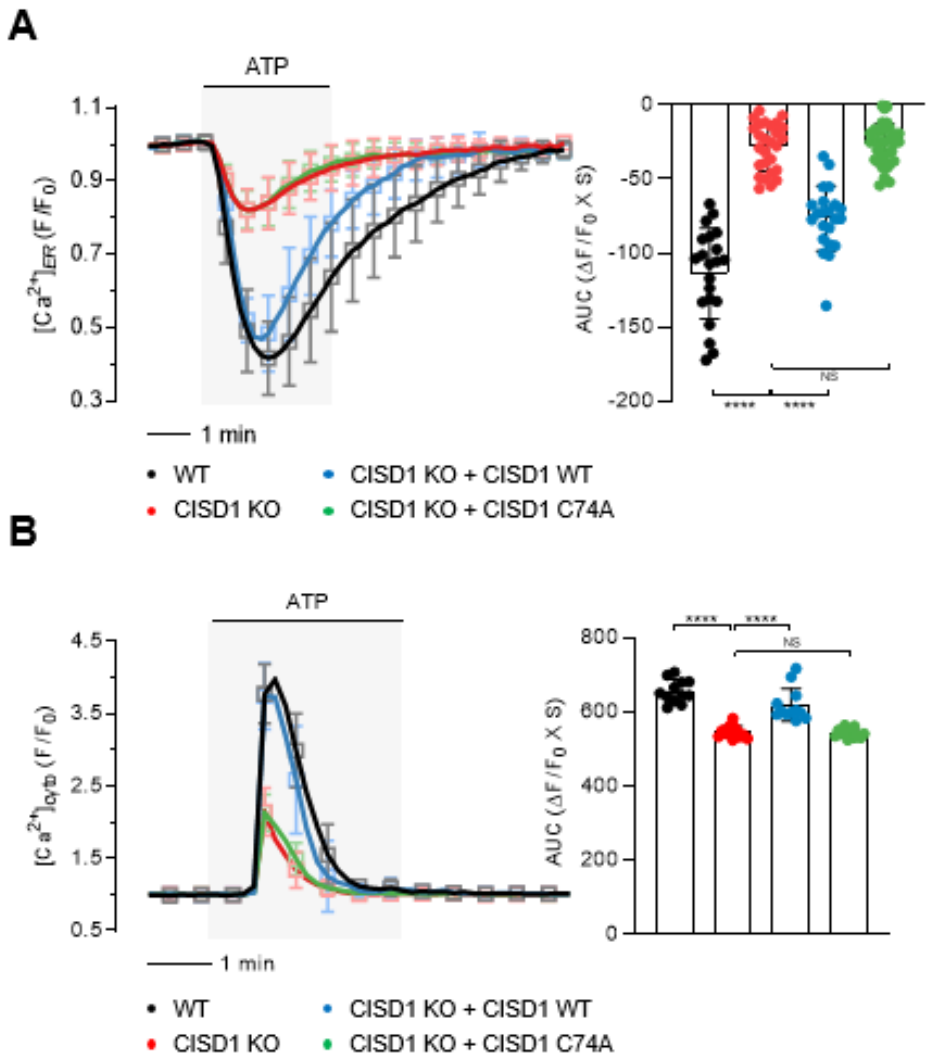

Figure 43. CISD1 C74 is critical for the interaction of CISD1 and IP$_3$R.

Measurement of ER **(A)** and cytosolic **(B)** calcium modulation in WT (black) and CISD1 KO (red) MEF cells. Similar experiments were also

conducted for CISD1 KO MEF cells expressing exogenous CISD1 WT (blue) or C74A mutant (green). 100 μM ATP was delivered to initiate IP_3R-mediated calcium release. The right side bar graphs indicate the quantification of the normalized calcium traces using AUC of calcium release during ATP treatment. $n > 100$ cells.

Pioglitazone alters the interaction between IP_3R and CISD1

Previous research discovered a link between the mitochondrial protein CISD1 and the anti-diabetic drug Thiazolidinedione (TZD), which is used to treat Type-2 diabetes (T2D). Pioglitazone, one of the antidiabetic drug, has also been reported to bind to the CISD proteins and inhibit the [2Fe-2S] cluster transfer upon binding (Colca *et al.*, 2004; Tamir et al., 2013). Therefore, if pioglitazone had any effects on the previously discovered interaction between CISD1 and IP_3R, I assumed that pioglitazone could also affect the PD-related phenotypes and conducted the necessary experiments. First, to see if pioglitazone alters the interaction between IP_3R and the CISD proteins, I performed co-immunoprecipitation experiments with pioglitazone treatment on CISD1 and IP_3R1. In order to confirm the effect of pioglitazone with certainty, the degree of change was confirmed as the concentration was increased. Interestingly, the addition of pioglitazone reduced the binding between IP_3R1 and CISD1 in a dose-dependent manner **(Fig. 44)**. I thought that if the binding of IP_3R1 and CISD1 was reduced, the activity of IP_3R would be reduced as well, so I measured how IP_3R activity changes when pioglitazone is treated. Pioglitazone was added to all of the solutions used in this experiment and allowed to flow to validate the effects of the pioglitazone. As a result, I found that pioglitazone treatment reduced IP_3R activity **(Fig. 45)**.

Then, I looked into how pioglitazone affects the abnormal calcium flux in PINK1 and Parkin KO MEF cells. I measured the changes in calcium flux in response to ATP in pioglitazone in a dose-dependent manner. As expected, the increased ER calcium release in PINK1 and Parkin KO MEF cells was rescued with pioglitazone treatment. When pioglitazone dosage was increased in PINK1 and Parkin KO MEF cells, ER calcium release was reduced even further **(Fig. 46A and 47A)**. Pioglitazone also reduced the increased cytosolic calcium levels in PINK1 and Parkin KO cells in a dose-dependent manner **(Fig. 46B and 47B)**. The effect of pioglitazone on calcium regulation was confirmed in mammalian cells, and then it was investigated in flies to see if the same effect happened. Consistent with the results in mammalian cells, PINK1 and Parkin null flies showed increased ER calcium release and cytosolic calcium levels when compared to WT flies, which were rescued by pioglitazone treatment **(Fig. 48 and 49)**. Once again, this highlights the importance of CISD1 as a mediator between PINK1 and Parkin in controlling IP_3R activity.

Pioglitazone rescues the PD-related phenotypes of PINK1 or Parkin deficiency

Since it was confirmed that pioglitazone rescued the impaired calcium flux by regulating IP_3R activity in both mammalian cells and *Drosophila*, finally, I wondered whether pioglitazone could rescue the PD-related phenotypes in PINK1 and Parkin null flies. So, I conducted the experiments to see if feeding pioglitazone to PINK1 and Parkin null flies would rescue PD-related phenotypes. After dissolving pioglitazone in standard *Drosophila* medium to make the final concentration 1 mM, WT flies and PINK1 and Parkin null flies were raised to eat from birth, and their PD-related phenotypes were compared. According to the previous experiments, when the standard *Drosophila* medium was fed to the PINK1 and Parkin null flies, the PD-related phenotypes could be seen in PINK1 and Parkin null flies compared to WT flies. Surprisingly, pioglitazone feeding alleviated the PD-related phenotypes found in PINK1 and Parkin null flies, such as crushed thoraces, abnormal wing postures, increased apoptotic signals in thoraces, decreased climbing ability, and a reduced number of DA neurons **(Fig. 50, 51, 52, and 53)**. As a result, it can be considered that the calcium homeostasis of the impaired PINK1 and Parkin null flies was normalized by eating pioglitazone, and the PD-related phenotypes were also rescued. Taken together, my data suggest that pioglitazone is an effective

therapeutic to treat the PD pathogenesis caused by PINK1 and Parkin mutations.

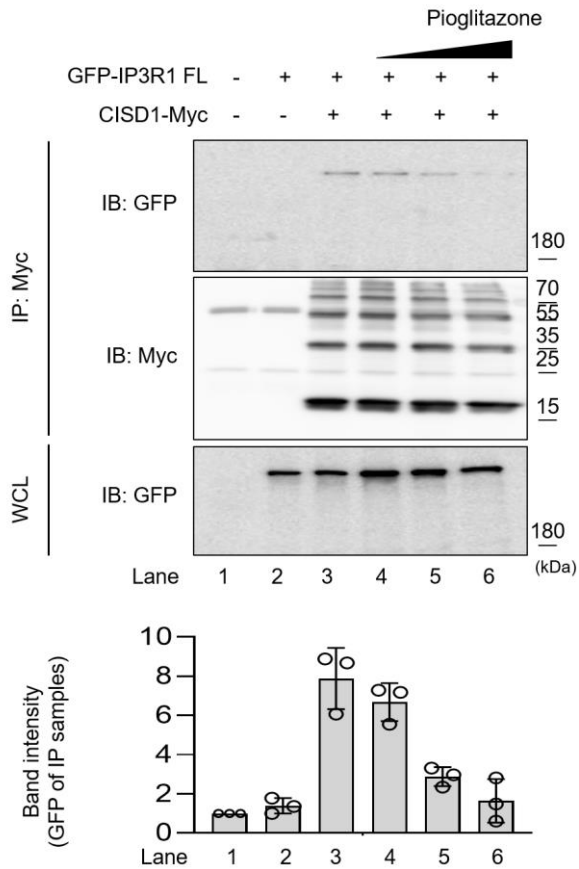

Figure 44. Pioglitazone inhibits the binding of IP_3R and CISD1.

HEK293T cells were transfected as indicated and treated with pioglitazone. Anti-Myc immunoprecipitates were analyzed for the association of IP_3R1 using immunoblot analyses. In a dose-dependent manner, pioglitazone reduced the binding of IP_3R and. Three independent experiments were done to quantitate the interaction between CISD1 and IP_3R1 (bar graphs in bottom).

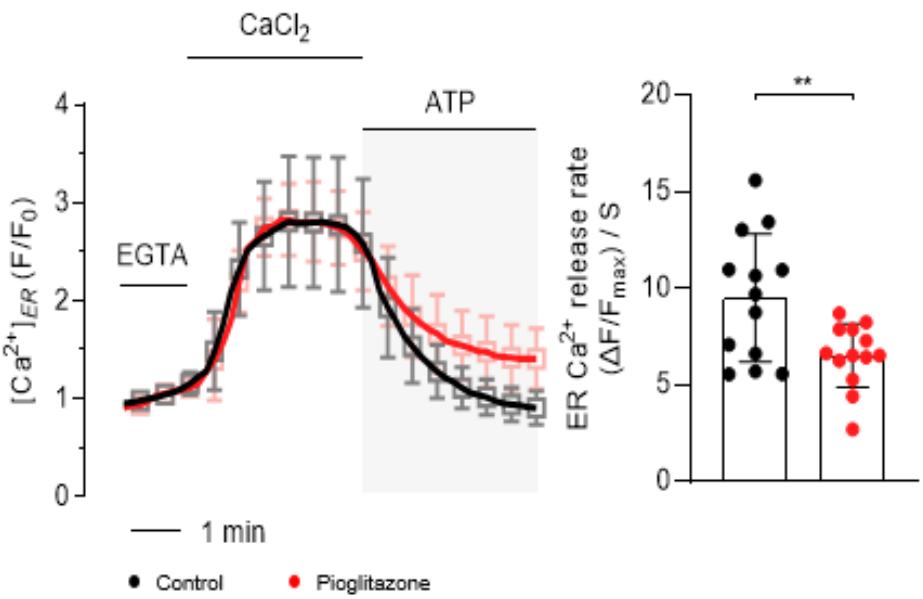

Figure 45. Pioglitazone treatment reduces IP_3R activity.

Measurement of ER calcium release through IP_3R. Control (black) and Pioglitazone treatment (red) in HEK293 cells. The bar graphs indicate the maximum rate of calcium release during ATP treatment. $n > 50$ cells.

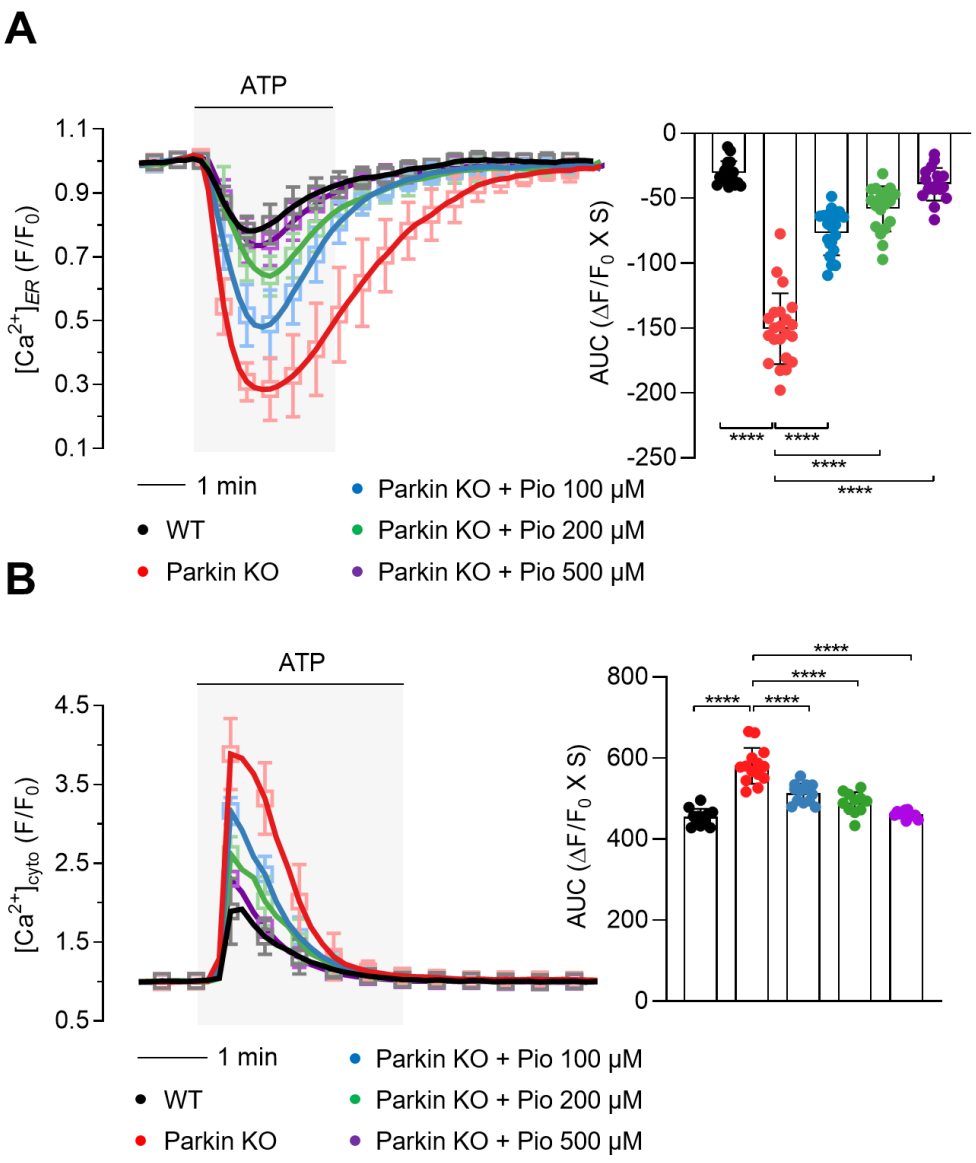

Figure 46. Pioglitazone restores the impaired calcium flux in Parkin KO cells.

Measurement of ER **(A)** and cytosol **(B)** calcium modulations in WT (black) and Parkin KO (red) cells when treated with indicated concentrations of pioglitazone (blue, green, and purple). The right side bar graphs indicate the area-under-the-curve (AUC) of calcium release during ATP treatment, which was used to quantify the normalized calcium traces. $n > 80$ cells.

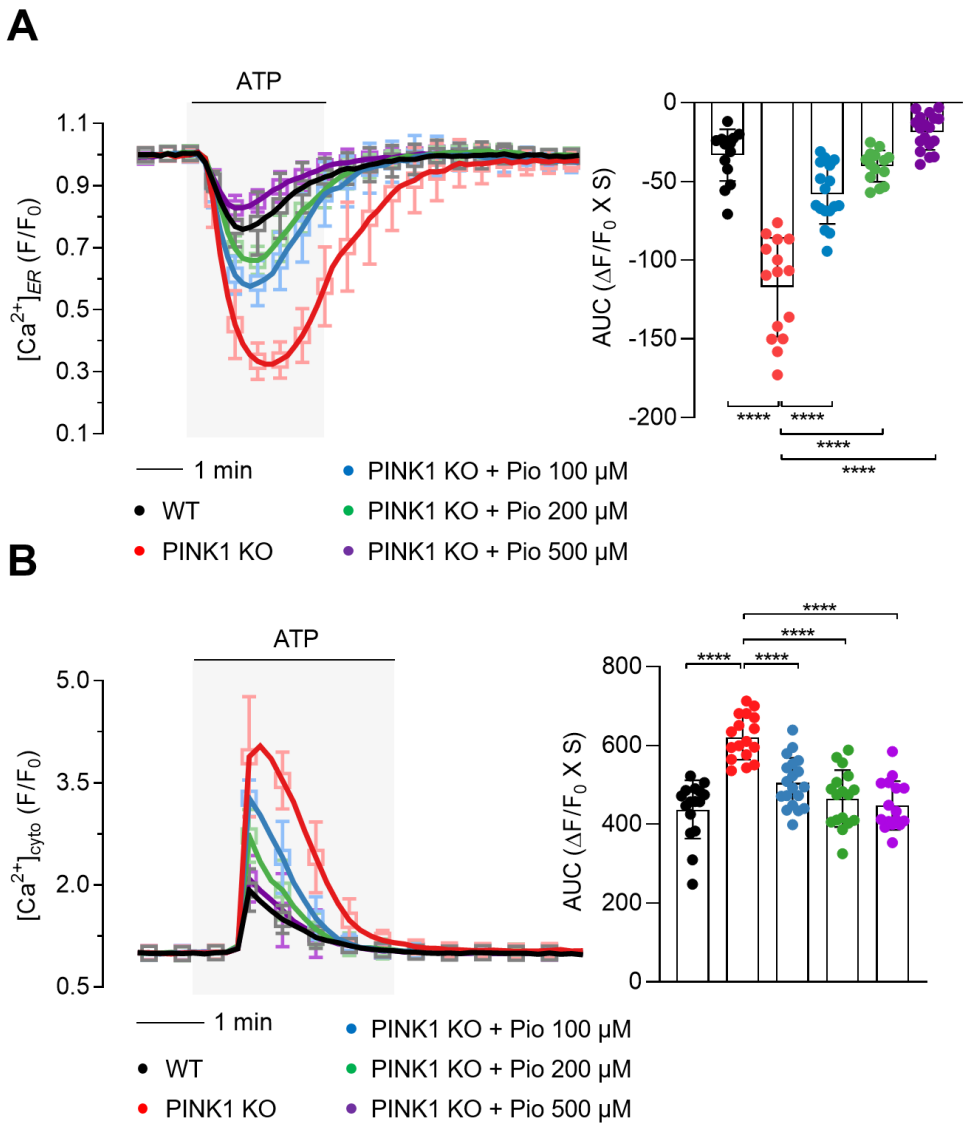

Figure 47. Pioglitazone restores the impaired calcium flux in PINK1 KO cells.

Measurement of ER **(A)** and cytosol **(B)** calcium modulations in WT (black)

and PINK1 KO (red) cells when treated with indicated concentrations of pioglitazone (blue, green, and purple). The right side bar graphs indicate the area-under-the-curve (AUC) of calcium release during ATP treatment, which was used to quantify the normalized calcium traces. $n > 100$ cells.

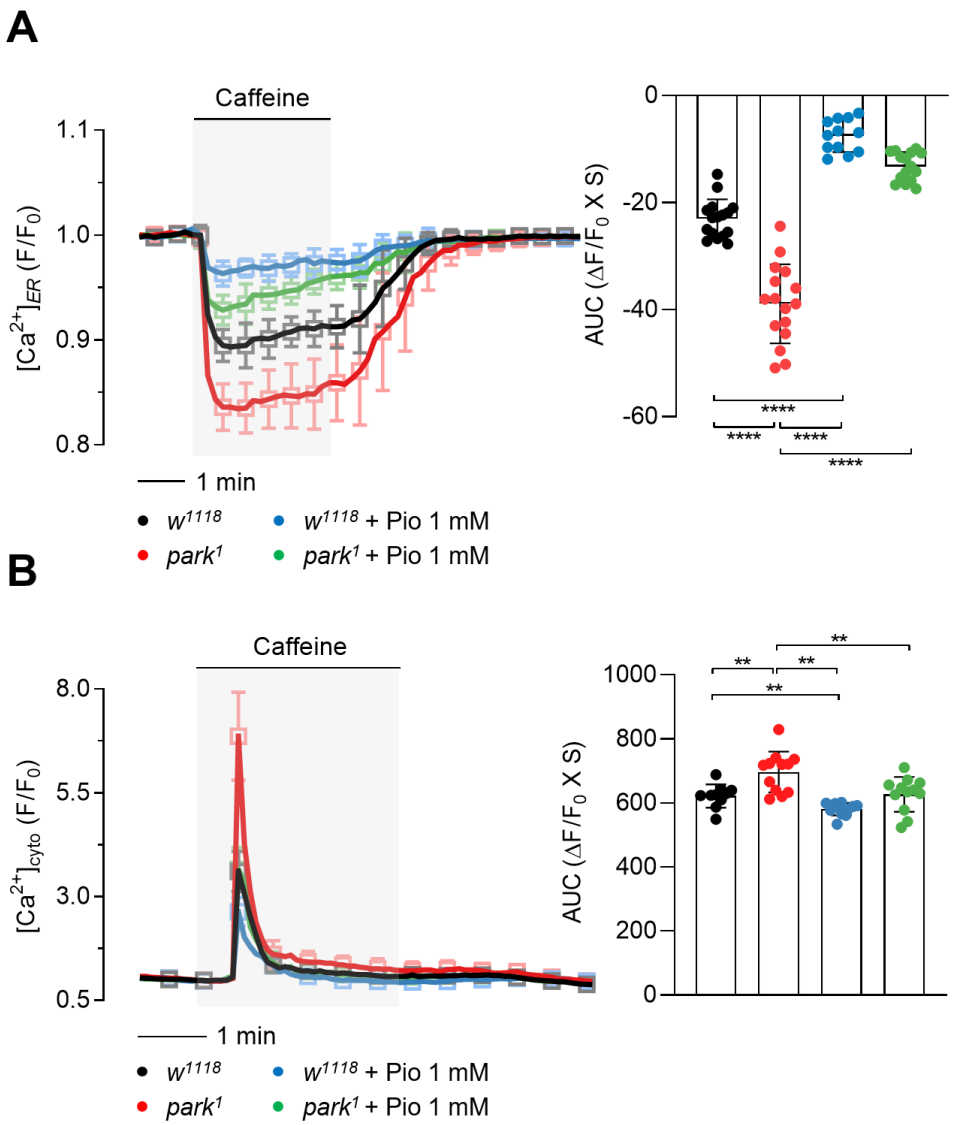

Figure 48. Pioglitazone restores the impaired calcium flux in Parkin null flies.

Measurement of ER **(A)** and cytosol **(B)** calcium modulations in WT (w^{1118}, black) and Parkin null mutant flies ($park^{1}$, red) when treated without or with

1 mM pioglitazone (blue and green). The right side bar graphs indicate the quantification of the normalized calcium traces using AUC of calcium release during caffeine treatment. $n > 10$ flies.

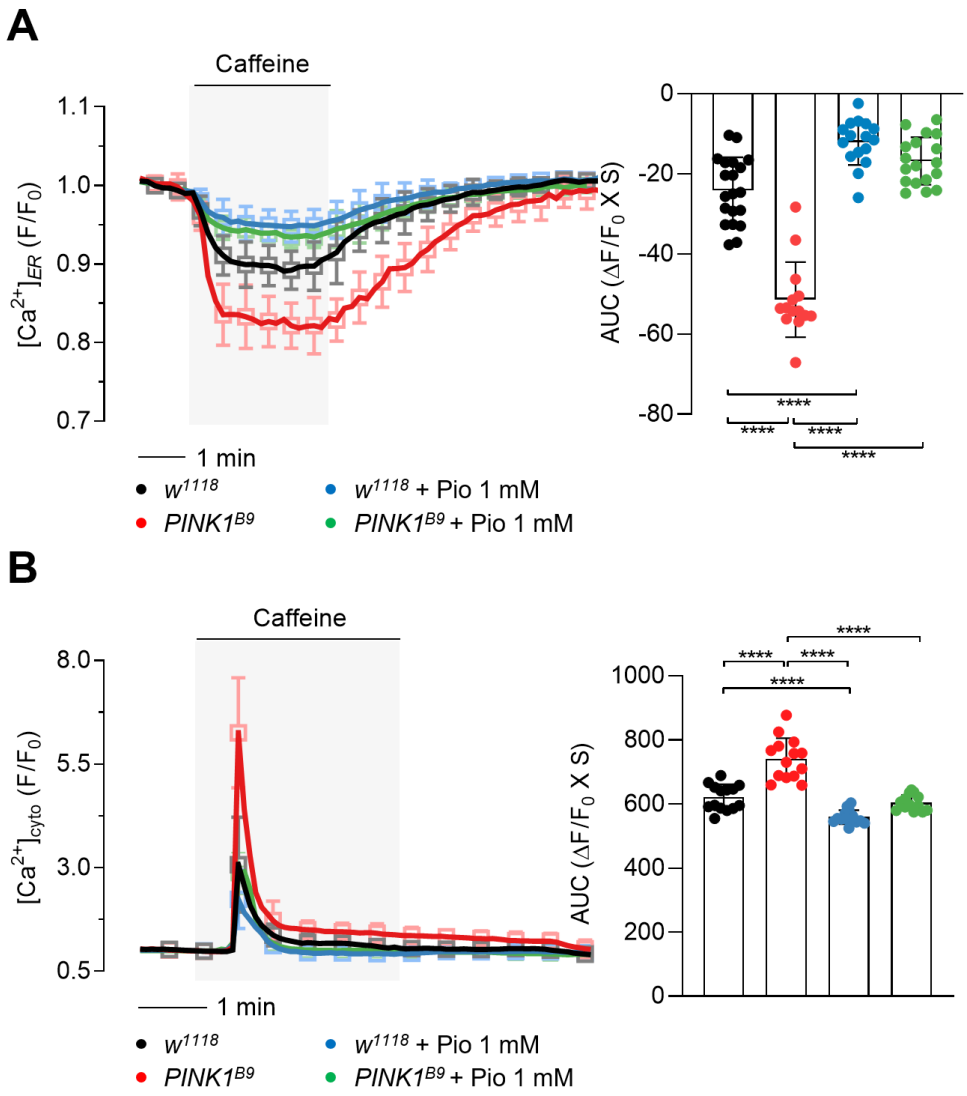

Figure 49. Pioglitazone restores the impaired calcium flux in PINK1 null flies.

Measurement of ER **(A)** and cytosol **(B)** calcium modulations in WT (w^{1118}, black) and PINK1 null mutant flies ($PINK1^{B9}$, red) when treated without or

with 1 mM pioglitazone (blue and green). The right side bar graphs indicate the quantification of the normalized calcium traces using AUC of calcium release during caffeine treatment. $n > 13$ flies.

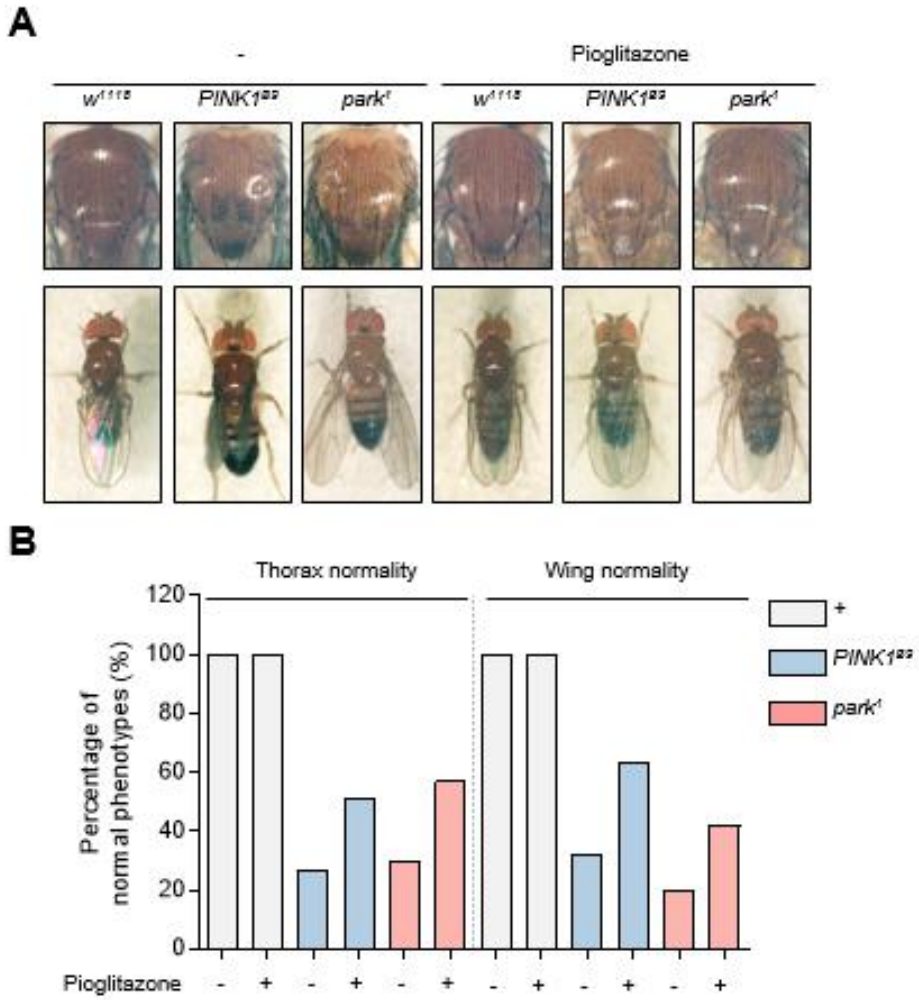

Figure 50. Pioglitazone rescues the abnormal thoracic and wing phenotypes of PINK1 and Parkin null flies.

Images of *Drosophila* thoracic (top panels) and wing posture (bottom panels) phenotypes **(A)** and percentages of the flies having normal phenotypes **(B)**. The flies in right panels (Pioglitazone) were fed with 1 mM pioglitazone (+) and compared with controls (-).

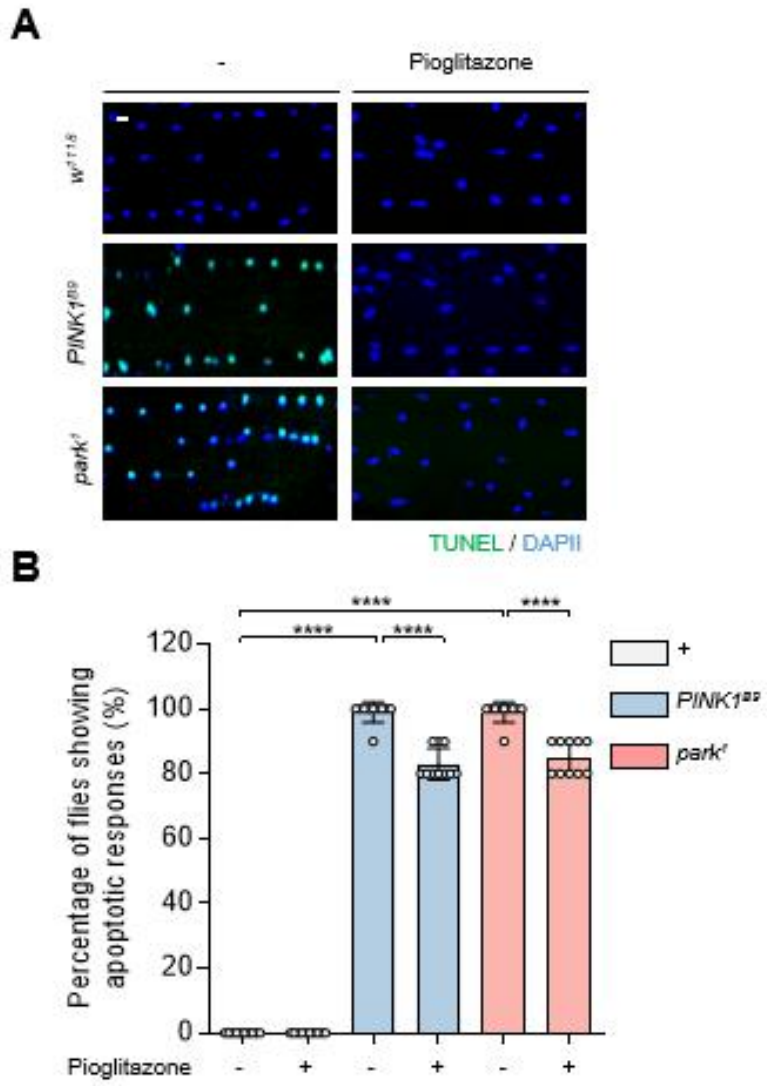

Figure 51. Pioglitazone rescues the increased apoptosis of PINK1 and Parkin null flies.

Images **(A)** and quantification **(B)** of the TUNEL assays of the adult flight muscles with indicated genotypes. + flies were fed with 1 mM pioglitazone. Green (TUNEL) and blue (DAPI). *n* = 10. Scale bar, 5 μm.

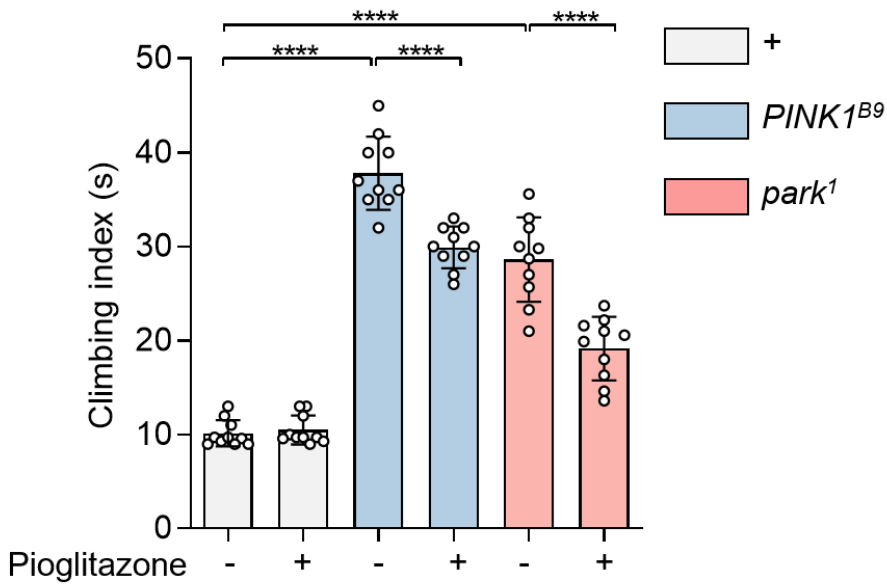

Figure 52. Pioglitazone rescues the impaired climbing ability of PINK1 and Parkin null flies.

Measurement of the climbing ability in the adult flies with indicated genotypes. + flies were fed with 1 mM pioglitazone. *n* = 10.

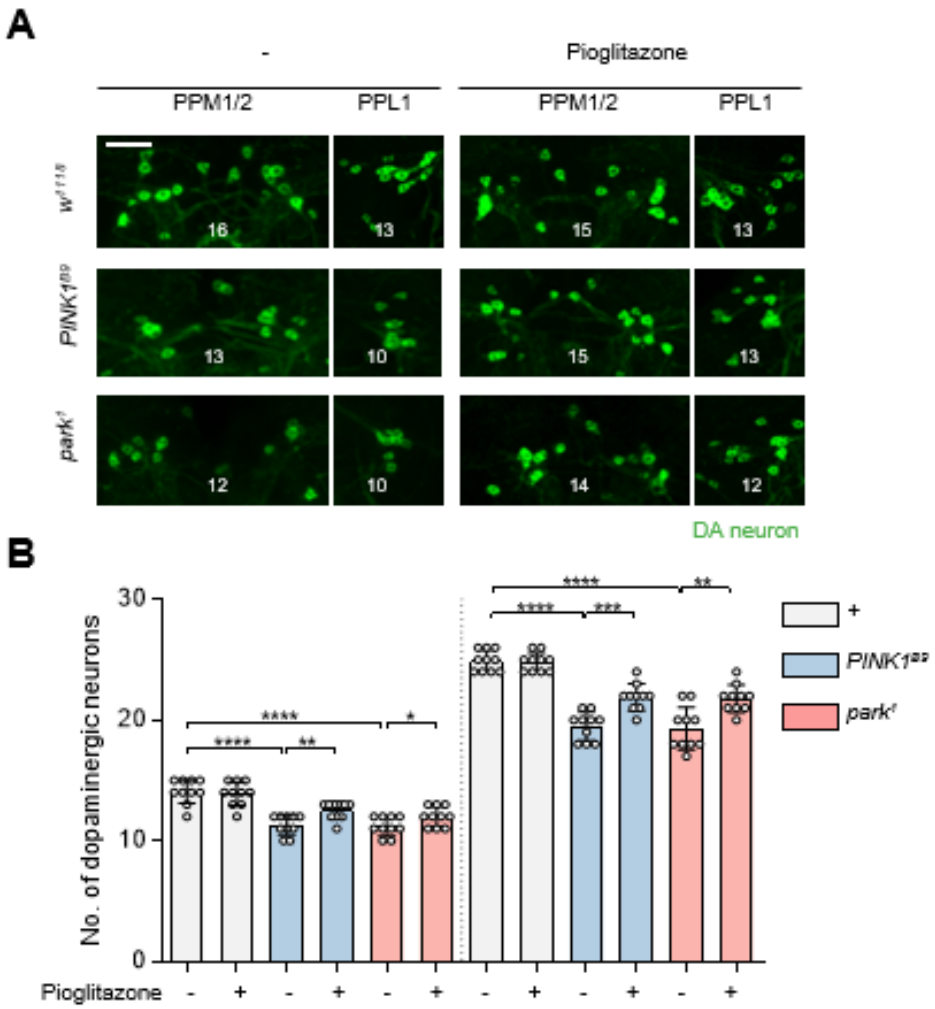

Figure 53. Pioglitazone rescues the reduced number of DA neurons of PINK1 and Parkin null flies.

Immunofluorescence images **(A)** and number **(B)** of DA neurons in PPM1/2 (top), and PPL1 (bottom) regions of adult fly brains with indicated genotypes. + flies were fed with 1 mM pioglitazone. Green (DA neuron). *n* = 10. Scale bar, 20 μm.

Discussions

PINK1 and Parkin regulates IP_3R-mediated ER calcium release through CISD1

My study provides a strong foundation for understanding the fundamental relationship between PINK1 or Parkin deficiency-induced PD development and intracellular calcium abnormalities. In summary, I found that calcium homeostasis was abnormal, such as increased ER calcium release and cytosolic calcium levels in PINK1 and Parkin KO mammalian cells and *Drosophila*. And it was discovered that this is a phenomenon caused by an increase in IP_3R activity. Next, through the genetic screen, I found that CISD1, a substrate of Parkin, regulates ER calcium release by direct interaction with IP_3R. These findings suggest that PINK1, Parkin, CISD1, and IP_3R all have a role in maintaining ER and cytosolic calcium homeostasis through the same critical pathway in cells **(Fig. 54A)**. By regulating IP_3R activity, CISD knockdown rescued the abnormal ER calcium release, resulting in the rescue of PD-related phenotypes in PINK1 and Parkin null flies. This indicates that restoring intracellular calcium homeostasis can alleviate PD pathogenesis. The same as the knockdown of CISD, pioglitazone, an anti-diabetic drug, also reduced ER calcium release

by blocking direct interaction between CISD and IP_3R, restoring the PD-related phenotypes induced by PINK1 and Parkin loss in mammalian cells and *Drosophila* **(Fig. 54B)**.

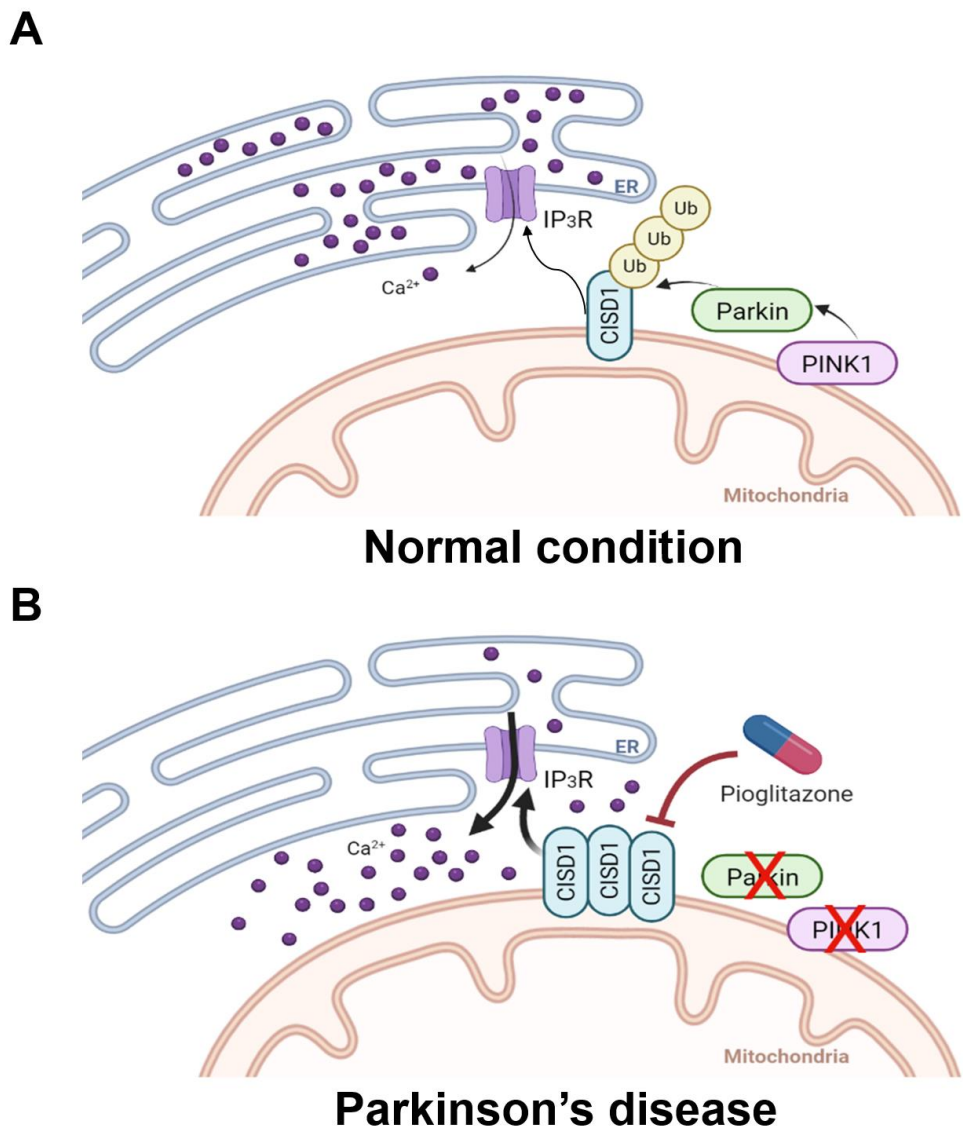

Figure 54. ER and cytosolic calcium homeostasis are regulated by the PINK1-Parkin pathway.

Under normal circumstances **(A)**, PINK1 activates the Parkin E3 ligase, causing CISD1 on the outer mitochondrial membrane to be ubiquitinated

and degraded. Parkin inhibits CISD1, which typically activates the ER calcium channel IP_3R, resulting in decreased IP_3R activity and cytosolic calcium levels. Through this system, the ER and cytosolic calcium homeostasis is properly maintained to keep the normal condition. However, under Parkinson's disease conditions **(B)** caused by the PINK1 or Parkin loss, CISD1 is not ubiquitinated by Parkin, and its protein level is increased. Thus, increased CISD1 protein levels result in increased IP_3R activity and cytosolic calcium levels, causing calcium homeostasis to be disrupted. Disrupted calcium homeostasis leads to PD-related phenotypes. The treatment of pioglitazone, a CISD1 inhibitor, suppresses IP_3R activity and rescues calcium homeostasis, thereby rescuing the PD phenotypes caused by PINK1 and Parkin deficient. Image was generated from Biorender.

The significance of ER calcium

The ER is the main calcium storing organelle in the cells. Calcium released from the ER is important for cell signaling and also serves as a protein quality control system in the ER lumen. Misfolded proteins, such as α-synuclein, produce a reduction in ER luminal calcium, which causes ER stress and triggers the unfolded protein response. Despite the fact that this is a normal physiological response to stress, chronic ER system overload, as seen in PD, can lead to cell death due to severe problems with cytosolic calcium homeostasis, protein biosynthesis, calcium-mediated signaling pathways, and other organelle functions that rely heavily on ER contacts.

There are additional experiments that need to be done in the future to explain the importance of intracellular calcium homeostasis. I only measured calcium changes in the ER and cytosol during ATP treatment. However, I believe that measuring basal calcium levels when ATP is not stimulated is a necessary additional experiment. I plan to investigate whether ER calcium is low and cytosolic calcium is high in PINK1 and Parkin KO even in the basal situation without ATP stimulation. In addition, the protein levels of the downstream of the calcium-mediated signaling pathway must be checked to determine whether the signaling pathway has been altered. According to the above findings, PINK1 and Parkin KO significantly increased ER calcium release compared to WT, and thus

cytosolic calcium. Therefore, it is thought that CaMKII, downstream of calcium signaling, will be highly activated due to the increase of cytosolic calcium in PINK1 and Parkin KO. If I measure the protein levels of phospho-CaMKII, a marker of CaMKII activation, I will be able to confirm whether calcium signaling pathway is actually altered in PINK1 and Parkin KO. And if I can confirm whether these changes are restored with knockdown of IP_3R and CISD1, I'll be able to support my results.

Calcium regulation of PD-related genes

Interestingly, certain PD-related genes encode proteins that help to deplete calcium reserves in the ER. In the European population, the gene BST1 (Bone marrow stromal cell antigen-1) is associated with sporadic PD. BST1 is an adenosine diphosphate ribose (ADP) cyclase that generates cyclic ADP ribose (cADPR), a strong and ubiquitous calcium mobilizer, to regulate calcium release from the ER via the ryanodine receptors (RyR). Phospholipase A2G6 (PLA2G6) provides an additional link between ER calcium homeostasis and PD. Autosomal recessive mutations in PLA2G6 lead to early-onset parkinsonism. PLA2G6 is a plasma membrane-associated calcium-dependent phospholipase A2 enzyme. It interacts with the ER- calcium sensor stromal interaction molecule 1 (STIM1) and stimulates refilling of the intracellular calcium stores by activating calcium channels at the plasma membrane, it is called store-operated calcium entry (SOCE). The reduction of PLA2G6 function hampers SOCE, resulting in a decrease in the proper calcium refilling of the ER. In animal models, disrupting SOCE causes autophagy, gradual loss of dopaminergic (DA) neurons in the SNc, and age-dependent L-3,4-dihydroxyphenylalanine (L-DOPA)-sensitive motor impairment. In animal models, disrupting SOCE causes autophagy, gradual loss of dopaminergic (DA) neurons in the SNc, and age-dependent L-3,4-dihydroxyphenylalanine (L-DOPA)-sensitive

motor impairment. Overexpression of a dominant-negative form of the SOCE channel in the *Drosophila* brain, Orai1, reduces expression of both tyrosine hydroxylase (TH) and the dopamine transporter (DAT), indicating a function for SOCE in the normal physiology of DA neurons in the SNc. These findings suggest that SOCE is critical for maintaining appropriate dopamine levels in the brain, and that abnormalities may result in PD-like disease. According to my reported results, the ER-mitochondria contact site is strengthened in DA neurons of PINK1 null flies, and the mitochondrial calcium level is enhanced, resulting in mitochondrial enlargement and neuronal death. The PINK1 mutant phenotypes were rescued by inhibiting components of the ER-mitochondria interaction sites, or by pharmacological manipulation using the 2APB, an IP_3R1 inhibitor. I discovered that modulating ER calcium prevented PD pathogenesis caused by the deletion of PINK1 or Parkin, implying that the CISD1-mediated IP_3R activity regulation mechanism is related to PD pathogenesis. These findings suggested that inhibiting IP_3R could be a potential therapeutic strategy for Parkinson's disease pathogenesis.

Importance of CISD1 and the PINK1-Parkin pathway in MAM maintenance

Through physical contact sites, such as the ER-mitochondria linkages known as mitochondria-associated membranes (MAMs), defects in ER calcium homeostasis can have severe impacts on other organelles (Csordás et al., 2006; Paillusson et al., 2016; Raffaello et al., 2016a; Rizzuto et al., 1998; Rowland and Voeltz, 2012; Xu et al., 2020). The mitochondrial calcium uniporter (MCU) complex in the inner mitochondrial membrane and IP_3R on the ER membrane are abundant in MAMs. MCU and IP_3R are linked by Grp75, a glucose-regulated protein that connects IP_3R to the voltage-dependent anion channel type 1 (VDAC1) on the outer mitochondrial membrane, allowing calcium exchange between the ER and mitochondria (Szabadkai *et al.*, 2006). These connections allow for calcium exchange between ER and mitochondria, and tight regulation of mitochondrial luminal calcium concentration. Mitochondrial luminal calcium is essential for the Krebs cycle and for driving the electron transport chain through complexes III and V. Both biochemical processes are required to keep the mitochondrial membrane potential and ATP levels stable. Furthermore, PINK1 and Parkin null mammalian cells or *Drosophila* showed increased mitochondrial calcium levels, and increased mitochondrial calcium uptake resulted in enhanced apoptosis. Thus, tight

regulation of mitochondrial luminal calcium concentration via MAM is critical. Interestingly, my previous research has shown that inhibiting MCU or VDAC1 partially rescues the PD phenotypes of PINK1 and Parkin deletion flies due to reducing mitochondrial calcium uptake, implying that regulating MAMs may alleviate PD pathogenesis (Ham Su et al., 2020). Furthermore, my results showed that CISD1 binds to and regulates IP_3R activity directly, and that CISD1 is found in MAMs (Kwak *et al.*, 2020). CISD1 is also found on the outer membrane of mitochondria because it has a transmembrane domain at the N terminus, and its structure allows the C terminus to be extended into the cytosol **(Fig. 4)**. IP_3R extends to the cytosol while acting as a channel in the ER membrane, and IP_3R is also found in MAM (Ye et al., 2021). Therefore, structurally, I believe it is possible to bind CISD1 and IP_3R in MAM **(Fig. 55)**. In summary, these findings suggest that CISD1 and the PINK1-Parkin pathway are important for the formation and maintenance of MAM structure, as well as ER-mitochondrial calcium transduction, which is necessary for mitochondrial physiology and pathologic phenotypes.

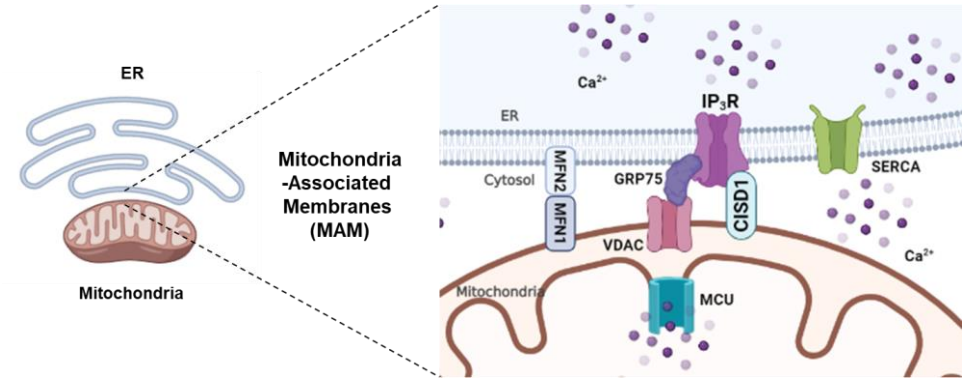

Figure 55. In MAM, CISD1 and IP$_3$R are expected to bind.

Image was generated from Biorender.

Potential of pioglitazone as a therapeutic agent for PD

Despite the fact that calcium regulation is important in the pathogenesis of Parkinson's disease, none of the calcium-regulated medications tested in prior trials had proven to be effective in alleviating symptoms in PD patients (Pioglitazone in early Parkinson's disease: a phase 2, multicentre, double-blind, randomised trial, 2015; Isradipine Versus Placebo in Early Parkinson Disease: A Randomized Trial, 2020; Brauer et al., 2020; Swart and Hurley, 2016; Wu et al., 2018). My study proposed that pioglitazone, a thiazolidinedione (TZD) and anti-diabetic drug, may help to slow the progression of Parkinson's disease. Pioglitazone has been shown to protect against not only diabetes but also Parkinson's disease in prior clinical tests. Other researches, on the other hand, have found that pioglitazone has no effect on PD pathogenesis. The role of pioglitazone in the treatment of Parkinson's disease is still debated (Pioglitazone in early Parkinson's disease: a phase 2, multicentre, double-blind, randomised trial, 2015; Brauer *et al.*, 2020; Chang et al., 2021; Wu *et al.*, 2018). However, my findings clearly indicated that feeding pioglitazone to flies rescued PD-related phenotypes caused by PINk1 or Parkin deficiency, such as impaired climbing ability and dopaminergic neuron loss. Furthermore, pioglitazone treatment reduces ER calcium release and cytosolic calcium levels in PINK1 and Parkin KO mammalian cells and *Drosophila*. These results indicate that

pioglitazone can protect against Parkinson's disease pathogenesis caused by calcium dysregulation in intracellular organelles. This suggests that future clinical trials of pioglitazone and its analogs should focus on PD patients with PINK1 or Parkin mutations.

However, more experiments are still needed to explain the exact mechanism and target of the damaged calcium recovery effect of pioglitazone. It is known that pioglitazone activates peroxisome proliferator activated receptor-γ (PPAR-γ) as described in the introduction. Therefore, it is necessary to check whether the effect of pioglitazone is due to the change of the membrane potential by the activated PPAR-γ or whether it affects the binding to CISD1 and IP_3R as in my experiment. Three experiments are possible to determine the calcium regulation mechanism and target of pioglitazone. First, I plan to see whether the calcium rescuing effect of pioglitazone still exists when E75 and E78, the PPAR-γ homologs of *Drosophila*, are knocked down. Second, it should be checked whether the effect of pioglitazone does not appear in CISD1 KO. Third, when the amount of CISD1 expression in cells is increased by concentration, an experiment can be performed to confirm whether the effect of pioglitazone is also increased.

Furthermore, it is necessary to determine whether the membrane potential is affected by PPAR-γ by measuring the difference in membrane

potential before and after pioglitazone treatment. In my experiment, I discovered that the binding of CISD1 and IP_3R influenced IP_3R activity **(Fig. 42)**. Also, as the concentration of pioglitazone increased, the binding of CISD1 and IP_3R decreased, and the activity of IP_3R decreased accordingly **(Fig. 44)**. Therefore, if there is no effect on the membrane potential at the concentration where the calcium change of pioglitazone was confirmed, it can be assumed that pioglitazone changed the calcium homeostasis by affecting the binding of CISD1 and IP_3R.

Part II

Fumarate modulates intracellular calcium homeostasis by inhibiting SERCA

Results

Identification of a novel factor regulating mitochondrial calcium flux using a genetic screen

In previous research, I confirmed that when MCU was overexpressed in the eyes of *Drosophila* using *gmr*-Gal4, layers in the eyes collapsed and were impaired (Choi *et al.*, 2017). As MCU functions as a calcium transporter in mitochondria, an increase in calcium import into the mitochondria led to this consequence. By using the phenotype of this *Drosophila*, I went through a modifier genetic screen test to find a new gene inside the mitochondria that may alter the mitochondrial calcium homeostasis.

I obtained a pool of mitochondria-related genes that are conserved from human to *Drosophila* through bioinformatics **(Fig. 56)**. Among the 22,017 human genes reported, I acquired 1,592 genes related to mitochondria ontologically. From these 1,592 genes, 369 gene orthologs existing in *Drosophila* were identified from the information obtained by Ensembl, HomoloGene, and Unigene. I ordered at least two lines of RNAi of each of these genes from the VDRC stock center, Bloomington stock center, and NIG-fly stock center to establish a pool of 724 *Drosophila* RNAi

for screen test. Overexpressed MCU and RNAi of each of these genes were crossed using *gmr*-GAL4, and the eyes of *Drosophila* were examined. I tried to find a specific RNAi that could rescue or worsen the phenotype of MCU overexpression, which destroys the eye of *Drosophila*. Among them, fumarate hydratase (FH) and succinate dehydrogenase subunit D (SDHD) were distinguished as modifiers. The overexpression of MCU in the eyes of *Drosophila* damaged the eyes, and the co-expression of FH RNAi exacerbated the level of impairment. In the case of SDHD, however, the damage was rescued **(Fig. 57)**. FH is an enzyme that catalyzes the chemical process that uses fumarate as a substrate to produce malate, and SDHD is a component of succinate dehydrogenase that catalyzes fumarate production from succinate **(Fig. 58)**. Both are highly important for the proper operation of the TCA cycle in mitochondria. Given these results, as the amount of fumarate increases, the eyes become more damaged, implying that the overexpression of the MCU has aggravated. It was also discovered that when the amount of fumarate was reduced, the eyes were rescued, implying that MCU overexpression was restored. As a result, I hypothesized that fumarate, a key metabolite of the TCA cycle, would affect MCU function, and I investigated whether fumarate actually alters the mitochondrial calcium influx.

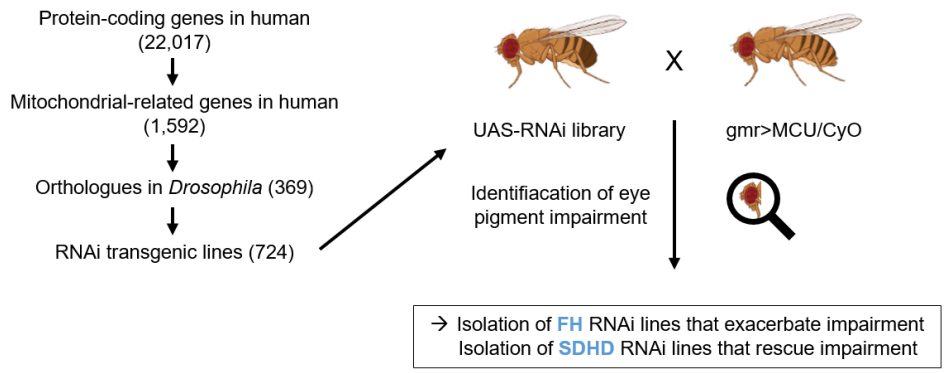

Figure 56. Schemes for acquiring an RNAi library through bioinformatics and for the genetic screen of the regulator of intracellular calcium homeostasis.

1,592 genes were discovered related to mitochondria ontologically among the 22,017 human genes listed. From the information gathered by Ensembl, HomoloGene, and Unigene, 369 gene orthologs that exist in *Drosophila* were identified. To establish a pool of 724 RNAi of *Drosophila* for screen, at least two lines of RNAi of each of these genes were ordered from many *Drosophila* stock centers. After overexpressing the MCU gene in *Drosophila* eyes with *gmr*-GAL4, they were crossed with each RNAi library to confirm the result of the impaired eye phenotype.

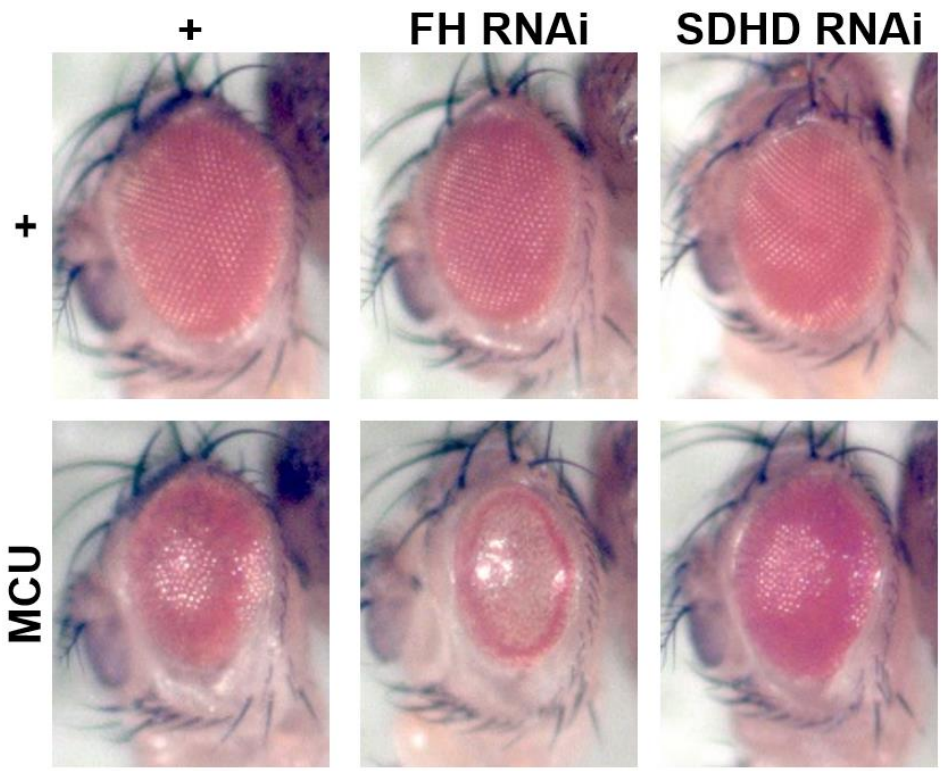

Figure 57. Results of genetic screen that alters MCU overexpression phenotype.

MCU overexpression (MCU/+) in the eyes of *Drosophila* damages the eyes compared to control (+/+). And the co-expression of FH RNAi exacerbated the level of impairment (MCU/FH RNAi). On the other side, co-expression of SDHD RNAi rescued the impaired phenotype (MCU/SDHD RNAi)

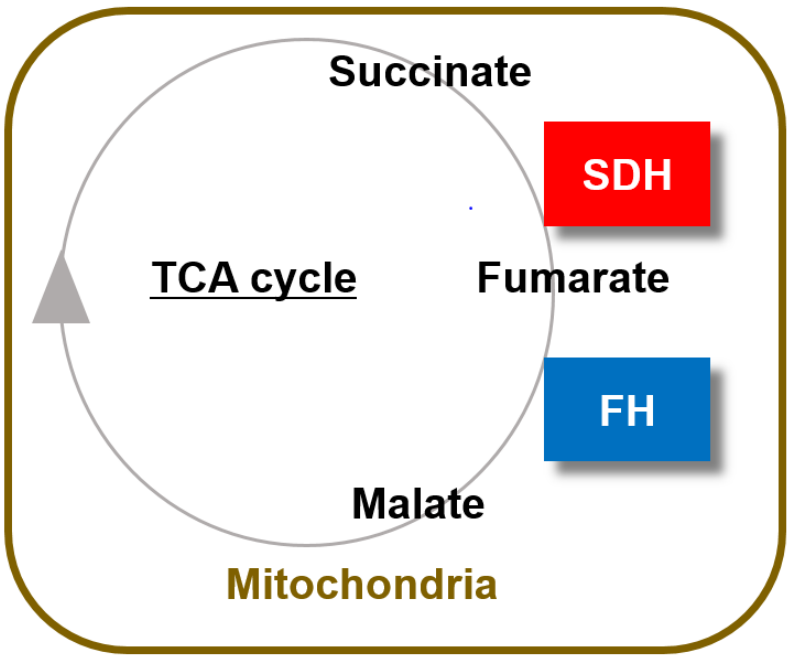

Figure 58. Functions of SDH and FH enzymes in the TCA cycle.

FH and SDH are enzymes that play an important role in the TCA cycle. SDHD is a component of succinate dehydrogenase that catalyzes fumarate production from succinate. FH is an enzyme that catalyzes the chemical reaction that uses fumarate as a substrate to produce malate.

Genes regulating fumarate metabolism in mitochondria affect mitochondrial calcium influx

To investigate the above experimental results in relation to alteration in mitochondrial calcium flux via MCU, I used the *Drosophila* calcium imaging system. After expression of mito-Pericam, a mitochondrial calcium indicator, in the muscle tissue of *Drosophila* larvae using *mef2*-GAL4, mitochondrial calcium flux was observed with caffeine treatment **(Fig. 12)**. The knockdown of FH may have caused an increase in calcium uptake that harmed the eyes further, whereas the knockdown of SDHD had the opposite effect. Indeed, the results from monitoring the mitochondrial calcium uptake through mito-Pericam in the muscle tissues of *Drosophila* demonstrated that the application of the knockdown of FH evoked an increase in the mitochondrial calcium influx **(Fig. 59A)** and the knockdown of SDHD led to a decrease **(Fig. 59B)**. FH and SDHD eliminate fumarate and produce fumarate, respectively, along the steps of the TCA cycle **(Fig. 58)**. Hence, considering the opposite effects they have on the genetic interaction and calcium flux in *Drosophila*, I came to examine fumarate as a new regulatory metabolite for mitochondrial calcium homeostasis.

Dimethyl fumarate (DMF) is a membrane permeable fumarate with methyl groups on both sides. that can raise the level of fumarate inside the cells. Since the change in mitochondrial calcium influx caused by

genetically altering fumarate amount has previously been found, I investigated whether mitochondrial calcium changes when DMF is treated. Surprisingly, application of DMF induced a rise in mitochondrial calcium influx in the muscular tissues of *Drosophila* **(Fig. 60A)**. On the other hand, the addition of another TCA metabolite, dimethyl succinate (DMS) and dimethyl malate (DMM), did not evoke any difference in mitochondrial calcium import compared with the control **(Fig. 60B and 60C)**. Taken together, fumarate and the enzymes that catalyze the production and elimination of fumarate in the TCA cycle seem to alter the mitochondrial calcium dynamics.

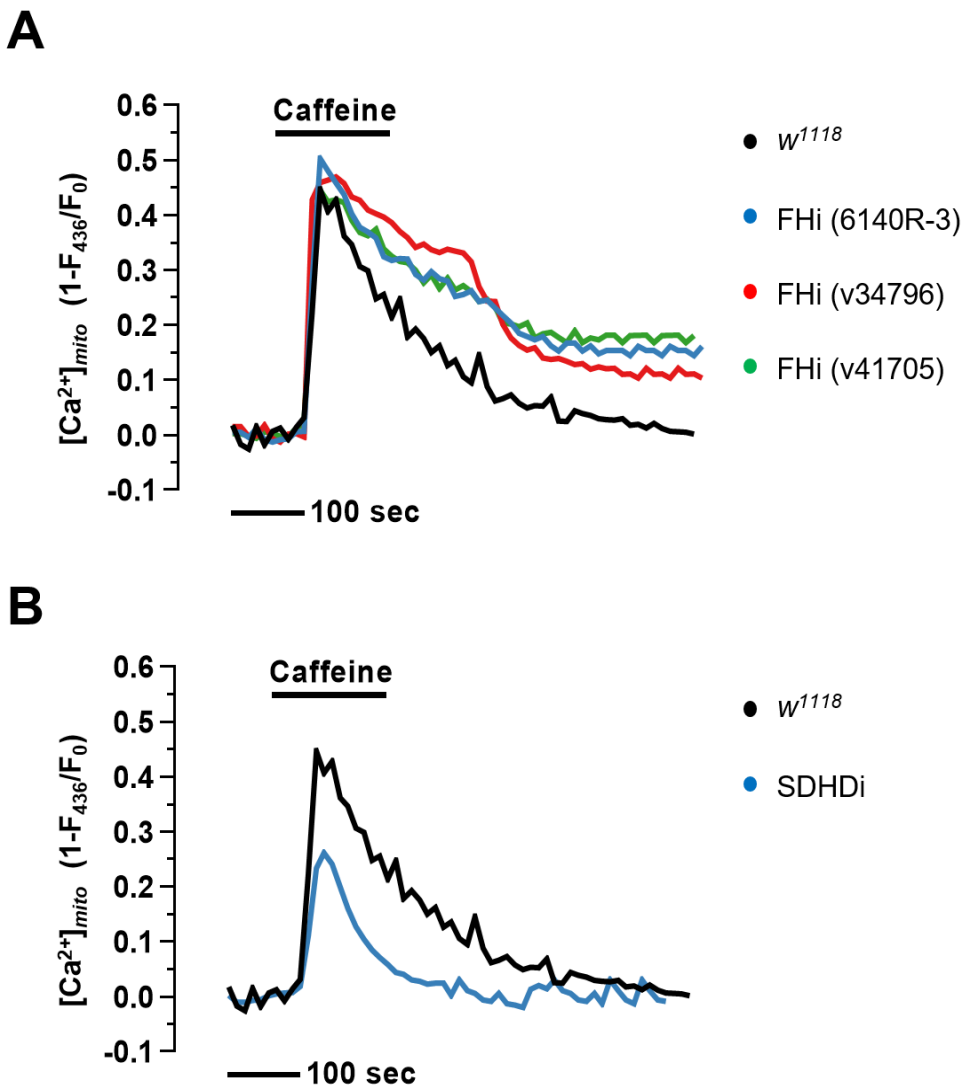

Figure 59. Mitochondrial calcium imaging results of FH and SDHD knockdown in *Drosophila*.

When compared to WT (*w1118,* black), the mitochondrial calcium influx increased in all three RNAi lines of FH (blue, red, and green) **(A)**. However,

the knockdown of SDHD (blue) showed a decreased mitochondrial calcium influx compared to the WT (*w1118*, black) **(B)**. 10 mM caffeine was treated for 3 minutes.

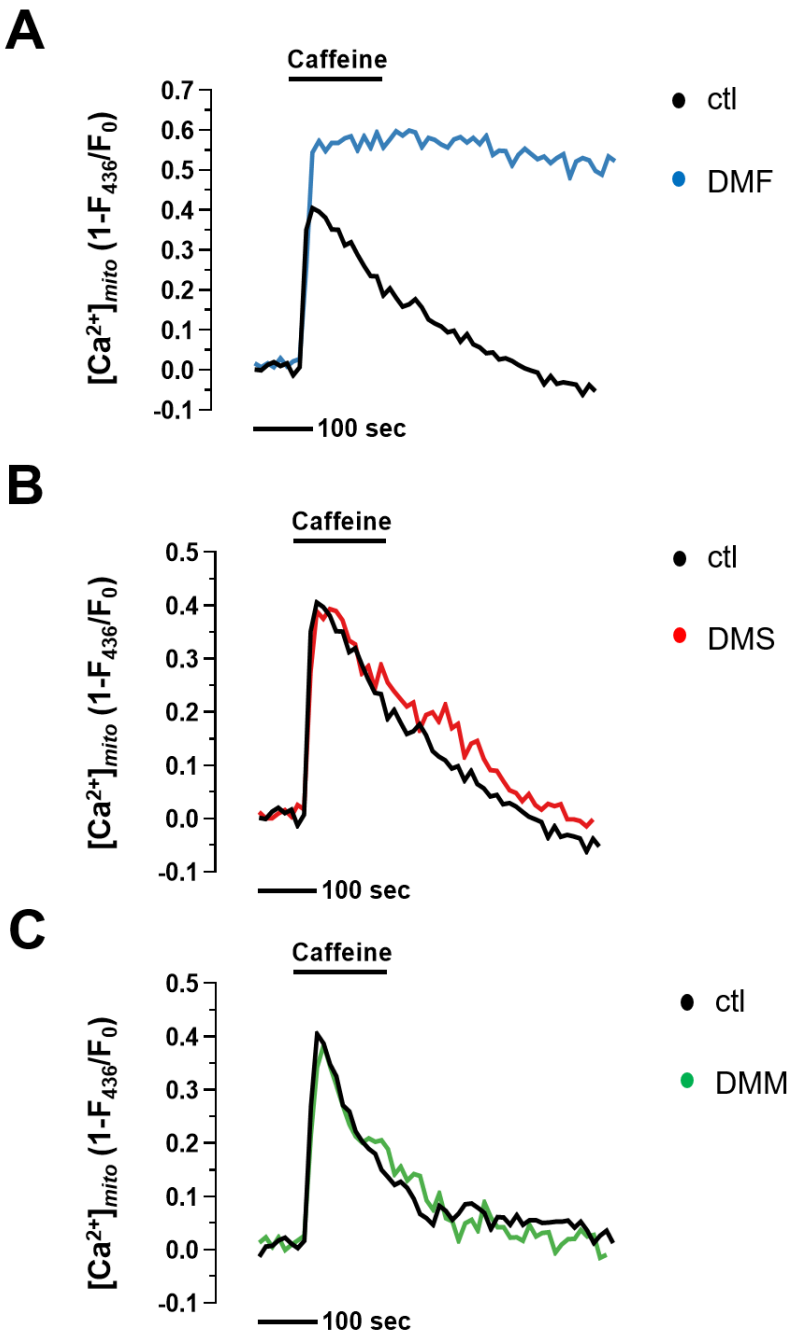
A
Caffeine
0.7
0.6
0.5
0.4
0.3
0.2
0.1
0.0
-0.1
[Ca2+]mito (1-F436/F0)
100 sec
ctl
DMF
B
Caffeine
0.5
0.4
0.3
0.2
0.1
0.0
-0.1
[Ca2+]mito (1-F436/F0)
100 sec
ctl
DMS
C
Caffeine
0.5
0.4
0.3
0.2
0.1
0.0
-0.1
[Ca2+]mito (1-F436/F0)
100 sec
ctl
DMM

Figure 60. DMF increases mitochondrial calcium influx in *Drosophila.*

Treatment of dimethyl fumarate (DMF) (blue) showed an increase in mitochondrial calcium influx compared to control (black) **(A)**. However, treatment of dimethyl succinate (DMS) (red) **(B)** and dimethyl malate (DMM) (green) **(C)**, two other TCA metabolites, had no effect on mitochondrial calcium influx when compared to the control (black). The concentration of treated DMF, DMS, and DMM is 3 mM each. 10 mM caffeine was treated for 3 minutes.

Fumarate regulates intracellular calcium levels in *Drosophila* and mammalian cells

Since it was confirmed that changing the amount of fumarate in *Drosophila* genetically or by DMF treatment altered mitochondrial calcium influx, I performed mammalian cell calcium imaging to confirm whether the same phenomenon occurred in mammalian cells. Surprisingly, when FH siRNA was transfected in HEK293 cells, an increase in mitochondrial calcium influx was observed **(Fig. 61A)**, and when SDHD siRNA was transfected, a decrease in mitochondrial calcium influx was confirmed **(Fig. 61B)**. It was also confirmed that when HEK293 cells were treated with DMF, mitochondrial influx was reduced **(Fig. 61C)**. According to these findings, fumarate regulates mitochondrial calcium influx, a phenomenon that has been observed not just in *Drosophila* but also in mammalian cells.

Next, I investigated whether this phenomenon affects calcium homeostasis in organelles other than mitochondrial calcium. First, for FH knockdown, the ER calcium graph was measured to move under the control line, and for SDHD knockdown, the ER calcium graph was measured to move up **(Fig. 62A)**. Accordingly, it was confirmed that cytosolic calcium was increased in FH knockdown and decreased in SDHD knockdown **(Fig. 62B)**. Following that, calcium changes in the ER and cytosol were measured in the treatment of DMF without genetics, similar to FH knockdown with a

large amount of fumarate **(Fig. 63A and 63B)**. In the same way that mitochondrial calcium changes in mammalian cells were similar to those in *Drosophila*, ER **(Fig. 64A)** and cytosolic **(Fig. 64B)** calcium changes in FH and SDHD knockdown cells were also similar to those in *Drosophila*. Finally, DMF treatment caused ER **(Fig. 65A)** and cytosolic **(Fig. 65B)** calcium changes in the cells in the same way that it did in *Drosophila*. Then I wondered what happens to calcium flux when the SDHD inhibitor, which reduces the amount of fumarate in the cells, is used instead of DMF, which increases the amount of fumarate in the cells. Surprisingly, carboxin, a known SDHD inhibitor, generated the same results as SDHD knockdown, in contrast to the treatment of DMF **(Fig. 66A and 66B)**.

To summarize, FH knockdown and DMF application hampered calcium reuptake in the ER, and SDHD knockdown induced a reduction in ER calcium flux, which is conserved in *Drosophila* and mammalian cells. In contrast, the expression of FH RNAi and the treatment of DMF increased calcium transport in the cytosol and mitochondria, whereas SDHD RNAi expression and the treatment of carboxin had the opposite effect. As a result, I established that the level of fumarate affects the intracellular calcium homeostasis.

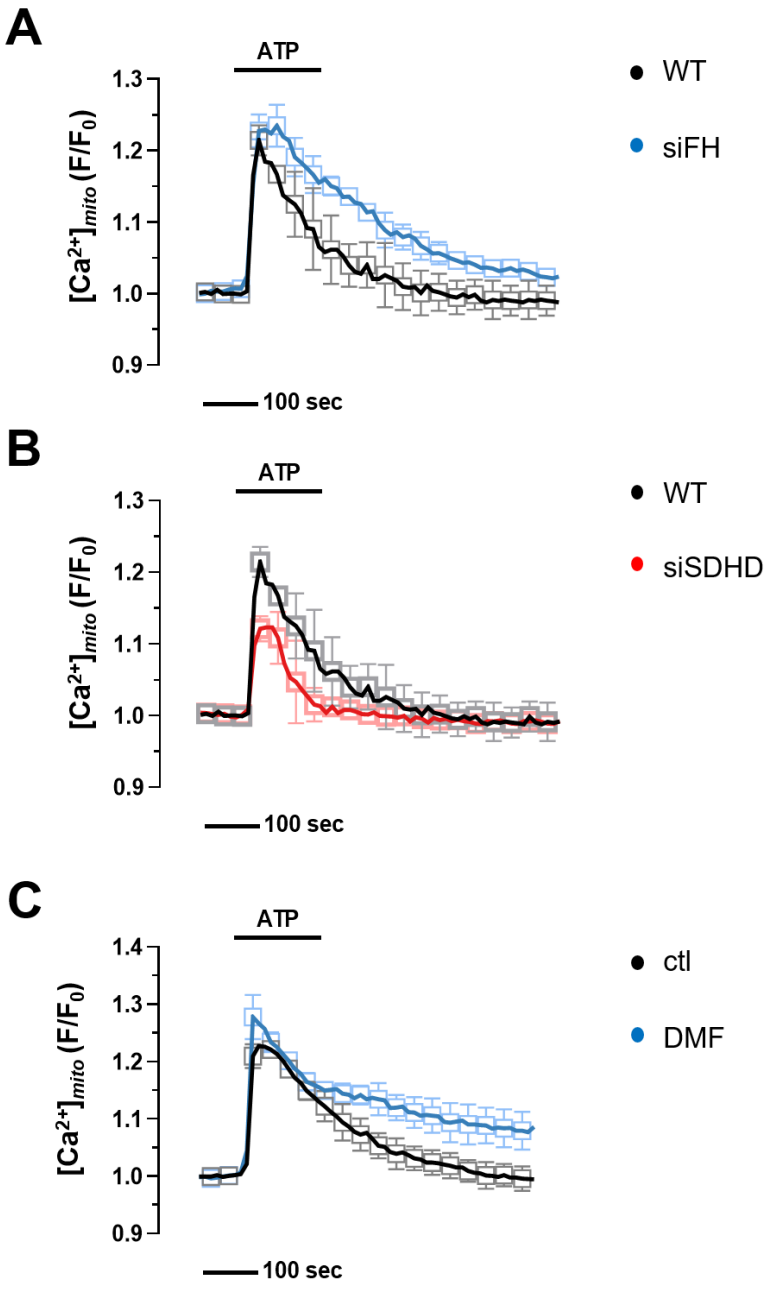
A
ATP
1.3
1.2
1.1
1.0
0.9
[Ca2+]mito (F/F0)
100 sec
WT
siFH
B
ATP
1.3
1.2
1.1
1.0
0.9
[Ca2+]mito (F/F0)
100 sec
WT
siSDHD
C
ATP
1.4
1.3
1.2
1.1
1.0
0.9
[Ca2+]mito (F/F0)
100 sec
ctl
DMF

Figure 61. Mitochondrial calcium imaging results in mammalian cells with treatment of FH siRNA, SDHD siRNA and DMF.

Measurement of mitochondrial calcium modulations when FH siRNA **(A)**, SDHD siRNA **(B)** was transfected in HEK293 cells. Treatment of 3 mM dimethyl fumarate (DMF) was also measured in HEK293 cells **(C)**. 100 μM ATP was delivered to initiate IP_3R-mediated calcium release.

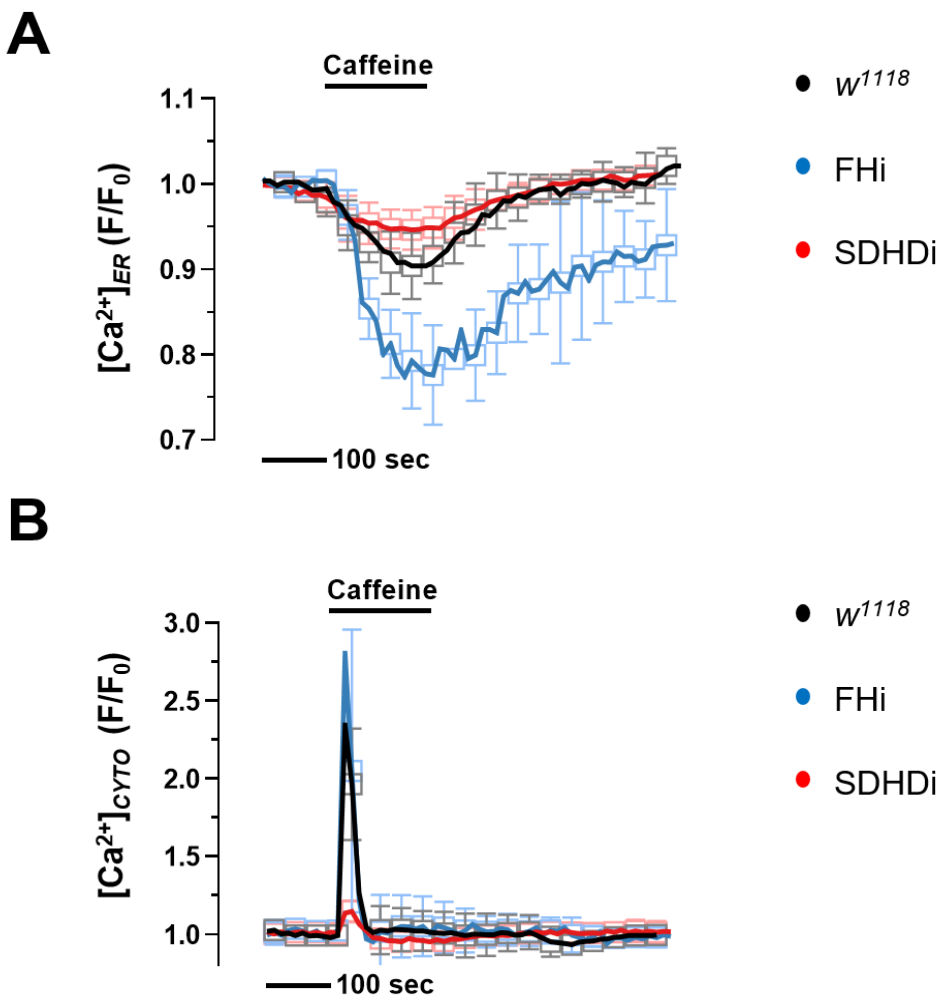

Figure 62. ER and cytosolic calcium flux in *Drosophila* with knockdown of FH or SDHD.

Measurement of ER **(A)** and cytosolic **(B)** modulation in WT (*w1118*, black), knockdown of FH (blue), and knockdown of SDHD (red). 10 mM caffeine was treated for 3 minutes.

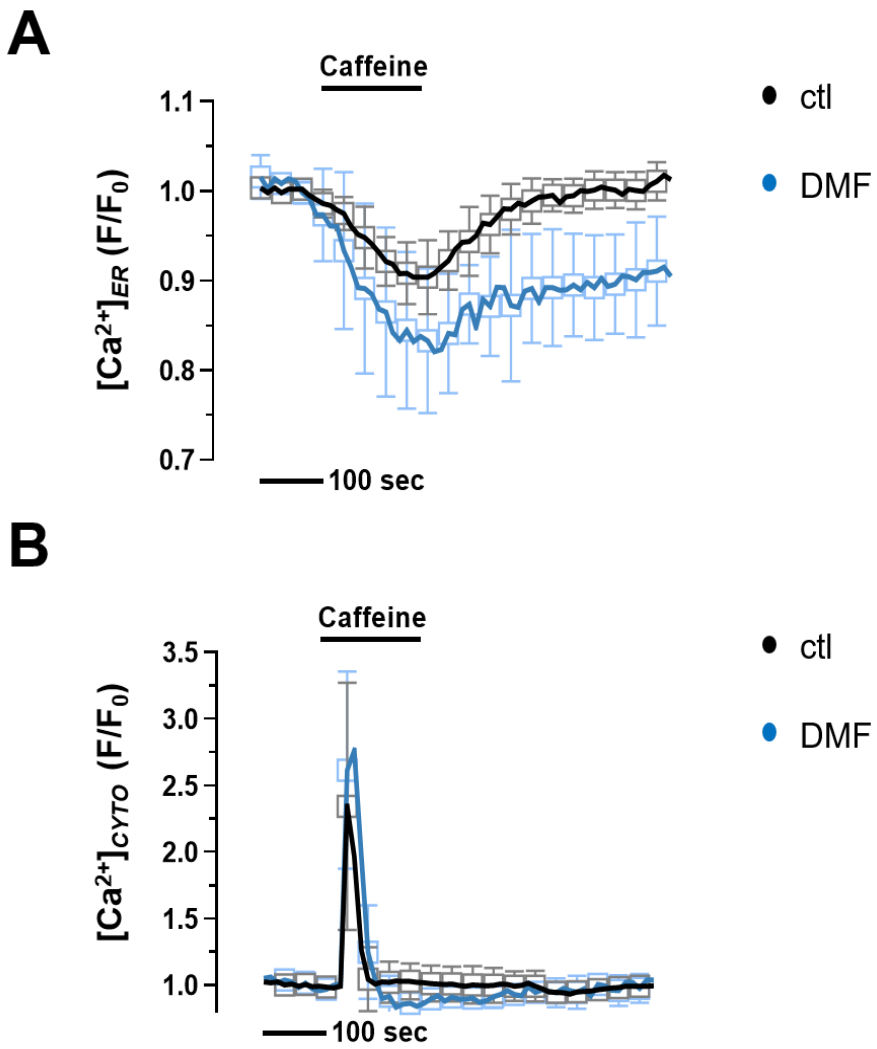

Figure 63. ER and cytosolic calcium flux in *Drosophila* with DMF treatment.

Measurement of ER **(A)** and cytosolic **(B)** modulation in control (black), and treatment of dimethyl fumarate (DMF) (blue). DMF 5mM was treated for *Drosophila* calcium imaging. 10 mM caffeine was treated for 3 minutes.

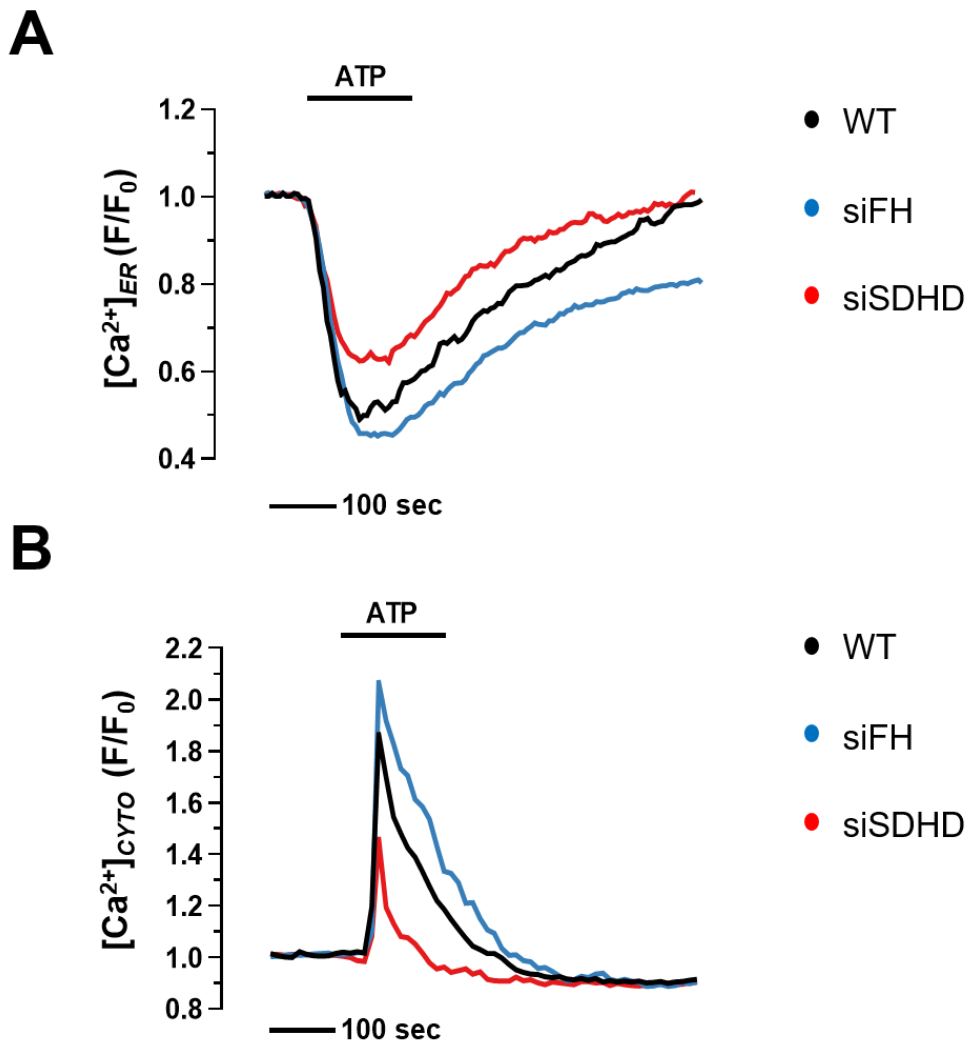

Figure 64. ER and cytosolic calcium flux in HEK293 cells with knockdown of FH or SDHD.

Measurement of ER **(A)** and cytosolic **(B)** modulation in WT (black), knockdown of FH (blue), and knockdown of SDHD (red). 100 µM ATP was delivered to initiate IP_3R-mediated calcium release.

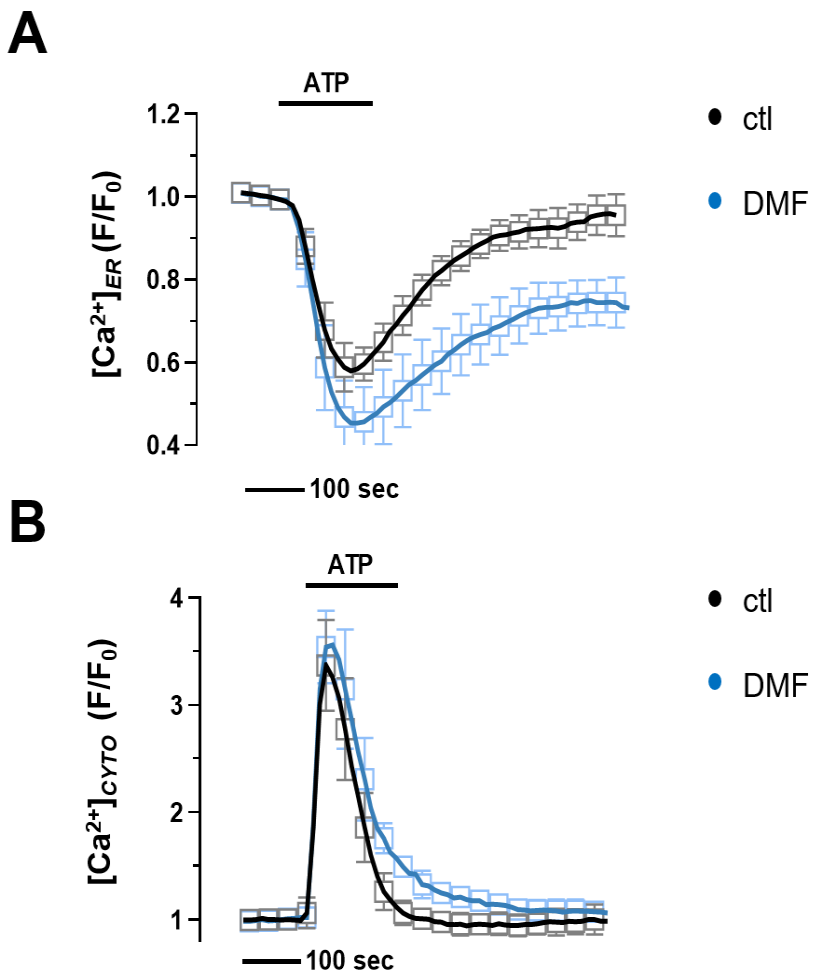

Figure 65. ER and cytosolic calcium flux in HEK293 cells with DMF treatment.

Measurement of ER **(A)** and cytosolic **(B)** modulation in control (black), and treatment of dimethyl fumarate (DMF) (blue). 3mM DMF was treated for mammalian cell calcium imaging.100 μM ATP was delivered to initiate IP_3R-mediated calcium release.

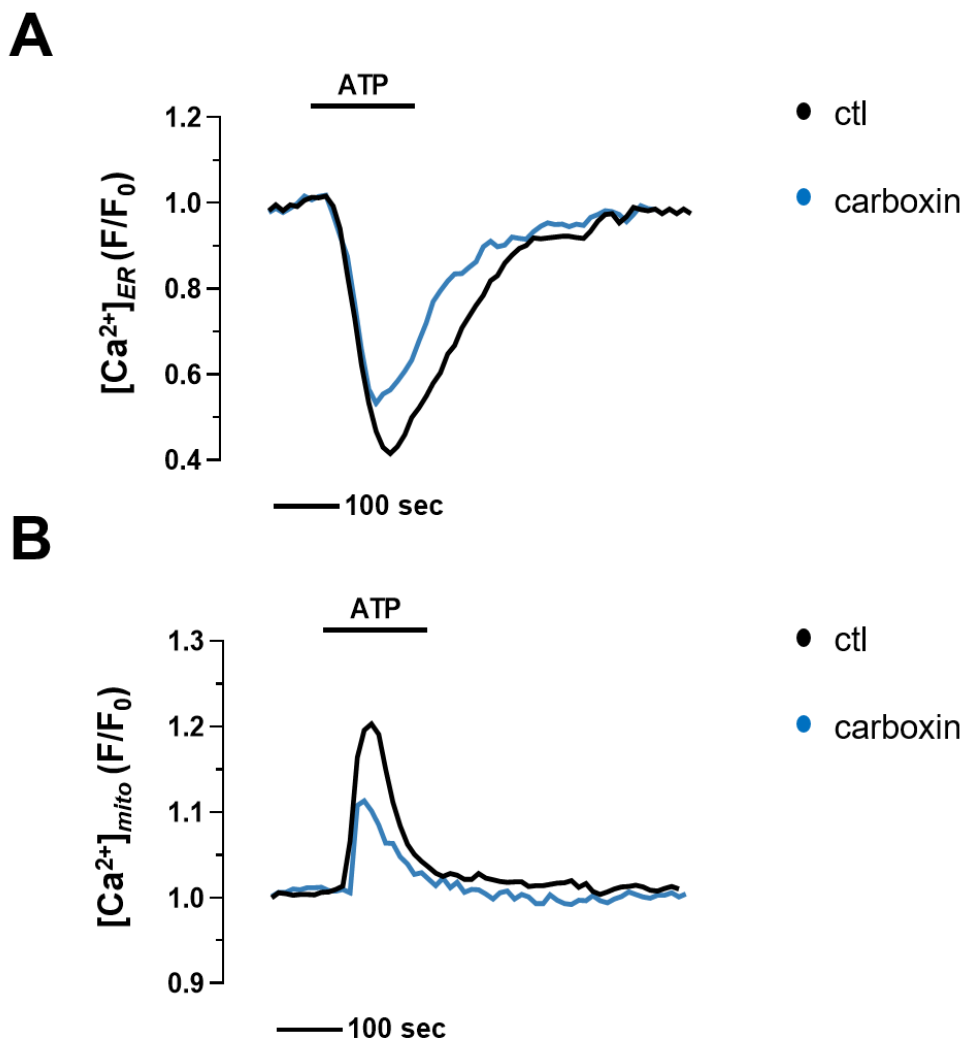

Figure 66. Carboxin, a SDHD inhibitor, alters ER and mitochondrial calcium flux in HEK293 cells.

Measurement of ER **(A)** and mitochondrial **(B)** calcium modulation in control (black), and treatment of carboxin 0.5 mM, a SDHD inhibitor (blue). 100 μM ATP was delivered to initiate IP_3R-mediated calcium release.

Fumarate alters intracellular calcium levels through regulating ER calcium channels

According to previous results, the amount of fumarate regulates the intracellular calcium flux in both mammalian cells and *Drosophila*. Calcium from the endoplasmic reticulum (ER) and extracellular environment accumulates in the cytosol, and then it is exported out to the extracellular, imported back into the ER through SERCA, or taken up by mitochondria via MCU and lysosomes. Thus, an increase in calcium influx in mitochondria by fumarate is intimately engaged to different subcellular components. So I tried to figure out which organelle calcium channels fumarate has an effect on.

First, when the ER calcium channel was inhibited, I measured the mitochondrial calcium flux to see if DMF still had an effect, and when the mitochondrial calcium channel was damaged, I measured ER calcium to see if DMF still had an effect. Even under ATP stimulation, cells treated with the IP_3R inhibitor 2-aminoethoxydiphenyl borate (2APB) have no ER calcium flux **(Fig. 67A)**. In this circumstance, 2APB reduced mitochondrial calcium influx in comparison to the control. Furthermore, the simultaneous treatment of DMF and 2APB was unable to compensate for this reduction in mitochondrial calcium influx **(Fig. 67B)**. This indicates that the effect of DMF does not appear if the ER calcium channel is dysfunctional. However,

it was confirmed that the effect of DMF was still shown in MCU knockout MEF cells in which the mitochondrial calcium channel was disrupted **(Fig. 68)**. Taken together, it is completely obvious that DMF alters intracellular calcium by affecting ER calcium channels rather than mitochondrial calcium channels.

Fumarate alters intracellular calcium levels through the ER calcium influx channel, SERCA

Next, I attempted to determine whether DMF affects the influx or efflux channels of ER calcium. First, the function of SERCA to uptake the cytosol calcium into ER was exploited. Calcium clearance in the cytosol is achieved by calcium exportation through the plasma membrane or importation into the ER via SERCA. Based on the results previously reported, the plasma membrane calcium efflux channels are known to be blocked when vanadate is treated (Introini et al., 2018). When the cytosolic calcium clearance mechanism through the plasma membrane is blocked with vanadate, only cytosol calcium clearance through the SERCA can be measured. When thapsigargin (TG), a SERCA inhibitor, is applied in the vanadate-treated condition, it is observed that the cytosol calcium cannot be imported into the ER through SERCA and is maintained at a constant concentration. Under vanadate treatment, the addition of DMF had the same effect as the application of thapsigargin (TG) **(Fig. 69)**. Since both DMF and TG inhibited cytosolic calcium clearance via SERCA, it was assumed that DMF would inhibit SERCA similarly to TG.

In order to verify this in more detail, the SERCA activity measurement experiment was performed to confirm that DMF inhibits SERCA activity. Previously, in part I, ER calcium influx and efflux were

measured to confirm IP_3R activity. The experiment was repeated in part II with a few changes. Permeabilization was achieved by treating intact cells with escin, one of the detergents. As a result, calcium ions might pass through cell membranes more easily. Using this effect, once the cytoplasmic concentration is controlled and stabilized, and then the solution containing MgATP is flowed, the ER calcium uptake occurs by providing energy to the SERCA. The level of SERCA activity can be measured and compared using this ER calcium uptake experiment. When TG, a SERCA inhibitor, was treated in this experiment, the activity of SERCA was inhibited, resulting in no calcium uptake by MgATP **(Fig. 70A)**. Then it was ascertained whether DMF, like TG, had no calcium uptake by MgATP. As a result, it was found that DMF decreased calcium uptake to the ER in a dose-dependent manner **(Fig. 70B)**. Overall, fumarate may obstruct SERCA, blocking calcium uptake into the ER and, as a result, altering the cellular calcium flux. Taking the previous calcium imaging graphs into account, as the ER calcium uptake of SERCA was blocked, the calcium in the cytosol increased, and the calcium entering the mitochondria also increased.

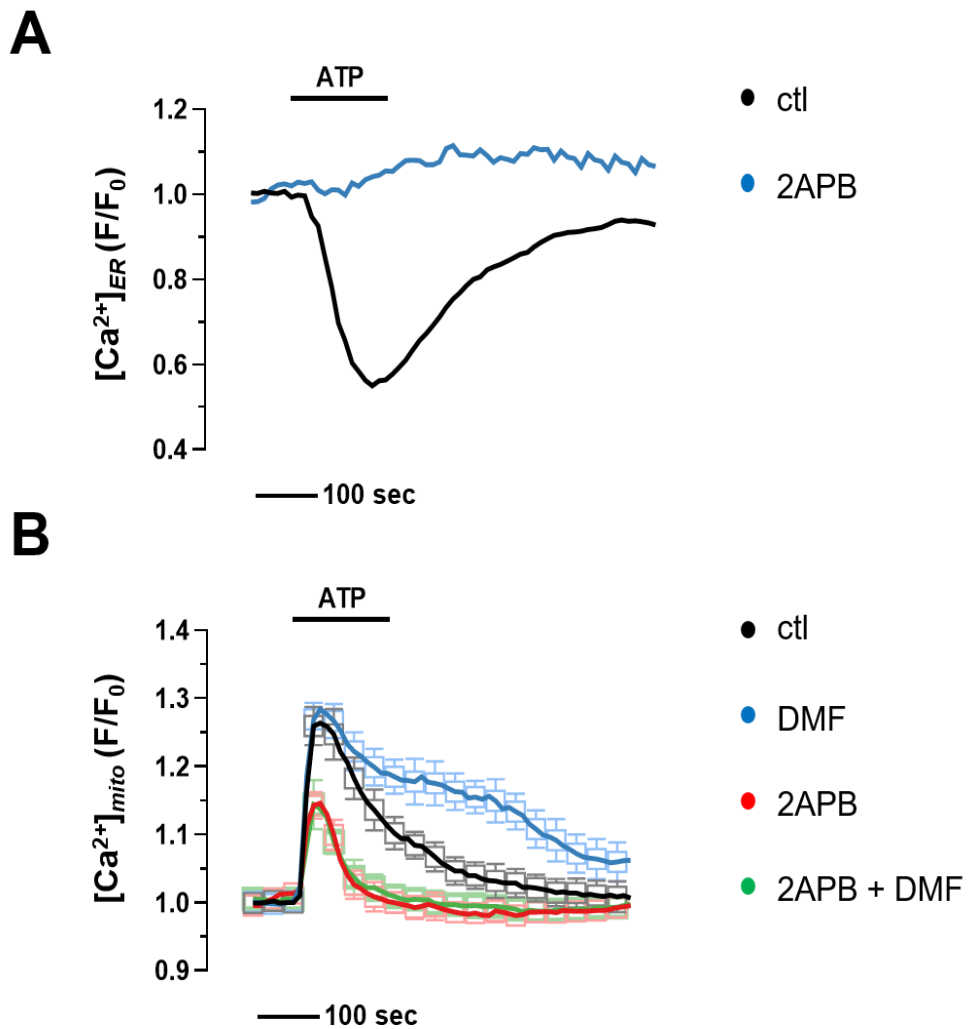

Figure 67. Effect of DMF is dependent on ER calcium channels.

Measurement of ER calcium modulation in control (black), and when treated with the IP_3R inhibitor 2-aminoethoxydiphenyl borate (2APB) 100 µM in HEK293 cells (blue) **(A)**. Measurement of mitochondrial calcium

modulation in control (black), treatment of 3 mM DMF (blue), treatment of 2APB (red), and simultaneous treatment of DMF and 2APB (green) **(B)**. 100 μM ATP was delivered to initiate IP_3R-mediated calcium release.

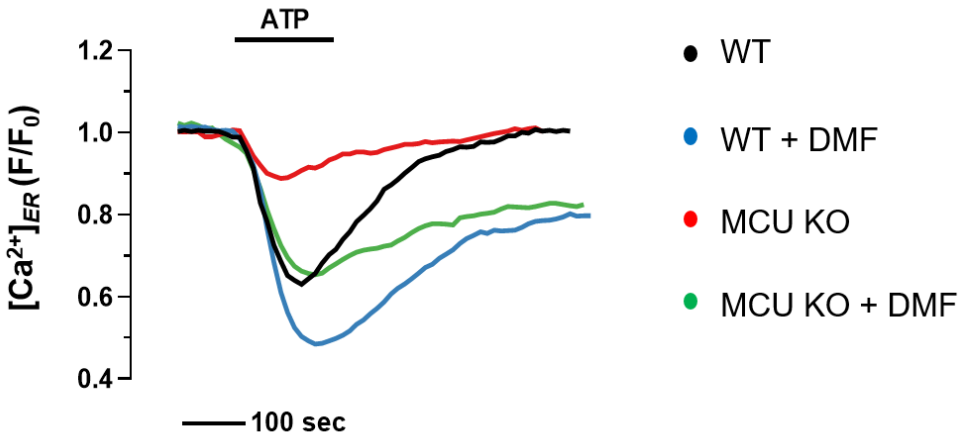

Figure 68. Effect of DMF is independent on MCU mitochondrial calcium channel.

Measurement of ER calcium modulation of WT (black) and MCU KO (red) MEF cells. Similar experiments were also conducted for WT (blue) and MCU KO (green) when treated with 3mM DMF.

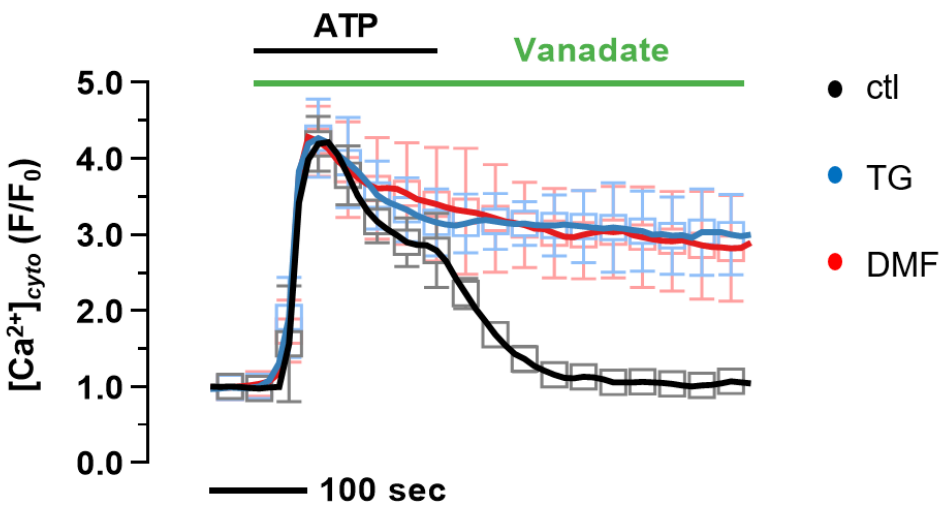

Figure 69. Cytosolic calcium clearance via SERCA is inhibited by DMF. Measurement of clearance of cytosolic calcium of control (black), treatment of 1 μM TG, a SERCA inhibitor (blue), and treatment of 3 mM DMF (red) in HEK293 cells. When vanadate is administered, the plasma membrane calcium efflux channels are blocked, keeping the SERCA as the only calcium-clearing pump.

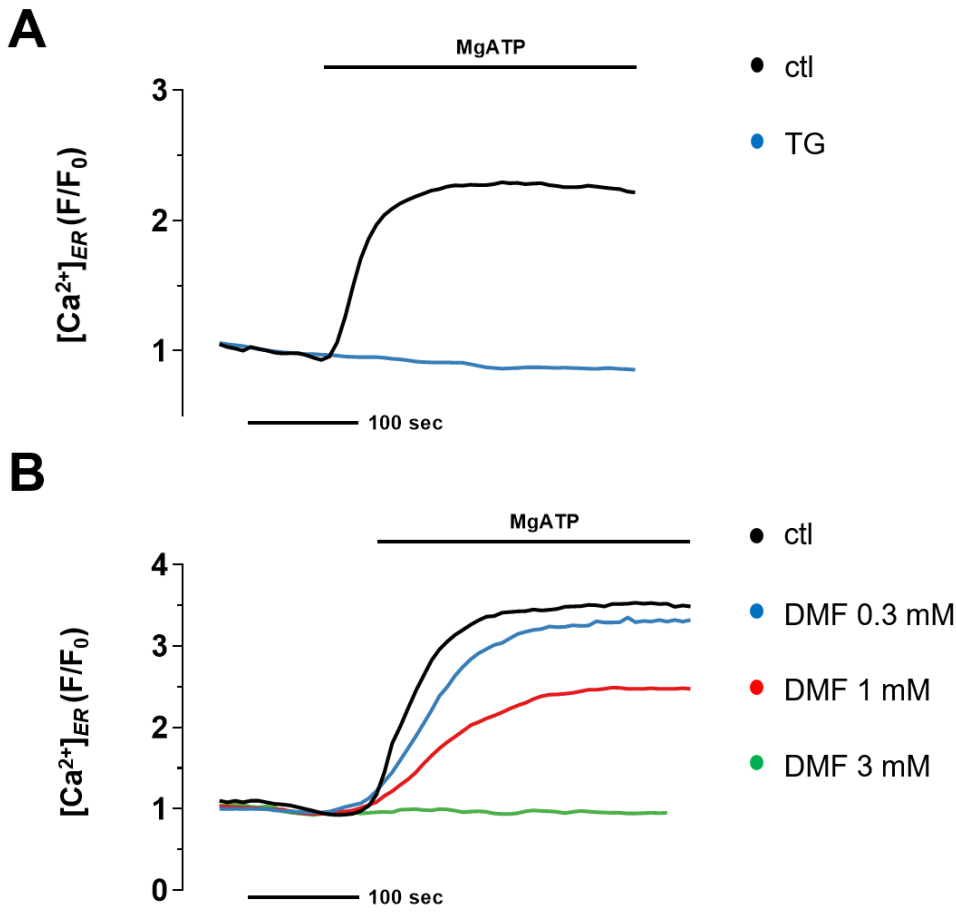

Figure 70. DMF reduces calcium uptake to the ER in a dose-dependent manner.

Measurement of SERCA activity when treated with TG 1 μM, a SERCA inhibitor, in permeabilized HEK293 cells by escin **(A)**. Measurement of SERCA activity when treated with indicated concentrations of DMF (blue, red, and green) in permeablized HEK293 cells by escin **(B)**.

Fumarate inhibits ER calcium uptake by succinating cysteine 876 of SERCA

Next, I observed how fumarate inhibits the activity of SERCA, resulting in a decrease in calcium import into the ER. Thus, by changing the media, I investigated the persistence of the effect of fumarate at lower concentrations. The reduction in ER calcium flux following fumarate treatment was measured again in cells after one hour of media change. This finding shows that the effect of fumarate on SERCA repression lasts at least one hour. I hypothesized that this change is caused by the post translational modification of the enzyme rather than fumarate directly binding to SERCA as an inhibitor.

In fact, an increase in fumarate concentration induces succination of many proteins, and an enzyme that eliminates this process has not yet been discovered. Hence, mass spectrometry was used to determine whether SERCA was succinated after DMF treatment. First, SERCA3 was cloned and overexpressed in the HEK293 cell line. The cell lines were then separated into fumarate-treated and untreated samples. After obtaining SERCA3 from these two groups, the mass-spectrum of these two SERCA3 was analyzed. As a result, fumarate turned out to succinate several cysteine residues of SERCA. Since no specific succinated cysteine with high efficiency was found, a point mutant form was generated in which several

cysteines from the mass data were replaced with serine that could not be succinated, respectively. After overexpressing each CS mutant in HEK293 cells, DMF was treated and compared to the WT to see if the DMF effect remained. As a result, when measuring ER calcium modulation, it was confirmed that the SERCA inhibition effect of DMF did not appear when SERCA3 C876S was overexpressed **(Fig. 71)**. Even when mitochondrial calcium was measured instead of ER calcium, the effect of DMF was not seen when SERCA3 C876S was overexpressed **(Fig. 72)**. This cysteine residue 876 is situated in the ER lumen, and is conserved across *Homo Sapiens*, *Drosophila Melanogaster* **(Fig. 73)**. Since HEK293 cell line mainly expressed a SERCA2 transcript among SERCA isoforms, I also generated a SERCA2 C875S mutant, and it was confirmed that the effect of DMF did not appear even when SERCA2 C875S was overexpressed. Therefore, the hypothesis that fumarate inhibits SERCA by succinating the 876 cysteine site could be validated.

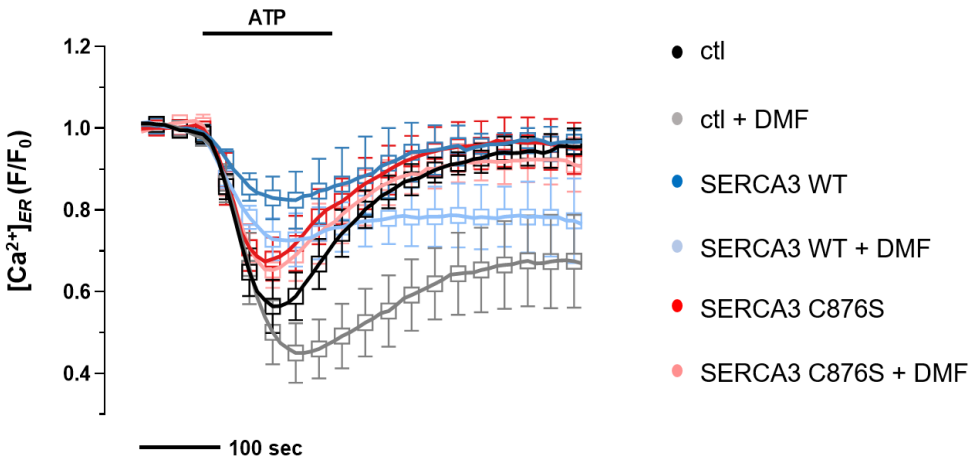

Figure 71. Inhibitory effect of DMF on SERCA is lost by SERCA C876S mutation.

Measurement of ER calcium modulation of DMF-treated and untreated HEK293 cell was compared. The effect of DMF was demonstrated in both the control (black) and the overexpression of SERCA3 WT (blue). However, DMF had no effect on the overexpression of SERCA3 C876S (red). 3mM DMF was treated for mammalian cell calcium imaging.

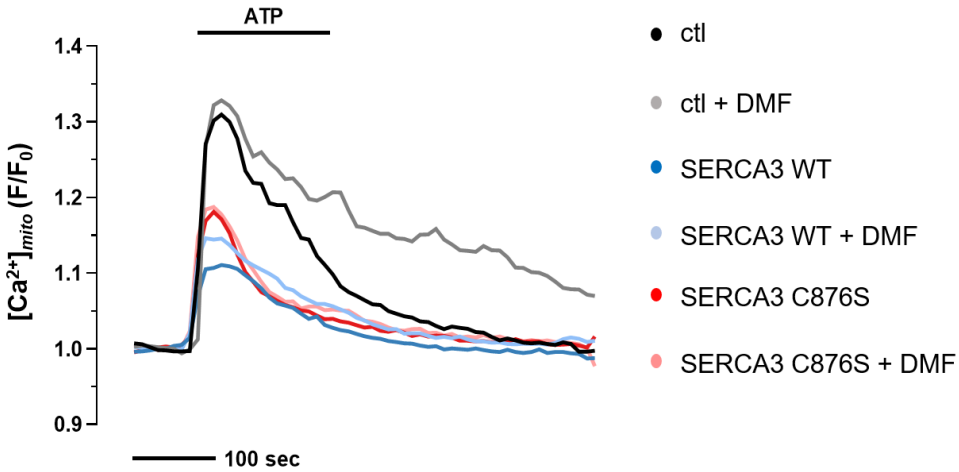

Figure 72. Inhibitory effect of DMF on mitochondrial calcium flux is lost by SERCA C876S mutation.

Measurement of mitochondrial calcium modulation of DMF-treated and untreated HEK293 cell was compared. The effect of DMF was demonstrated in both the control (black) and the overexpression of SERCA3 WT (blue). However, DMF had no effect on the overexpression of SERCA3 C876S (red). 3mM DMF was treated for mammalian cell calcium imaging.

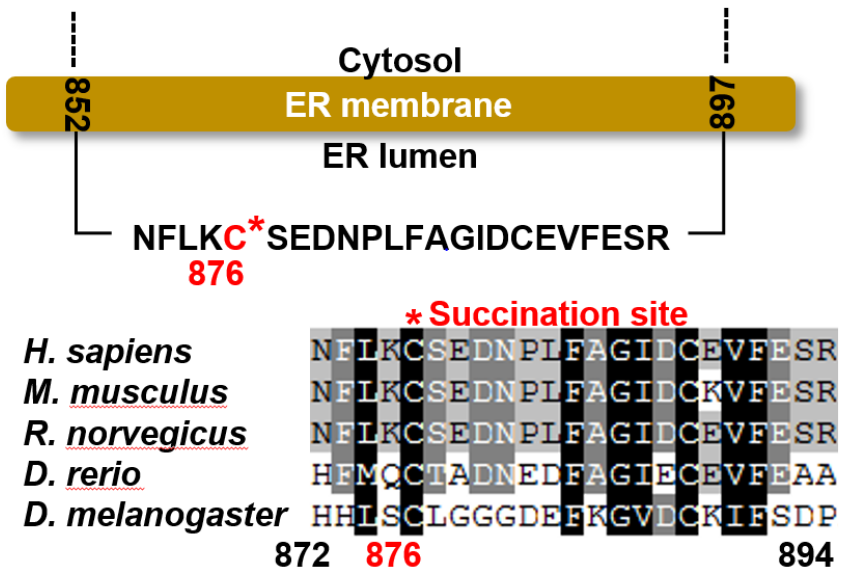

Figure 73. SERCA cysteine 876 residue is in the ER lumen and is highly conserved.

876 cysteine residue is located in ER lumen. Aligned SERCA3 protein sequences of *H. sapiens* (Q93084.2), *M. musculus* (Q64518.1), *R. norvegicus* (P18596.2), *D. rerio* (Q642Z0) and *D. melanogaster* (A0A0B4LGB7) with indication of the conserved cysteine residue in red.

High glucose medium induces SERCA cysteine 876 succination

To confirm the similar inhibitory effect of fumarate on SERCA by succinating cysteine 875, I used the clustered regularly interspaced short palindromic repeats (CRISPR)-Cas9 system to generate a C876S knock-in (KI) *Drosophila* model. There was no developmental problem found in C876S homo *Drosophila*, and it was viable until the adult stage. Nonetheless, for C876S KI flies, the ER calcium flux was reduced compared to the control, which was identical to the result obtained in mammalian cells with the expressed SERCA2 C875S mutant **(Fig. 74A)**. Alterations in fumarate concentration caused by FH or SDHD knockdown genetically had no effect on the ER calcium flux of C876S KI flies **(Fig. 74B)**. As a result, succination according to fumarate concentration did not occur in C876S KI flies in which endogenous 876 cysteine was replaced with serine, leading to no change in ER calcium flux.

It is well known that glucose provides the main source of pyruvate entering the TCA cycle (Heyland et al., 2009; Shiratori et al., 2019). Therefore, I expected that when glucose was added, the TCA cycle would be activated, and the amount of fumarate in the cell would increase. So, calcium imaging was performed to investigate the effect of high glucose medium on SERCA succination, which ultimately inhibits SERCA activity. To prove this, it was measured whether the same effect as DMF treatment

appeared on ER calcium flux when high glucose medium was treated in a dose-dependent manner. As a result, 5 mM glucose was taken as a low-level control, and as the concentration of glucose increased to 50 mM and 100 mM, the line of the ER calcium graph fell **(Fig. 75)**. This finding implies that SERCA succination of fumarate is increased even after glucose treatment. The effects of glucose medium on ER calcium flux were also repeated in *Drosophila* **(Fig. 76)**. If glucose treatment completely activates the TCA cycle and raises the level of fumarate, I wondered what would happen if SDH, an enzyme that produces fumarate, did not function properly in this situation. So, I measured the ER calcium flux to see the effect of the glucose treatment when the carboxin, a SDH inhibitor, was treated or siSDHD was expressed in mammalian cells. As a result, both carboxin treatment **(Fig. 77A)** and SDHD knockdown **(Fig. 77B)** reduced the SERCA inhibition effect of high glucose. These results indicate that the fumarate generated in the TCA cycle causes the effect of SERCA inhibition by high glucose. Finally, it was investigated whether SERCA inhibition occurred in the SERCA C876S mutant after exposure to high glucose levels. ER calcium modulation was measured with high glucose medium after overexpressing SERCA3 WT and SERCA3 C876S in HEK293 cells. It was confirmed that the SERCA inhibition effect of high glucose medium did not appear when SERCA C876S was overexpressed, despite the fact that control

and SERCA3 WT overexpression showed SERCA inhibition **(Fig. 78)**. No high glucose medium effect on ER calcium flux was also repeated in SERCA C876S KI flies **(Fig. 79).** Overall, high glucose medium activated the TCA cycle and increased fumarate production, resulting in SERCA succination in mammalian cells and *Drosophila*.

Heart functions in *Drosophila* correlate with SERCA succination

The ultimate goal is to understand the physiological meaning of SERCA succination in vivo using the *Drosophila* model. When there was no stimulus, there were no problems with the developmental process or no apparent phenotypes in C876S KI flies in comparison to WT. Therefore, I observed various phenotypes comparing WT and C876S KI flies when fed with a high sugar diet (HSD) to induce hyperglycemia. Flies were fed with HSD (standard media with 1.0 M sucrose final concentration) to evoke specific aspects of diet-induced metabolic dysfunction, and the results were compared to those fed with a low sugar diet (final concentration of 0.15 M sucrose) as control. Since it is known that developmental delay occurs by HSD (Na et al., 2013b), I performed HSD after birth to see if there was a difference between WT and C876S KI flies. As a result, developmental delay occurred in both WT and C876S KI flies during HSD, but there was a difference in the final survival results. There was no difference in survival between WT and C876S KI flies in low sugar as control, but when high sugar was fed, WT died before becoming adult flies **(Fig. 80A)**, whereas C876S KI became adult normally **(Fig. 80B)**.

Next, since there is a developmental delay when HSD is given from birth, I tried to see the difference between WT and C876S KI flies when HSD was given after maturation into adults. Since it is known that SERCA

is most highly expressed in the muscle and heart, these two tissues were examined. Among several experiments, a difference in heartbeat rate between WT and C876S KI flies was discovered when HSD was fed. After dissecting adult flies to obtain the hearts of *Drosophila*, the heart beat for 1 minute was recorded as beats per minute (BPM). Surprisingly, WT showed tachycardia with significantly higher heart BPM than controls when HSD was fed for 48 hours **(Fig. 81A).** But, there was no difference in the heart BPM between the control and the HSD fed in SERCA C876S KI flies **(Fig. 81B)**. Although more studies are still needed, this result indicates that fumarate-induced alterations in calcium homeostasis can cause a heart dysfunction.

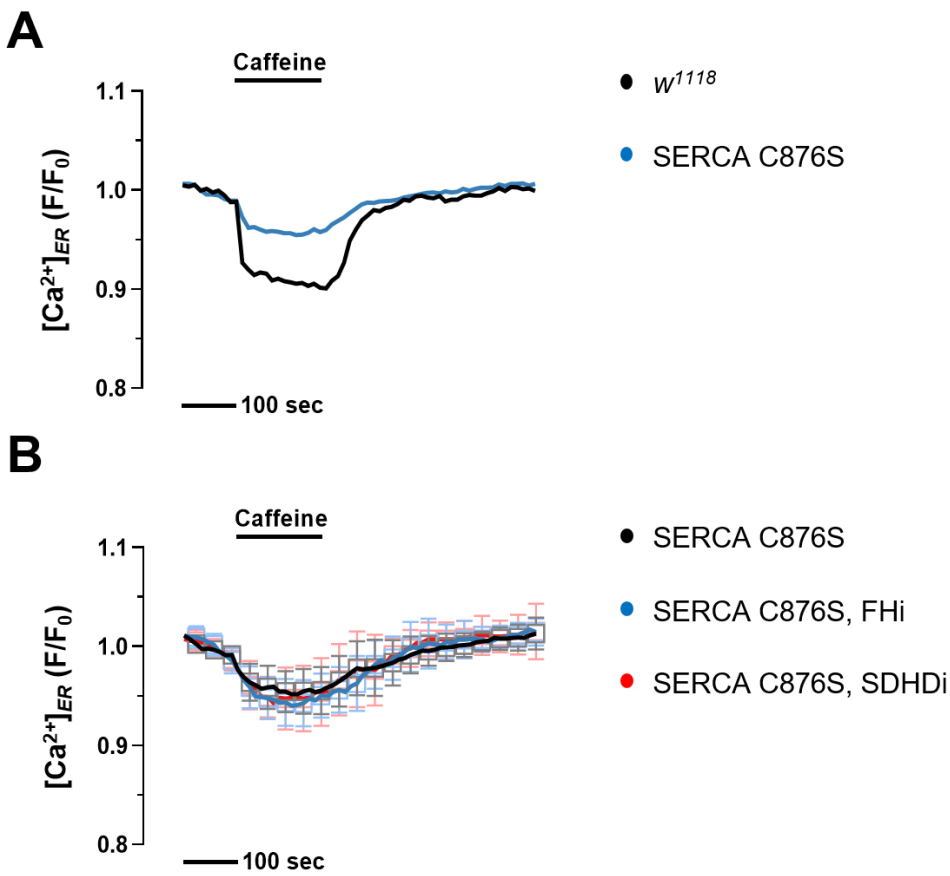

Figure 74. Knockdown of FH or SDHD has no effect on ER calcium flux in SERCA C876S KI flies.

Measurement of ER calcium in WT (*w1118*, black), and SERCA C876S KI flies (blue) **(A)**. Comparison of ER calcium modulation in SERCA C876S KI flies caused by knockdown of FH (SERCA C876S, FHi, blue) or SDHD (SERCA C876S, SDHDi, red) to control (SERCA C876S, black) **(B)**.

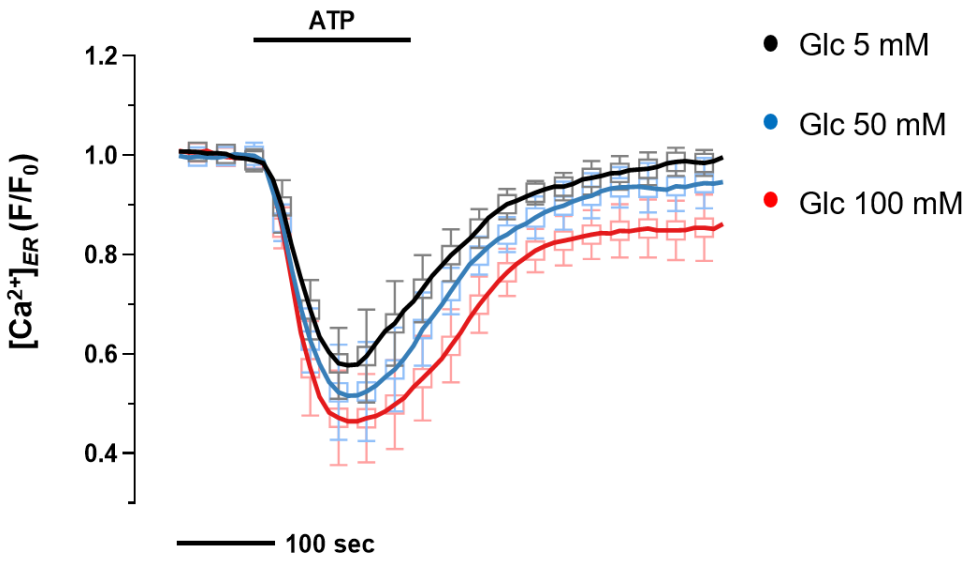

Figure 75. High glucose media induce SERCA succination and inhibition in HEK293 cells.

Measurement of ER calcium modulation in treatment of glucose 5 mM as a low-level control (black), treatment of glucose 50 mM (blue), and treatment of glucose 100 mM as a high-level (red). 100 µM ATP was delivered to initiate IP_3R-mediated calcium release.

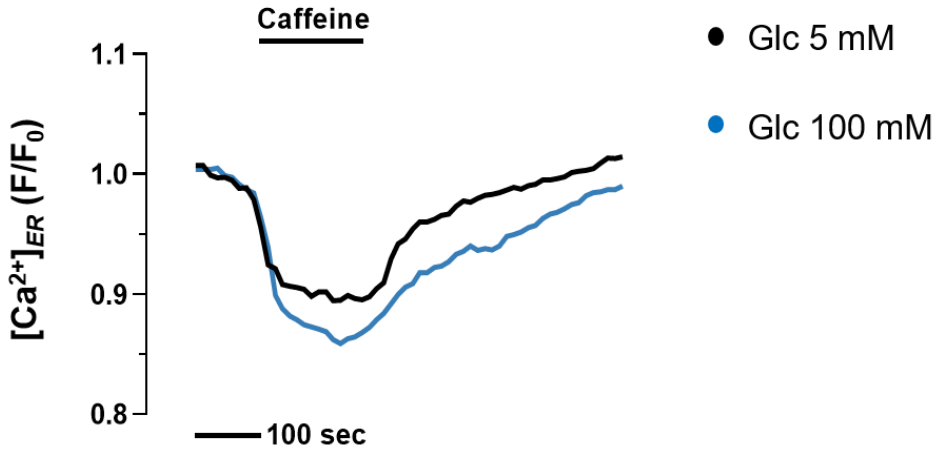

Figure 76. High glucose media induce SERCA succination and inhibition in *Drosophila*.

Measurement of ER calcium modulation in treatment of glucose 5 mM as a low-level control (black), treatment of glucose 100 mM as a high-level (blue). 10 mM caffeine was treated for 3 minutes.

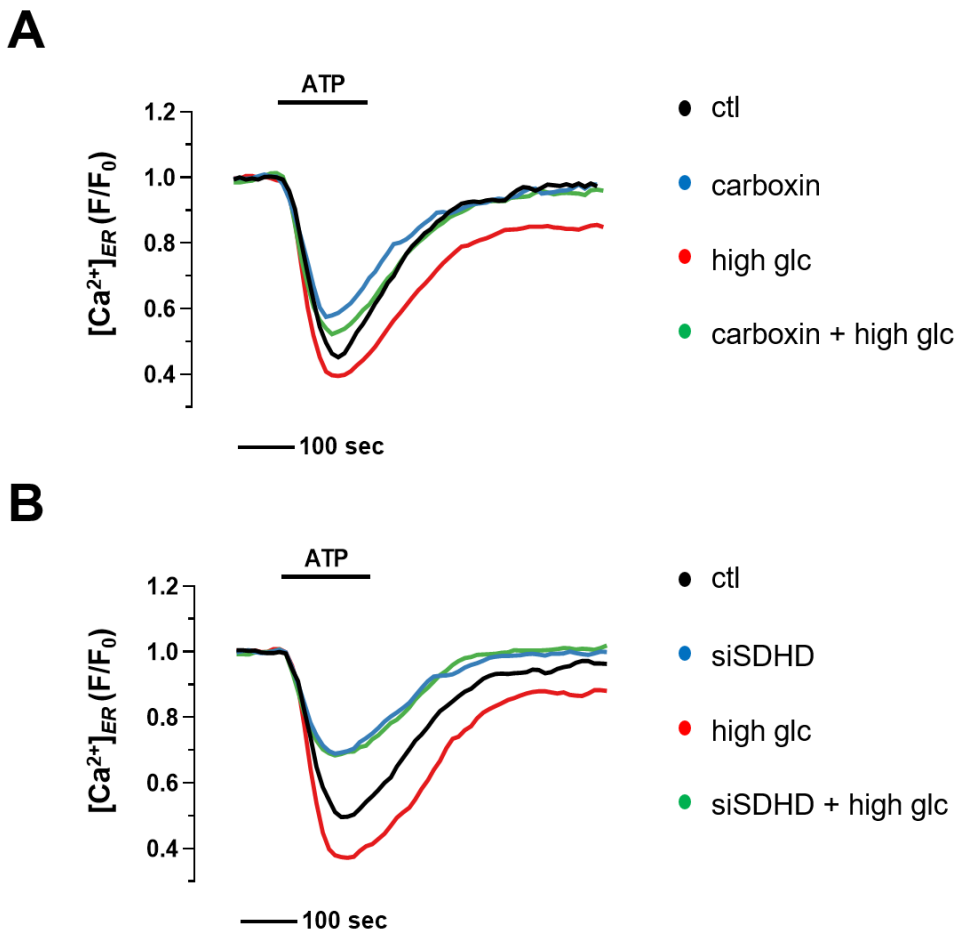

Figure 77. SDH mediates high glucose media-induced SERCA inhibition in HEK293 cells.

Measurement of ER calcium modulation in control (black), treatment of carboxin 0.5 mM (blue), treatment of glucose 100 mM as a high-level (red), and simultaneous treatment of carboxin and high glucose (green) **(A)**. Measurement of ER calcium modulation in control (black), knockdown of

SDHD (blue), treatment of glucose 100 mM as a high-level (red), and treatment of high glucose for the knockdown of SDHD (green) **(B)**. 100 μM ATP was delivered to initiate IP_3R-mediated calcium release.

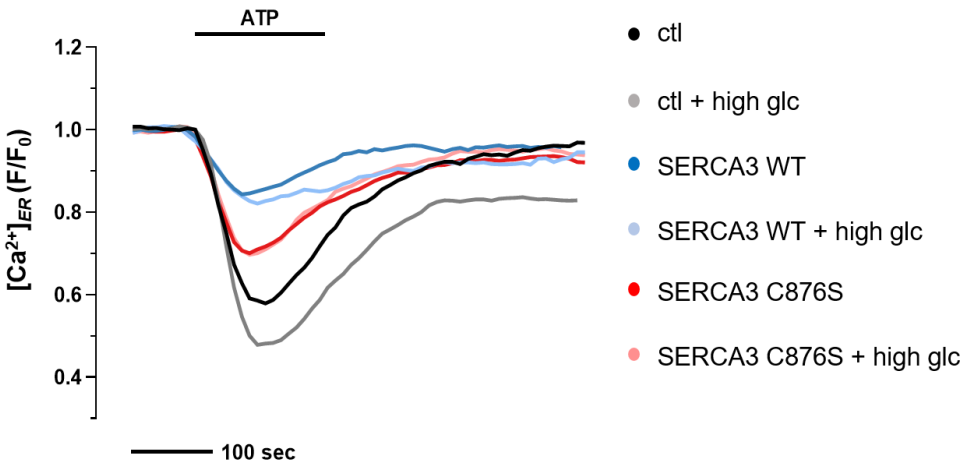

Figure 78. SERCA C876 succination is necessary for high glucose media-induced SERCA inhibition in HEK293 cells.

Measurement of ER calcium modulation of glucose 100 mM treatment as a high-level in HEK293 cell was compared. The effect of high glucose was demonstrated in both the control (black) and the overexpression of SERCA3 WT (blue). However, high glucose had no effect on the overexpression of SERCA3 C876S (red).

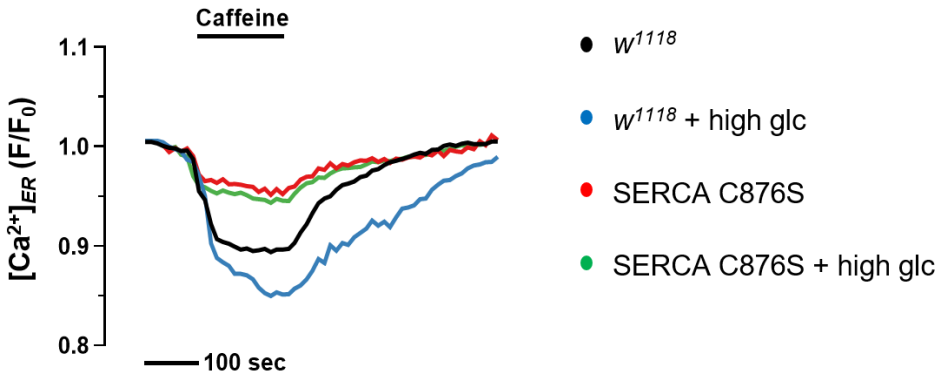

Figure 79. Loss of the effect of HSD on ER calcium flux in SERCA C876S KI flies

Measurement of ER calcium modulation in WT (*w1118*, black), glucose 100 mM treatment as a high-level for WT (blue), SERCA C876S KI flies as control (red), and glucose 100 mM treatment as a high-level for 10 mM for SERCA C876S KI flies (green).

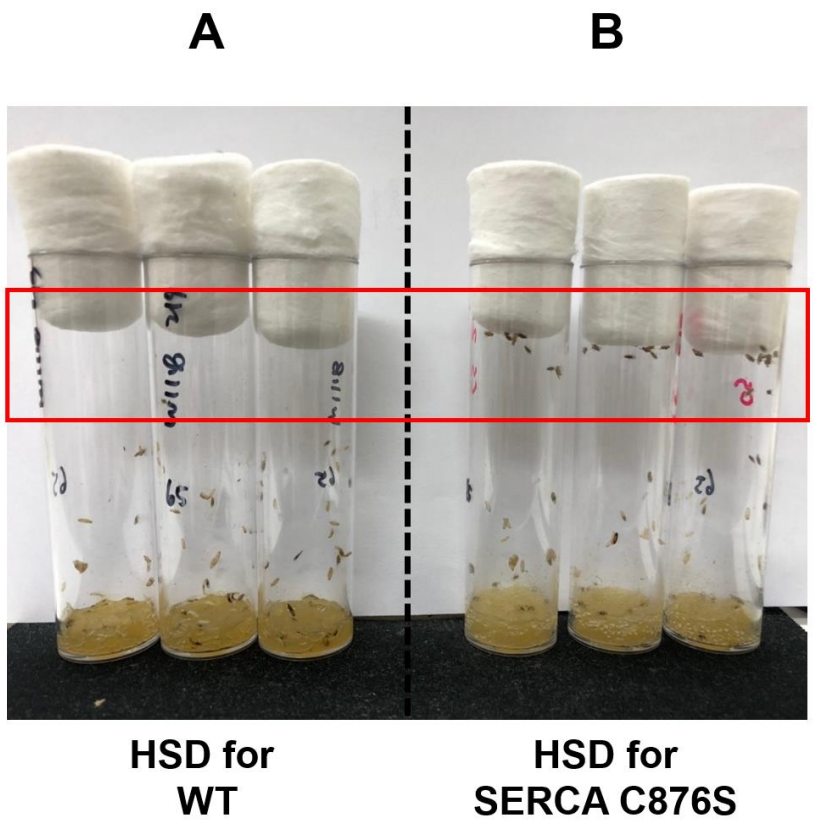

Figure 80. In HSD, WT does not mature into an adult and dies, whereas SERCA C876S KI matures into an adult.

A high sugar diet (HSD) was performed after birth, and the survival rate was compared and measured between WT (*w1118*) **(A)** and SERCA C876S KI **(B)** flies. The eggs were received for a specific period of time, and they were raised until they became adults.

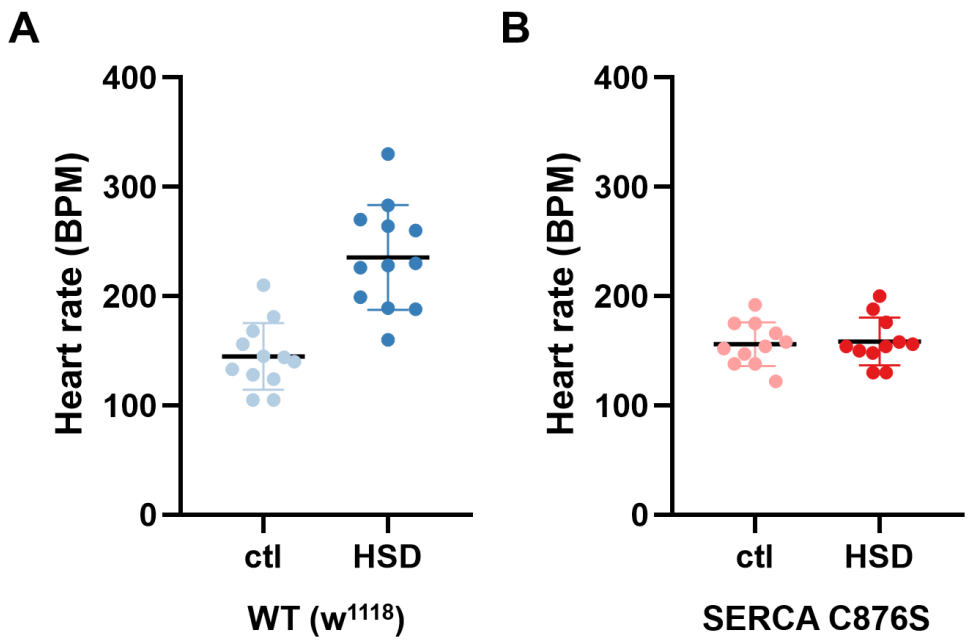

Figure 81. HSD induces tachycardia in WT but not in SERCA C876S KI flies.

Measurement of heart beat per minute in WT (w^{1118}) **(A)** and SERCA C876S KI **(B)** flies. Adult flies were fed a medium with a final concentration of sucrose of 0.15 M for control and a medium with a final concentration of sucrose of 1 M for HSD for 48 hours. The heartbeat rates of adult flies were recorded and quantified in BPM after they were dissected to obtain the heart. Each spot on the graph represents the BPM of one individual adult fly. $n >$ 11.

Discussions

Fumarate modulates intracellular calcium homeostasis by inhibiting SERCA

Based on the results so far, I believe that my study will contribute to a better understanding of the regulation of intracellular calcium homeostasis. Multicellular organisms have diverse metabolic activities that vary with development and changes in extracellular nutrient supplies and intracellular metabolic pathways. It is speculated that calcium homeostasis may be altered and adjusted as a result of the metabolic changes caused by SERCA succination. In summary **(Fig. 82)**, under high glucose medium, higher pyruvate would activate the TCA cycle in the mitochondria, resulting in enhanced synthesis of fumarate, an intermediate metabolite. Therefore, the increased fumarate induced a PTM called succination on the cysteine 876 residue of SERCA, an ER calcium influx channel, and inhibits SERCA. Following that, the ER failed to reuptake cytosolic calcium, resulting in impaired cellular calcium homeostasis. In *Drosophila*, when a high sugar diet was fed to induce hyperglycemia, tachycardia was occurred as a result of the disruption of calcium homeostasis. To confirm the succination on the cysteine 876 residue of SERCA in vivo, I generated a SERCA C876S

knock-in fly that cannot be succinated by fumarate. Since intracellular calcium homeostasis in SERCA C876S KI flies was not changed when fumarate levels were modulated, fumarate should target the 876 cysteine of SERCA. Finally, it was confirmed that SERCA C876S KI showed no heartbeat abnormalities when HSD was fed. Since I discovered that fumarate regulates intracellular calcium homeostasis, I suggest that modulating fumarate levels could be used to treat a variety of disease caused by abnormalities in intracellular calcium homeostasis.

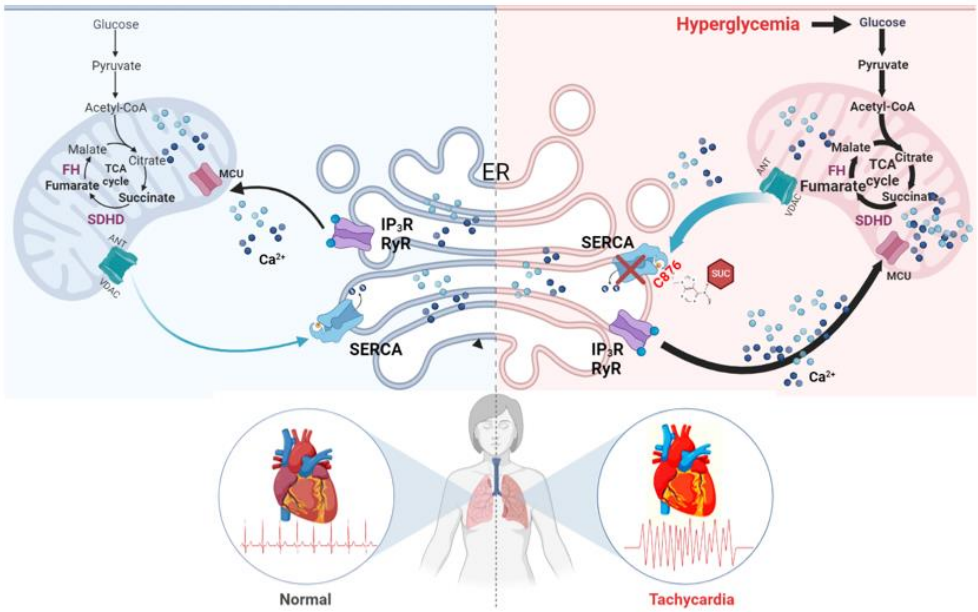

Figure 82. Fumarate regulates intracellular calcium homeostasis by inhibiting SERCA.

Under normal conditions, the TCA cycle is properly activated, ensuring that the amount of fumarate is appropriately maintained and intracellular calcium homeostasis is well maintained. As a result, the heart beat remains constant, allowing the body to remain healthy. In the case of hyperglycemia, however, the TCA cycle is highly activated, and the amount of fumarate, an intermediate, is significantly increased. Then, fumarate inhibits SERCA, an ER calcium influx channel, by succinating its cysteine 876 residue, causing calcium homeostasis to be disrupted. Once calcium homeostasis is disrupted, the heart beats much faster than normal, resulting in tachycardia. Image was generated from Biorender.

Metabolites directly regulate intracellular calcium homeostasis

Several studies have examined the impact of mitochondrial calcium on TCA cycle flux and mitochondrial ATP production. Nevertheless, it is unclear whether TCA cycle substrates directly regulate mitochondrial calcium channels. A recent study evaluated the effect on MCU activity using pharmacological and genetic modulations to limit the mitochondrial transport and entry of TCA cycle substrates generated by glycolysis and fatty acid oxidation (Nemani et al., 2020). Changes in fuel availability or mitochondrial transporter function cause changes in TCA metabolite levels. It was shown that the changes in mitochondrial metabolism activate EGR1, a transcription factor that affects MCU complex expression (Tomar and Elrod, 2020). Other studies on metabolites and calcium regulation have also found that 25,26-Dihydroxycholecalcifron, a metabolite of vitamin D, influences intestinal calcium transport activity. These findings, nevertheless, do not indicate that metabolites directly regulate the activity of calcium channels. However, here I discovered that fumarate directly regulates the activity of SERCA. Furthermore, my studies show that metabolites produced in mitochondria not only regulate the activity of mitochondrial calcium channels but also control the calcium channel of the ER, the largest calcium storage in the cell, affecting overall intracellular calcium homeostasis. It is well understood that when intracellular calcium

homeostasis is disrupted, various problems occur, leading to neurodegenerative diseases. Since fumarate modulates intracellular calcium homeostasis, I believe that manipulation of fumarate levels could cure several diseases caused by abnormal intracellular calcium homeostasis.

It is well known that metabolites are produced during the digestion of carbohydrates and proteins by the gut microbiota (Donohoe et al., 2011; Fernández-Veledo and Vendrell, 2019). Therefore, the microbiome can be considered as a source that can provide fumarate in the human body. I intend to perform additional experiments to determine whether fumarate produced in the intestine affects only the site of production, or whether fumarate can regulate calcium by moving to other organs and cells along the bloodstream. Although it is not pure fumarate, there are research results that a drug called dimethyl fumarate moves through the bloodstream and is absorbed into cells (Andersen et al., 2018). Therefore, rather than regulating intracellular calcium concentration locally in the gut, fumarate produced by the gut microbiota may travel through the bloodstream and affect other organs and tissues. It would be an interesting study if I could demonstrate that fumarate, a metabolite produced in the intestine after food consumption, can move through the bloodstream and alter calcium homeostasis in heart cells, thereby altering heart beat.

Diseases associated with fumarate levels

Protein succination is also increased in the kidney of a fumarate hydratase (FH)-deficient conditional knockout mouse that develops renal cysts (Pollard et al., 2007). The amount of fumarate increases when FH is deleted, and the FH loss-of-function mutation is known to be a driver of hereditary leiomyomatosis and renal cell calcinoma (HLRCC) (Panarsky et al., 2020). This lesion has two major oncogenic effects. First, it directly stimulates a metabolic transition to Warburg metabolism by disrupting the Krebs cycle, causing cells to shift to alternative pathways in order to maintain the balance of energy required for survival and proliferation. Second, excess fumarate leads to accumulation of members of the hypoxia inducible factor family of transcription factors (Kaelin, 2002; Yang et al., 2012). The deletion of the FH gene results in decreased oxidative phosphorylation capability, increased lactate generation, and fast glycolytic flow, all of which indicate impaired Krebs cycle activity and are typical of the Warburg effect (Yang et al., 2010). Thus, FH functions as a tumor suppressor gene. In addition, excess fumarate is an oncometabolite in itself. The dysregulation of the hypoxia inducible factor (HIF) family of transcription factors is central to the oncogenic pathways of renal cell carcinomas. Mutations in the oncogenic driver Von Hippel Landau (VHL) gene, for example, hinder the VHL protein's ability to ubiquitinate HIFs for

further degradation. The accumulation of fumarate in FH null cells blocks the prolyl hydroxylase of HIF1, causing HIFs to fail to be identified by VHL and therefore accumulate. This accumulation and dysregulation may result in the renal cell carcinoma oncogenic pathway (Isaacs et al., 2005). As mentioned above, although diseases related to FH have been well studied, diseases related to SDH, an enzyme with the opposite role to FH, are rare in humans, but there are several disease cases. SDH is encoded by four nuclear genes and the structure of SDH genes are conserved throughout evolution. The SDHA mutations, the first mutations in a nuclear gene discovered to produce a mitochondrial RC deficiency cause classic mitochondrial encephalopathy, namely Leigh syndrome (Bourgeron et al., 1995; Parfait et al., 2000). Subunit B, C, and D mutations have recently been linked to paraganglioma and phaeochromocytomas, both of which are benign vascularized tumors of the head and neck (Astuti et al., 2001; Baysal *et al.*, 2000; Niemann and Müller, 2000).

A variety of physiological impacts due to increased protein succination

In several biological processes, succination at cysteine residues of proteins can result in loss of enzymatic activity or protein function. Succination of essential members of the iron-sulfur cluster biogenesis family of proteins, including Iscu and Nfu1, causes defects in iron-sulfur biosynthesis, which is required for respiratory chain complexes (Tyrakis et al., 2017). In addition to the loss of fumarate hydratase, hyperpolarization of the inner mitochondrial membrane, in combination with mitochondrial, ER, and oxidative stress, increases intracellular fumarate concentration and protein succination in 3T3 adipocytes grown in high glucose medium (Nagai et al., 2007). And also, in the epididymal, subcutaneous, and mesenteric adipocytes of the db/db (leptin receptor deficient) obese mouse, an animal model of type 2 diabetes, similar elevations and patterns of protein succination were observed (Frizzell et al., 2009). Succination was similarly enhanced in the ob/ob (leptin deficient) mouse's adipose tissue, and to a lesser level in the diet induced obese (DIO) mouse, which is insulin resistant but not diabetic. Succination of adiponectin prevents the production of oligomeric species and secretory forms of the protein, resulting in lower levels of plasma adiponectin in diabetes (Thomas *et al.*, 2012). According to these previous reports that show increased succination in high glucose medium or in a diabetic mouse, it is reasonable to predict

that hyperglycemia in my experiments would enhance SERCA succination.

From the above results, it was confirmed that the physiology of survival was different depending on the succination. In contrast to WT flies, fumarate-induced succination of SERCA does not occur in SERCA C876S KI flies, resulting in no fumarate-induced calcium change in my results. In WT, increased fumarate by the high sugar diet inhibited SERCA and altered calcium homeostasis. This calcium alteration may have an effect on insulin secretion, for example, so that WT was lethal. However, in C876S KI, calcium did not change even during HSD, so C876S KI would have survived under normal insulin secretion. Therefore, it is necessary to conduct an experiment to check insulin producing cells (IPCs) by dilp2 staining or mRNA level measurement to see if there is a difference in insulin secretion in WT and C876S KI.

Relationship between calcium homeostasis and cardiac functions

Calcium plays an important role in the electrical activity and pumping function of the heart. The heart is driven by regular excitations generated in the sinus node as the natural pacemaker. In the diastolic depolarization (DD) phase of the action potential (AP), a delicate balance of inward and outward transmembrane currents, as well as the intricate interplay of the calcium and membrane clocks, known as the coupled clock mechanism, regulate the spontaneous beating of sinus node myocytes and its rate (Tsutsui et al., 2018; Yaniv et al., 2015). Calcium also binds to machinery within the cell that helps the cell to squeeze together, which makes the heart pump blood. It is widely established that heart muscle contraction requires intracellular calcium release from the sarcoplasmic reticulum. Indeed, the calcium content in the cytosol of cardiac myocytes increases 10-fold with each heartbeat, from a resting level of 100 nM to 1 M (Marks et al., 2002). Because the level of calcium elevation during systole is directly related to the contraction of heart muscle, a failure in signaling that precludes effective elevation of cytosolic calcium would presumably affect contractility. A failure in calcium removal from the cytosol during diastole, on the other hand, would impair cardiac relaxation, which is critical because it permits the heart chambers to refill with blood in preparation for the next beat (Marks, 2003).

Further works on Part II

In the above experiments, it was assumed that the amount of fumarate would increase due to activation of the TCA cycle under high glucose conditions. However, I have not actually measured whether the amount of fumarate increased in high glucose conditions, and this measurement is an experiment that must be done in the future. I plan to conduct an experiment with Dr. Cholsoon Jang at UC Irvine to directly measure the level of fumarate produced when a high concentration of glucose, which can be traced using isotope labeling, is treated. However, according to the paper that measured the amount of metabolites in the TCA cycle under high glucose (55 mM), it was shown to increase the amount of metabolites produced by the TCA cycle (Jiang et al., 2018). And in my experiment, it was confirmed that the SERCA inhibition effect increased as the concentration of high glucose increased (50 mM, 100 mM) **(Fig. 75)**. As a result, I believe that the amount of fumarate will increase at the high glucose concentration I tested, and thus SERCA inhibition will increase.

Next, various experiments to find the physiological meaning of the part II are still in progress. Among them, tachycardia was confirmed as a result of SERCA inhibition in WT flies fed a high sugar diet. However, these results were obtained when HSD was fed for a short period of time (48hrs). If SERCA inhibition persists for a long term, intracellular calcium

homeostasis is impaired because calcium reuptake does not occur in the ER, and heart beat will eventually decrease. However, in the short term, I believe it is a phenomenon that the heart beat is temporarily increased due to an increase in cytosol calcium, as demonstrated by my experimental results. The correlations between calcium and heartbeat are not explained clearly in these studies. Therefore, I will continue to investigate the correlation between the heart and intracellular calcium homeostasis by using specific GAL4 expressed in the heart.

Conclusion

Since maintaining intracellular calcium homeostasis is essential, I tried to comprehend and clarify the mechanism of several calcium channels that regulate calcium homeostasis. As a result of various experiments, an important calcium regulation mechanism in the pathogenesis of Parkinson's disease was discovered, and a treatment for it was proposed. Furthermore, I identified a novel factor that regulates intracellular calcium homeostasis by modulating SERCA activity, and I attempted to decipher its physiological significance.

In part I, I discovered that PINK1 and Parkin, the causing genes of Parkinson's disease, manipulate the activity of IP_3R, thereby regulating ER calcium release, and that this alteration in calcium homeostasis results in the occurrence of PD-related phenotypes in PINK1 and Parkin null flies. It was also confirmed that CISD1, which is downstream of the PINK1-Parkin pathway, interacts directly with IP_3R and that Parkin specifically ubiquitinates CISD1. As a result, I observed that CISD knockdown rescues PD-related phenotypes in PINK1 and Parkin null flies by restoring impaired calcium homeostasis. Finally, I discovered that pioglitazone, which is used to treat Type 2 diabetes, inhibits the interaction between IP_3R and CISD. Following that, pioglitazone treatment alleviated the PD-related phenotypes caused by PINK1 and Parkin deficiency in both mammalian cells and *Drosophila*, so it was proposed as a therapeutic drug for PD.

In part II, I performed a genetic screen and discovered that fumarate, a TCA cycle intermediate metabolite, may alters calcium homeostasis. In addition, I found that fumarate causes SERCA to be inhibited by a PTM known as succination on the cysteine 876 residue. When cysteine 876 of SERCA was substituted with serine, the inhibition of SERCA by fumarate did not occur in mammalian cells or *Drosophila*. Then I discovered that when *Drosophila* were given a high sugar diet (HSD) to induce hyperglycemia, symptoms of tachycardia occurred in WT but not in SERCA C876S, suggesting that fumarate can be an endogenous regulator of intracellular calcium homeostasis in response to cellular metabolic activities.

I believe that my studies will contribute significantly to a better understanding of the role of intracellular calcium regulation in the pathogenesis of PD. And also, they will provide a deeper understanding of how metabolites regulate intracellular calcium homeostasis.

References

Akerboom, J., Carreras Calderón, N., Tian, L., Wabnig, S., Prigge, M., Tolö, J., Gordus, A., Orger, M.B., Severi, K.E., Macklin, J.J., et al. (2013). Genetically encoded calcium indicators for multi-color neural activity imaging and combination with optogenetics. Front Mol Neurosci *6*, 2-2. 10.3389/fnmol.2013.00002.

Andersen, J.L., Gesser, B., Funder, E.D., Nielsen, C.J.F., Gotfred-Rasmussen, H., Rasmussen, M.K., Toth, R., Gothelf, K.V., Arthur, J.S.C., Iversen, L., and Nissen, P. (2018). Dimethyl fumarate is an allosteric covalent inhibitor of the p90 ribosomal S6 kinases. Nat Commun *9*, 4344. 10.1038/s41467-018-06787-w.

Apell, H.J. (2003). Structure-function relationship in P-type ATPases--a biophysical approach. Rev Physiol Biochem Pharmacol *150*, 1-35. 10.1007/s10254-003-0018-9.

Astuti, D., Latif, F., Dallol, A., Dahia, P.L., Douglas, F., George, E., Sköldberg, F., Husebye, E.S., Eng, C., and Maher, E.R. (2001). Gene mutations in the succinate dehydrogenase subunit SDHB cause susceptibility to familial pheochromocytoma and to familial paraganglioma. Am J Hum Genet *69*, 49-54. 10.1086/321282.

Barazzuol, L., Giamogante, F., Brini, M., and Calì, T. (2020). PINK1/Parkin Mediated Mitophagy, Ca(2+) Signalling, and ER-Mitochondria Contacts in Parkinson's Disease. Int J Mol Sci *21*, 1772. 10.3390/ijms21051772.

Baughman, J.M., Perocchi, F., Girgis, H.S., Plovanich, M., Belcher-Timme, C.A., Sancak, Y., Bao, X.R., Strittmatter, L., Goldberger, O., Bogorad, R.L., et al. (2011). Integrative genomics identifies MCU as an essential component of the mitochondrial calcium uniporter. Nature *476*, 341-345. 10.1038/nature10234.

Baysal, B.E., Ferrell, R.E., Willett-Brozick, J.E., Lawrence, E.C., Myssiorek, D., Bosch, A., van der Mey, A., Taschner, P.E., Rubinstein, W.S., Myers, E.N., et al. (2000). Mutations in SDHD, a mitochondrial complex II gene, in hereditary paraganglioma. Science *287*, 848-851. 10.1126/science.287.5454.848.

Benn, D.E., Croxson, M.S., Tucker, K., Bambach, C.P., Richardson, A.L., Delbridge, L., Pullan, P.T., Hammond, J., Marsh, D.J., and Robinson, B.G. (2003). Novel succinate dehydrogenase subunit B (SDHB) mutations in familial phaeochromocytomas and paragangliomas, but an absence of somatic SDHB

mutations in sporadic phaeochromocytomas. Oncogene *22*, 1358-1364. 10.1038/sj.onc.1206300.

Bezprozvanny, I., and Ehrlich, B.E. (1993). ATP modulates the function of inositol 1,4,5-trisphosphate-gated channels at two sites. Neuron *10*, 1175-1184. 10.1016/0896-6273(93)90065-y.

Bi, J., Wang, W., Liu, Z., Huang, X., Jiang, Q., Liu, G., Wang, Y., and Huang, X. (2014). Seipin promotes adipose tissue fat storage through the ER Ca^{2+}-ATPase SERCA. Cell Metab *19*, 861-871. 10.1016/j.cmet.2014.03.028.

Blewett, M.M., Xie, J., Zaro, B.W., Backus, K.M., Altman, A., Teijaro, J.R., and Cravatt, B.F. (2016). Chemical proteomic map of dimethyl fumarate-sensitive cysteines in primary human T cells. Sci Signal *9*, rs10. 10.1126/scisignal.aaf7694.

Bonneau, B., Ando, H., Kawaai, K., Hirose, M., Takahashi-Iwanaga, H., and Mikoshiba, K. (2016). IRBIT controls apoptosis by interacting with the Bcl-2 homolog, Bcl2l10, and by promoting ER-mitochondria contact. Elife *5*. 10.7554/eLife.19896.

Bononi, A., Giorgi, C., Patergnani, S., Larson, D., Verbruggen, K., Tanji, M., Pellegrini, L., Signorato, V., Olivetto, F., Pastorino, S., et al. (2017). BAP1 regulates IP3R3-mediated Ca(2+) flux to mitochondria suppressing cell transformation. Nature *546*, 549-553. 10.1038/nature22798.

Bourgeron, T., Rustin, P., Chretien, D., Birch-Machin, M., Bourgeois, M., Viegas-Péquignot, E., Munnich, A., and Rötig, A. (1995). Mutation of a nuclear succinate dehydrogenase gene results in mitochondrial respiratory chain deficiency. Nat Genet *11*, 144-149. 10.1038/ng1095-144.

Brauer, R., Wei, L., Ma, T., Athauda, D., Girges, C., Vijiaratnam, N., Auld, G., Whittlesea, C., Wong, I., and Foltynie, T. (2020). Diabetes medications and risk of Parkinson's disease: a cohort study of patients with diabetes. Brain *143*, 3067-3076. 10.1093/brain/awaa262.

Britzolaki, A., Saurine, J., Klocke, B., and Pitychoutis, P.M. (2020). A Role for SERCA Pumps in the Neurobiology of Neuropsychiatric and Neurodegenerative Disorders. In Calcium Signaling, M.S. Islam, ed. (Springer International Publishing), pp. 131-161. 10.1007/978-3-030-12457-1_6.

Browne, P., Chandraratna, D., Angood, C., Tremlett, H., Baker, C., Taylor, B.V.,

and Thompson, A.J. (2014). Atlas of Multiple Sclerosis 2013: A growing global problem with widespread inequity. Neurology *83*, 1022-1024. 10.1212/WNL.0000000000000768.

Camara, A.K.S., Zhou, Y., Wen, P.-C., Tajkhorshid, E., and Kwok, W.-M. (2017). Mitochondrial VDAC1: A Key Gatekeeper as Potential Therapeutic Target. Frontiers in Physiology *8*. 10.3389/fphys.2017.00460.

Carreras-Sureda, A., Pihán, P., and Hetz, C. (2018). Calcium signaling at the endoplasmic reticulum: fine-tuning stress responses. Cell Calcium *70*, 24-31. 10.1016/j.ceca.2017.08.004.

Cha, G.-H., Kim, S., Park, J., Lee, E., Kim, M., Lee Sung, B., Kim Jin, M., Chung, J., and Cho Kyoung, S. (2005). Parkin negatively regulates JNK pathway in the dopaminergic neurons of Drosophila. Proceedings of the National Academy of Sciences *102*, 10345-10350. 10.1073/pnas.0500346102.

Chami, M., Gozuacik, D., Lagorce, D., Brini, M., Falson, P., Peaucellier, G., Pinton, P., Lecoeur, H., Gougeon, M.L., le Maire, M., et al. (2001). SERCA1 truncated proteins unable to pump calcium reduce the endoplasmic reticulum calcium concentration and induce apoptosis. The Journal of cell biology *153*, 1301-1314. 10.1083/jcb.153.6.1301.

Chang, N.C., Nguyen, M., Bourdon, J., Risse, P.A., Martin, J., Danialou, G., Rizzuto, R., Petrof, B.J., and Shore, G.C. (2012). Bcl-2-associated autophagy regulator Naf-1 required for maintenance of skeletal muscle. Hum Mol Genet *21*, 2277-2287. 10.1093/hmg/dds048.

Chang, Y.H., Yen, S.J., Chang, Y.H., Wu, W.J., and Lin, K.D. (2021). Pioglitazone and statins lower incidence of Parkinson disease in patients with diabetes mellitus. European Journal of Neurology *28*, 430-437. https://doi.org/10.1111/ene.14542.

Cherra, S.J., 3rd, Steer, E., Gusdon, A.M., Kiselyov, K., and Chu, C.T. (2013). Mutant LRRK2 elicits calcium imbalance and depletion of dendritic mitochondria in neurons. Am J Pathol *182*, 474-484. 10.1016/j.ajpath.2012.10.027.

Choi, S., Quan, X., Bang, S., Yoo, H., Kim, J., Park, J., Park, K.S., and Chung, J. (2017). Mitochondrial calcium uniporter in Drosophila transfers calcium between the endoplasmic reticulum and mitochondria in oxidative stress-

induced cell death. J Biol Chem *292*, 14473-14485. 10.1074/jbc.M116.765578.

Clapham, D.E. (2007). Calcium signaling. Cell *131*, 1047-1058. 10.1016/j.cell.2007.11.028.

Cockman, M.E., Masson, N., Mole, D.R., Jaakkola, P., Chang, G.W., Clifford, S.C., Maher, E.R., Pugh, C.W., Ratcliffe, P.J., and Maxwell, P.H. (2000). Hypoxia inducible factor-alpha binding and ubiquitylation by the von Hippel-Lindau tumor suppressor protein. J Biol Chem *275*, 25733-25741. 10.1074/jbc.M002740200.

Colca, J.R., McDonald, W.G., Waldon, D.J., Leone, J.W., Lull, J.M., Bannow, C.A., Lund, E.T., and Mathews, W.R. (2004). Identification of a novel mitochondrial protein ("mitoNEET") cross-linked specifically by a thiazolidinedione photoprobe. Am J Physiol Endocrinol Metab *286*, E252-260. 10.1152/ajpendo.00424.2003.

Compston, A., and Coles, A. (2008). Multiple sclerosis. Lancet *372*, 1502-1517. 10.1016/s0140-6736(08)61620-7.

Contreras, L., Drago, I., Zampese, E., and Pozzan, T. (2010). Mitochondria: The calcium connection. Biochimica et Biophysica Acta (BBA) - Bioenergetics *1797*, 607-618. https://doi.org/10.1016/j.bbabio.2010.05.005.

Csordás, G., Renken, C., Várnai, P., Walter, L., Weaver, D., Buttle, K.F., Balla, T., Mannella, C.A., and Hajnóczky, G. (2006). Structural and functional features and significance of the physical linkage between ER and mitochondria. J Cell Biol *174*, 915-921. 10.1083/jcb.200604016.

Danielpur, L., Sohn, Y.S., Karmi, O., Fogel, C., Zinger, A., Abu-Libdeh, A., Israeli, T., Riahi, Y., Pappo, O., Birk, R., et al. (2016). GLP-1-RA Corrects Mitochondrial Labile Iron Accumulation and Improves β-Cell Function in Type 2 Wolfram Syndrome. J Clin Endocrinol Metab *101*, 3592-3599. 10.1210/jc.2016-2240.

de Brito, O.M., and Scorrano, L. (2008). Mitofusin 2 tethers endoplasmic reticulum to mitochondria. Nature *456*, 605-610. 10.1038/nature07534.

De Stefani, D., Raffaello, A., Teardo, E., Szabò, I., and Rizzuto, R. (2011). A forty-kilodalton protein of the inner membrane is the mitochondrial calcium uniporter. Nature *476*, 336-340. 10.1038/nature10230.

Donohoe, D.R., Garge, N., Zhang, X., Sun, W., O'Connell, T.M., Bunger, M.K., and Bultman, S.J. (2011). The microbiome and butyrate regulate energy metabolism and autophagy in the mammalian colon. Cell Metab *13*, 517-526. 10.1016/j.cmet.2011.02.018.

Drui, G., Carnicella, S., Carcenac, C., Favier, M., Bertrand, A., Boulet, S., and Savasta, M. (2014). Loss of dopaminergic nigrostriatal neurons accounts for the motivational and affective deficits in Parkinson's disease. Mol Psychiatry *19*, 358-367. 10.1038/mp.2013.3.

Eng, C., Kiuru, M., Fernandez, M.J., and Aaltonen, L.A. (2003). A role for mitochondrial enzymes in inherited neoplasia and beyond. Nat Rev Cancer *3*, 193-202. 10.1038/nrc1013.

Ernster, L., and Dallner, G. (1995). Biochemical, physiological and medical aspects of ubiquinone function. Biochim Biophys Acta *1271*, 195-204. 10.1016/0925-4439(95)00028-3.

Essin, K., and Gollasch, M. (2009). Role of ryanodine receptor subtypes in initiation and formation of calcium sparks in arterial smooth muscle: comparison with striated muscle. J Biomed Biotechnol *2009*, 135249-135249. 10.1155/2009/135249.

Fan, G., Baker, M.L., Wang, Z., Baker, M.R., Sinyagovskiy, P.A., Chiu, W., Ludtke, S.J., and Serysheva, I.I. (2015). Gating machinery of InsP3R channels revealed by electron cryomicroscopy. Nature *527*, 336-341. 10.1038/nature15249.

Fernández-Veledo, S., and Vendrell, J. (2019). Gut microbiota-derived succinate: Friend or foe in human metabolic diseases? Rev Endocr Metab Disord *20*, 439-447. 10.1007/s11154-019-09513-z.

Frizzell, N., Rajesh, M., Jepson, M.J., Nagai, R., Carson, J.A., Thorpe, S.R., and Baynes, J.W. (2009). Succination of thiol groups in adipose tissue proteins in diabetes: succination inhibits polymerization and secretion of adiponectin. J Biol Chem *284*, 25772-25781. 10.1074/jbc.M109.019257.

Gandhi, S., Wood-Kaczmar, A., Yao, Z., Plun-Favreau, H., Deas, E., Klupsch, K., Downward, J., Latchman, D.S., Tabrizi, S.J., Wood, N.W., et al. (2009). PINK1-associated Parkinson's disease is caused by neuronal vulnerability to calcium-induced cell death. Mol Cell *33*, 627-638. 10.1016/j.molcel.2009.02.013.

Giguère, N., Burke Nanni, S., and Trudeau, L.E. (2018). On Cell Loss and Selective Vulnerability of Neuronal Populations in Parkinson's Disease. Front Neurol *9*, 455. 10.3389/fneur.2018.00455.

Gillard, G.O., Collette, B., Anderson, J., Chao, J., Scannevin, R.H., Huss, D.J., and Fontenot, J.D. (2015). DMF, but not other fumarates, inhibits NF-κB activity in vitro in an Nrf2-independent manner. J Neuroimmunol *283*, 74-85. 10.1016/j.jneuroim.2015.04.006.

Glaves, J.P., Primeau, J.O., Espinoza-Fonseca, L.M., Lemieux, M.J., and Young, H.S. (2019). The Phospholamban Pentamer Alters Function of the Sarcoplasmic Reticulum Calcium Pump SERCA. Biophysical journal *116*, 633-647. 10.1016/j.bpj.2019.01.013.

Golinelli-Cohen, M.P., Lescop, E., Mons, C., Gonçalves, S., Clémancey, M., Santolini, J., Guittet, E., Blondin, G., Latour, J.M., and Bouton, C. (2016). Redox Control of the Human Iron-Sulfur Repair Protein MitoNEET Activity via Its Iron-Sulfur Cluster. J Biol Chem *291*, 7583-7593. 10.1074/jbc.M115.711218.

Gorski, P.A., Trieber, C.A., Ashrafi, G., and Young, H.S. (2015). Regulation of the sarcoplasmic reticulum calcium pump by divergent phospholamban isoforms in zebrafish. The Journal of biological chemistry *290*, 6777-6788. 10.1074/jbc.M114.585604.

Guzman, J.N., Ilijic, E., Yang, B., Sanchez-Padilla, J., Wokosin, D., Galtieri, D., Kondapalli, J., Schumacker, P.T., and Surmeier, D.J. (2018). Systemic isradipine treatment diminishes calcium-dependent mitochondrial oxidant stress. J Clin Invest *128*, 2266-2280. 10.1172/jci95898.

Ham, S.J., Lee, D., Xu, W.J., Cho, E., Choi, S., Min, S., Park, S., and Chung, J. (2021). Loss of UCHL1 rescues the defects related to Parkinson's disease by suppressing glycolysis. Sci Adv *7*. 10.1126/sciadv.abg4574.

Ham Su, J., Lee, D., Yoo, H., Jun, K., Shin, H., and Chung, J. (2020). Decision between mitophagy and apoptosis by Parkin via VDAC1 ubiquitination. Proceedings of the National Academy of Sciences *117*, 4281-4291. 10.1073/pnas.1909814117.

Hamada, K., Miyatake, H., Terauchi, A., and Mikoshiba, K. (2017). IP(3)-mediated gating mechanism of the IP(3) receptor revealed by mutagenesis and

X-ray crystallography. Proceedings of the National Academy of Sciences of the United States of America *114*, 4661-4666. 10.1073/pnas.1701420114.

Heyland, J., Fu, J., and Blank, L.M. (2009). Correlation between TCA cycle flux and glucose uptake rate during respiro-fermentative growth of Saccharomyces cerevisiae. Microbiology *155*, 3827-3837. https://doi.org/10.1099/mic.0.030213-0.

Hoffman, N.E., Chandramoorthy, H.C., Shanmughapriya, S., Zhang, X.Q., Vallem, S., Doonan, P.J., Malliankaraman, K., Guo, S., Rajan, S., Elrod, J.W., et al. (2014). SLC25A23 augments mitochondrial Ca^{2+} uptake, interacts with MCU, and induces oxidative stress-mediated cell death. Mol Biol Cell *25*, 936-947. 10.1091/mbc.E13-08-0502.

Holt, S.H., Darash-Yahana, M., Sohn, Y.S., Song, L., Karmi, O., Tamir, S., Michaeli, D., Luo, Y., Paddock, M.L., Jennings, P.A., et al. (2016). Activation of apoptosis in NAF-1-deficient human epithelial breast cancer cells. J Cell Sci *129*, 155-165. 10.1242/jcs.178293.

Hsu, C.-C., Tseng, L.-M., and Lee, H.-C. (2016). Role of mitochondrial dysfunction in cancer progression. Exp Biol Med (Maywood) *241*, 1281-1295. 10.1177/1535370216641787.

Huang, E., Qu, D., Huang, T., Rizzi, N., Boonying, W., Krolak, D., Ciana, P., Woulfe, J., Klein, C., Slack, R.S., et al. (2017). PINK1-mediated phosphorylation of LETM1 regulates mitochondrial calcium transport and protects neurons against mitochondrial stress. Nature Communications *8*, 1399. 10.1038/s41467-017-01435-1.

Introini, V., Crick, A., Tiffert, T., Kotar, J., Lin, Y.C., Cicuta, P., and Lew, V.L. (2018). Evidence against a Role of Elevated Intracellular Ca(2+) during Plasmodium falciparum Preinvasion. Biophys J *114*, 1695-1706. 10.1016/j.bpj.2018.02.023.

Isaacs, J.S., Jung, Y.J., Mole, D.R., Lee, S., Torres-Cabala, C., Chung, Y.-L., Merino, M., Trepel, J., Zbar, B., Toro, J., et al. (2005). HIF overexpression correlates with biallelic loss of fumarate hydratase in renal cancer: Novel role of fumarate in regulation of HIF stability. Cancer Cell *8*, 143-153. https://doi.org/10.1016/j.ccr.2005.06.017.

Isradipine Versus Placebo in Early Parkinson Disease: A Randomized Trial. (2020). Ann Intern Med *172*, 591-598. 10.7326/m19-2534.

Jiang, B.-p., Lv, Q.-y., Xiang, J.-m., Le, L., Hu, K.-p., Xu, L.-j., and Xiao, P.-g. (2018). Inhibition of metabolic disorders in vivo and in vitro by main constituent of Coreopsis tinctoria. Chinese Herbal Medicines *10*, 157-168. https://doi.org/10.1016/j.chmed.2018.03.004.

Jiang, D., Zhao, L., and Clapham, D.E. (2009). Genome-wide RNAi screen identifies Letm1 as a mitochondrial Ca2+/H+ antiporter. Science *326*, 144-147. 10.1126/science.1175145.

Jiang, D., Zhao, L., Clish, C.B., and Clapham, D.E. (2013). Letm1, the mitochondrial Ca2+/H+ antiporter, is essential for normal glucose metabolism and alters brain function in Wolf-Hirschhorn syndrome. Proc Natl Acad Sci U S A *110*, E2249-2254. 10.1073/pnas.1308558110.

Jiang, X., Jin, T., Zhang, H., Miao, J., Zhao, X., Su, Y., and Zhang, Y. (2019). Current Progress of Mitochondrial Quality Control Pathways Underlying the Pathogenesis of Parkinson's Disease. Oxid Med Cell Longev *2019*, 4578462. 10.1155/2019/4578462.

Kaelin, W.G., Jr. (2002). Molecular basis of the VHL hereditary cancer syndrome. Nat Rev Cancer *2*, 673-682. 10.1038/nrc885.

Kent, A.C., El Baradie, K.B.Y., and Hamrick, M.W. (2021). Targeting the Mitochondrial Permeability Transition Pore to Prevent Age-Associated Cell Damage and Neurodegeneration. Oxid Med Cell Longev *2021*, 6626484-6626484. 10.1155/2021/6626484.

Khaliq, Z.M., and Bean, B.P. (2010). Pacemaking in dopaminergic ventral tegmental area neurons: depolarizing drive from background and voltage-dependent sodium conductances. J Neurosci *30*, 7401-7413. 10.1523/jneurosci.0143-10.2010.

Kim, U., Kim, C.Y., Lee, J.M., Oh, H., Ryu, B., Kim, J., and Park, J.H. (2020). Correction to: Phloretin Inhibits the Human Prostate Cancer Cells through the Generation of Reactive Oxygen Species. Pathol Oncol Res *26*, 2011-2012. 10.1007/s12253-019-00667-4.

Kiuru, M., Launonen, V., Hietala, M., Aittomäki, K., Vierimaa, O., Salovaara,

R., Arola, J., Pukkala, E., Sistonen, P., Herva, R., and Aaltonen, L.A. (2001). Familial cutaneous leiomyomatosis is a two-hit condition associated with renal cell cancer of characteristic histopathology. Am J Pathol *159*, 825-829. 10.1016/s0002-9440(10)61757-9.

Kornberg, M.D., Bhargava, P., Kim, P.M., Putluri, V., Snowman, A.M., Putluri, N., Calabresi, P.A., and Snyder, S.H. (2018). Dimethyl fumarate targets GAPDH and aerobic glycolysis to modulate immunity. Science *360*, 449-453. 10.1126/science.aan4665.

Kostic, M., Ludtmann, M.H., Bading, H., Hershfinkel, M., Steer, E., Chu, C.T., Abramov, A.Y., and Sekler, I. (2015). PKA Phosphorylation of NCLX Reverses Mitochondrial Calcium Overload and Depolarization, Promoting Survival of PINK1-Deficient Dopaminergic Neurons. Cell Rep *13*, 376-386. 10.1016/j.celrep.2015.08.079.

Kusminski, C.M., Chen, S., Ye, R., Sun, K., Wang, Q.A., Spurgin, S.B., Sanders, P.E., Brozinick, J.T., Geldenhuys, W.J., Li, W.H., et al. (2016). MitoNEET-Parkin Effects in Pancreatic α- and β-Cells, Cellular Survival, and Intrainsular Cross Talk. Diabetes *65*, 1534-1555. 10.2337/db15-1323.

Kusminski, C.M., Holland, W.L., Sun, K., Park, J., Spurgin, S.B., Lin, Y., Askew, G.R., Simcox, J.A., McClain, D.A., Li, C., and Scherer, P.E. (2012). MitoNEET-driven alterations in adipocyte mitochondrial activity reveal a crucial adaptive process that preserves insulin sensitivity in obesity. Nat Med *18*, 1539-1549. 10.1038/nm.2899.

Kwak, C., Shin, S., Park, J.-S., Jung, M., Nhung Truong Thi, M., Kang, M.-G., Lee, C., Kwon, T.-H., Park Sang, K., Mun Ji, Y., et al. (2020). Contact-ID, a tool for profiling organelle contact sites, reveals regulatory proteins of mitochondrial-associated membrane formation. Proceedings of the National Academy of Sciences *117*, 12109-12120. 10.1073/pnas.1916584117.

Lin, H., Su, X., and He, B. (2012). Protein lysine acylation and cysteine succination by intermediates of energy metabolism. ACS Chem Biol *7*, 947-960. 10.1021/cb3001793.

Lin, J., Zhou, T., Ye, K., and Wang, J. (2007). Crystal structure of human mitoNEET reveals distinct groups of iron–sulfur proteins. Proceedings of the

National Academy of Sciences *104*, 14640-14645. 10.1073/pnas.0702426104.

Linker, R.A., Lee, D.H., Ryan, S., van Dam, A.M., Conrad, R., Bista, P., Zeng, W., Hronowsky, X., Buko, A., Chollate, S., et al. (2011). Fumaric acid esters exert neuroprotective effects in neuroinflammation via activation of the Nrf2 antioxidant pathway. Brain *134*, 678-692. 10.1093/brain/awq386.

Mammucari, C., Raffaello, A., Vecellio Reane, D., Gherardi, G., De Mario, A., and Rizzuto, R. (2018). Mitochondrial calcium uptake in organ physiology: from molecular mechanism to animal models. Pflügers Archiv - European Journal of Physiology *470*, 1165-1179. 10.1007/s00424-018-2123-2.

Marks, A.R. (2003). Calcium and the heart: a question of life and death. The Journal of clinical investigation *111*, 597-600. 10.1172/JCI18067.

Marks, A.R., Reiken, S., and Marx, S.O. (2002). Progression of heart failure: is protein kinase a hyperphosphorylation of the ryanodine receptor a contributing factor? Circulation *105*, 272-275.

Marongiu, R., Spencer, B., Crews, L., Adame, A., Patrick, C., Trejo, M., Dallapiccola, B., Valente, E.M., and Masliah, E. (2009). Mutant Pink1 induces mitochondrial dysfunction in a neuronal cell model of Parkinson's disease by disturbing calcium flux. J Neurochem *108*, 1561-1574. 10.1111/j.1471-4159.2009.05932.x.

Matteucci, A., Patron, M., Vecellio Reane, D., Gastaldello, S., Amoroso, S., Rizzuto, R., Brini, M., Raffaello, A., and Calì, T. (2018). Parkin-dependent regulation of the MCU complex component MICU1. Scientific Reports *8*, 14199. 10.1038/s41598-018-32551-7.

Merkley, E.D., Metz, T.O., Smith, R.D., Baynes, J.W., and Frizzell, N. (2014). The succinated proteome. Mass Spectrom Rev *33*, 98-109. 10.1002/mas.21382.

Mhyre, T.R., Boyd, J.T., Hamill, R.W., and Maguire-Zeiss, K.A. (2012). Parkinson's disease. Subcell Biochem *65*, 389-455. 10.1007/978-94-007-5416-4_16.

Mittler, R., Darash-Yahana, M., Sohn, Y.S., Bai, F., Song, L., Cabantchik, I.Z., Jennings, P.A., Onuchic, J.N., and Nechushtai, R. (2019). NEET Proteins: A New Link Between Iron Metabolism, Reactive Oxygen Species, and Cancer. Antioxid Redox Signal *30*, 1083-1095. 10.1089/ars.2018.7502.

Modesti, L., Danese, A., Angela Maria Vitto, V., Ramaccini, D., Aguiari, G., Gafà, R., Lanza, G., Giorgi, C., and Pinton, P. (2021). Mitochondrial Ca2+ Signaling in Health, Disease and Therapy. Cells *10*. 10.3390/cells10061317.

Moi, P., Chan, K., Asunis, I., Cao, A., and Kan, Y.W. (1994). Isolation of NF-E2-related factor 2 (Nrf2), a NF-E2-like basic leucine zipper transcriptional activator that binds to the tandem NF-E2/AP1 repeat of the beta-globin locus control region. Proc Natl Acad Sci U S A *91*, 9926-9930. 10.1073/pnas.91.21.9926.

Montes Diaz, G., Hupperts, R., Fraussen, J., and Somers, V. (2018). Dimethyl fumarate treatment in multiple sclerosis: Recent advances in clinical and immunological studies. Autoimmunity Reviews *17*, 1240-1250. https://doi.org/10.1016/j.autrev.2018.07.001.

Moon, H.E., and Paek, S.H. (2015). Mitochondrial Dysfunction in Parkinson's Disease. Exp Neurobiol *24*, 103-116. 10.5607/en.2015.24.2.103.

Mrowietz, U., Altmeyer, P., Bieber, T., Röcken, M., Schopf, R.E., and Sterry, W. (2007). Treatment of psoriasis with fumaric acid esters (Fumaderm). J Dtsch Dermatol Ges *5*, 716-717. 10.1111/j.1610-0387.2007.06346.x.

Mrowietz, U., Christophers, E., and Altmeyer, P. (1998). Treatment of psoriasis with fumaric acid esters: results of a prospective multicentre study. German Multicentre Study. Br J Dermatol *138*, 456-460. 10.1046/j.1365-2133.1998.02124.x.

Na, J., Musselman, L.P., Pendse, J., Baranski, T.J., Bodmer, R., Ocorr, K., and Cagan, R. (2013a). A Drosophila model of high sugar diet-induced cardiomyopathy. PLoS Genet *9*, e1003175. 10.1371/journal.pgen.1003175.

Na, J., Musselman, L.P., Pendse, J., Baranski, T.J., Bodmer, R., Ocorr, K., and Cagan, R. (2013b). A Drosophila Model of High Sugar Diet-Induced Cardiomyopathy. PLOS Genetics *9*, e1003175. 10.1371/journal.pgen.1003175.

Nagai, R., Brock, J.W., Blatnik, M., Baatz, J.E., Bethard, J., Walla, M.D., Thorpe, S.R., Baynes, J.W., and Frizzell, N. (2007). Succination of protein thiols during adipocyte maturation: a biomarker of mitochondrial stress. J Biol Chem *282*, 34219-34228. 10.1074/jbc.M703551200.

Nechushtai, R., Karmi, O., Zuo, K., Marjault, H.-B., Darash-Yahana, M., Sohn,

Y.-S., King, S.D., Zandalinas, S.I., Carloni, P., and Mittler, R. (2020). The balancing act of NEET proteins: Iron, ROS, calcium and metabolism. Biochimica et Biophysica Acta (BBA) - Molecular Cell Research *1867*, 118805. https://doi.org/10.1016/j.bbamcr.2020.118805.

Nemani, N., Dong, Z., Daw, C.C., Madaris, T.R., Ramachandran, K., Enslow, B.T., Rubannelsonkumar, C.S., Shanmughapriya, S., Mallireddigari, V., Maity, S., et al. (2020). Mitochondrial pyruvate and fatty acid flux modulate MICU1-dependent control of MCU activity. Sci Signal *13*. 10.1126/scisignal.aaz6206.

Niemann, S., and Müller, U. (2000). Mutations in SDHC cause autosomal dominant paraganglioma, type 3. Nat Genet *26*, 268-270. 10.1038/81551.

Orrenius, S., Zhivotovsky, B., and Nicotera, P. (2003). Regulation of cell death: the calcium–apoptosis link. Nature Reviews Molecular Cell Biology *4*, 552-565. 10.1038/nrm1150.

Paddock, M.L., Wiley, S.E., Axelrod, H.L., Cohen, A.E., Roy, M., Abresch, E.C., Capraro, D., Murphy, A.N., Nechushtai, R., Dixon, J.E., and Jennings, P.A. (2007). MitoNEET is a uniquely folded 2Fe 2S outer mitochondrial membrane protein stabilized by pioglitazone. Proc Natl Acad Sci U S A *104*, 14342-14347. 10.1073/pnas.0707189104.

Paillusson, S., Stoica, R., Gomez-Suaga, P., Lau, D.H.W., Mueller, S., Miller, T., and Miller, C.C.J. (2016). There's Something Wrong with my MAM; the ER-Mitochondria Axis and Neurodegenerative Diseases. Trends Neurosci *39*, 146-157. 10.1016/j.tins.2016.01.008.

Paknejad, N., and Hite, R.K. (2018). Structural basis for the regulation of inositol trisphosphate receptors by Ca2+ and IP3. Nature Structural & Molecular Biology *25*, 660-668. 10.1038/s41594-018-0089-6.

Panarsky, R., Crooks, D.R., Lane, A.N., Yang, Y., Cassel, T.A., Fan, T.W., Linehan, W.M., and Moscow, J.A. (2020). Fumarate hydratase-deficient renal cell carcinoma cells respond to asparagine by activation of the unfolded protein response and stimulation of the hexosamine biosynthetic pathway. Cancer Metab *8*, 7. 10.1186/s40170-020-00214-9.

Parfait, B., Chretien, D., Rötig, A., Marsac, C., Munnich, A., and Rustin, P. (2000). Compound heterozygous mutations in the flavoprotein gene of the

respiratory chain complex II in a patient with Leigh syndrome. Hum Genet *106*, 236-243. 10.1007/s004390051033.

Park, J., Lee, S.B., Lee, S., Kim, Y., Song, S., Kim, S., Bae, E., Kim, J., Shong, M., Kim, J.-M., and Chung, J. (2006). Mitochondrial dysfunction in Drosophila PINK1 mutants is complemented by parkin. Nature *441*, 1157-1161. 10.1038/nature04788.

Park, S.J., Jeong, J., Park, Y.U., Park, K.S., Lee, H., Lee, N., Kim, S.M., Kuroda, K., Nguyen, M.D., Kaibuchi, K., and Park, S.K. (2015). Disrupted-in-schizophrenia-1 (DISC1) Regulates Endoplasmic Reticulum Calcium Dynamics. Sci Rep *5*, 8694. 10.1038/srep08694.

Perocchi, F., Gohil, V.M., Girgis, H.S., Bao, X.R., McCombs, J.E., Palmer, A.E., and Mootha, V.K. (2010). MICU1 encodes a mitochondrial EF hand protein required for Ca2+ uptake. Nature *467*, 291-296. 10.1038/nature09358.

Pioglitazone in early Parkinson's disease: a phase 2, multicentre, double-blind, randomised trial. (2015). Lancet Neurol *14*, 795-803. 10.1016/s1474-4422(15)00144-1.

Plovanich, M., Bogorad, R.L., Sancak, Y., Kamer, K.J., Strittmatter, L., Li, A.A., Girgis, H.S., Kuchimanchi, S., De Groot, J., Speciner, L., et al. (2013). MICU2, a paralog of MICU1, resides within the mitochondrial uniporter complex to regulate calcium handling. PLoS One *8*, e55785. 10.1371/journal.pone.0055785.

Pollard, P.J., Spencer-Dene, B., Shukla, D., Howarth, K., Nye, E., El-Bahrawy, M., Deheragoda, M., Joannou, M., McDonald, S., Martin, A., et al. (2007). Targeted inactivation of fh1 causes proliferative renal cyst development and activation of the hypoxia pathway. Cancer Cell *11*, 311-319. 10.1016/j.ccr.2007.02.005.

Prinz, J.C. (2003). The role of T cells in psoriasis. J Eur Acad Dermatol Venereol *17*, 257-270. 10.1046/j.1468-3083.2003.00720.x.

Raffaello, A., De Stefani, D., Sabbadin, D., Teardo, E., Merli, G., Picard, A., Checchetto, V., Moro, S., Szabò, I., and Rizzuto, R. (2013). The mitochondrial calcium uniporter is a multimer that can include a dominant-negative pore-forming subunit. Embo j *32*, 2362-2376. 10.1038/emboj.2013.157.

Raffaello, A., Mammucari, C., Gherardi, G., and Rizzuto, R. (2016a). Calcium

at the Center of Cell Signaling: Interplay between Endoplasmic Reticulum, Mitochondria, and Lysosomes. Trends Biochem Sci *41*, 1035-1049. 10.1016/j.tibs.2016.09.001.

Raffaello, A., Mammucari, C., Gherardi, G., and Rizzuto, R. (2016b). Calcium at the Center of Cell Signaling: Interplay between Endoplasmic Reticulum, Mitochondria, and Lysosomes. Trends in biochemical sciences *41*, 1035-1049. 10.1016/j.tibs.2016.09.001.

Ran, F.A., Hsu, P.D., Wright, J., Agarwala, V., Scott, D.A., and Zhang, F. (2013). Genome engineering using the CRISPR-Cas9 system. Nature Protocols *8*, 2281-2308. 10.1038/nprot.2013.143.

Rcom-H'cheo-Gauthier, A., Goodwin, J., and Pountney, D.L. (2014). Interactions between calcium and alpha-synuclein in neurodegeneration. Biomolecules *4*, 795-811. 10.3390/biom4030795.

Rizzuto, R., Pinton, P., Carrington, W., Fay, F.S., Fogarty, K.E., Lifshitz, L.M., Tuft, R.A., and Pozzan, T. (1998). Close contacts with the endoplasmic reticulum as determinants of mitochondrial Ca2+ responses. Science *280*, 1763-1766. 10.1126/science.280.5370.1763.

Rossi, A., Pizzo, P., and Filadi, R. (2019). Calcium, mitochondria and cell metabolism: A functional triangle in bioenergetics. Biochimica et Biophysica Acta (BBA) - Molecular Cell Research *1866*, 1068-1078. https://doi.org/10.1016/j.bbamcr.2018.10.016.

Rouzier, C., Moore, D., Delorme, C., Lacas-Gervais, S., Ait-El-Mkadem, S., Fragaki, K., Burté, F., Serre, V., Bannwarth, S., Chaussenot, A., et al. (2017). A novel CISD2 mutation associated with a classical Wolfram syndrome phenotype alters Ca2+ homeostasis and ER-mitochondria interactions. Hum Mol Genet *26*, 1599-1611. 10.1093/hmg/ddx060.

Rowland, A.A., and Voeltz, G.K. (2012). Endoplasmic reticulum–mitochondria contacts: function of the junction. Nature Reviews Molecular Cell Biology *13*, 607-615. 10.1038/nrm3440.

Rustin, P., Bourgeron, T., Parfait, B., Chretien, D., Munnich, A., and Rötig, A. (1997). Inborn errors of the Krebs cycle: a group of unusual mitochondrial diseases in human. Biochim Biophys Acta *1361*, 185-197. 10.1016/s0925-

4439(97)00035-5.

Rustin, P., Munnich, A., and Rötig, A. (2002). Succinate dehydrogenase and human diseases: new insights into a well-known enzyme. European Journal of Human Genetics *10*, 289-291. 10.1038/sj.ejhg.5200793.

Saleem, H., Tovey, S.C., Riley, A.M., Potter, B.V., and Taylor, C.W. (2013). Stimulation of inositol 1,4,5-trisphosphate (IP3) receptor subtypes by adenophostin A and its analogues. PLoS One *8*, e58027. 10.1371/journal.pone.0058027.

Sandebring, A., Dehvari, N., Perez-Manso, M., Thomas, K.J., Karpilovski, E., Cookson, M.R., Cowburn, R.F., and Cedazo-Mínguez, A. (2009). Parkin deficiency disrupts calcium homeostasis by modulating phospholipase C signalling. Febs j *276*, 5041-5052. 10.1111/j.1742-4658.2009.07201.x.

Schober, R., Waldherr, L., Schmidt, T., Graziani, A., Stilianu, C., Legat, L., Groschner, K., and Schindl, R. (2019). STIM1 and Orai1 regulate Ca2+ microdomains for activation of transcription. Biochimica et Biophysica Acta (BBA) - Molecular Cell Research *1866*, 1079-1091. https://doi.org/10.1016/j.bbamcr.2018.11.001.

Scorziello, A., Borzacchiello, D., Sisalli, M.J., Di Martino, R., Morelli, M., and Feliciello, A. (2020). Mitochondrial Homeostasis and Signaling in Parkinson's Disease. Front Aging Neurosci *12*, 100-100. 10.3389/fnagi.2020.00100.

Shao, J., Fu, Z., Ji, Y., Guan, X., Guo, S., Ding, Z., Yang, X., Cong, Y., and Shen, Y. (2016). Leucine zipper-EF-hand containing transmembrane protein 1 (LETM1) forms a Ca2+/H+ antiporter. Scientific Reports *6*, 34174. 10.1038/srep34174.

Shen, Z.Q., Chen, Y.F., Chen, J.R., Jou, Y.S., Wu, P.C., Kao, C.H., Wang, C.H., Huang, Y.L., Chen, C.F., Huang, T.S., et al. (2017). CISD2 Haploinsufficiency Disrupts Calcium Homeostasis, Causes Nonalcoholic Fatty Liver Disease, and Promotes Hepatocellular Carcinoma. Cell Rep *21*, 2198-2211. 10.1016/j.celrep.2017.10.099.

Shiratori, R., Furuichi, K., Yamaguchi, M., Miyazaki, N., Aoki, H., Chibana, H., Ito, K., and Aoki, S. (2019). Glycolytic suppression dramatically changes the intracellular metabolic profile of multiple cancer cell lines in a mitochondrial

metabolism-dependent manner. Scientific Reports *9*, 18699. 10.1038/s41598-019-55296-3.

Soman, S., Keatinge, M., Moein, M., Da Costa, M., Mortiboys, H., Skupin, A., Sugunan, S., Bazala, M., Kuznicki, J., and Bandmann, O. (2017). Inhibition of the mitochondrial calcium uniporter rescues dopaminergic neurons in pink1(-/-) zebrafish. Eur J Neurosci *45*, 528-535. 10.1111/ejn.13473.

Surmeier, D.J., Obeso, J.A., and Halliday, G.M. (2017). Selective neuronal vulnerability in Parkinson disease. Nature Reviews Neuroscience *18*, 101-113. 10.1038/nrn.2016.178.

Suzuki, J., Kanemaru, K., Ishii, K., Ohkura, M., Okubo, Y., and Iino, M. (2014). Imaging intraorganellar Ca2+ at subcellular resolution using CEPIA. Nature Communications *5*, 4153. 10.1038/ncomms5153.

Swart, T., and Hurley, M.J. (2016). Calcium Channel Antagonists as Disease-Modifying Therapy for Parkinson's Disease: Therapeutic Rationale and Current Status. CNS Drugs *30*, 1127-1135. 10.1007/s40263-016-0393-9.

Szabadkai, G.r., Bianchi, K., Va´rnai, P.t., De Stefani, D., Wieckowski, M.R., Cavagna, D., Nagy, A.I., Balla, T.s., and Rizzuto, R. (2006). Chaperone-mediated coupling of endoplasmic reticulum and mitochondrial Ca2+ channels. Journal of Cell Biology *175*, 901-911. 10.1083/jcb.200608073.

Tadini-Buoninsegni, F., Smeazzetto, S., Gualdani, R., and Moncelli, M.R. (2018). Drug Interactions With the Ca2+-ATPase From Sarco(Endo)Plasmic Reticulum (SERCA). Frontiers in Molecular Biosciences *5*. 10.3389/fmolb.2018.00036.

Tamir, S., Paddock, M.L., Darash-Yahana-Baram, M., Holt, S.H., Sohn, Y.S., Agranat, L., Michaeli, D., Stofleth, J.T., Lipper, C.H., Morcos, F., et al. (2015a). Structure-function analysis of NEET proteins uncovers their role as key regulators of iron and ROS homeostasis in health and disease. Biochim Biophys Acta *1853*, 1294-1315. 10.1016/j.bbamcr.2014.10.014.

Tamir, S., Paddock, M.L., Darash-Yahana-Baram, M., Holt, S.H., Sohn, Y.S., Agranat, L., Michaeli, D., Stofleth, J.T., Lipper, C.H., Morcos, F., et al. (2015b). Structure–function analysis of NEET proteins uncovers their role as key regulators of iron and ROS homeostasis in health and disease. Biochimica et

Biophysica Acta (BBA) - Molecular Cell Research *1853*, 1294-1315. https://doi.org/10.1016/j.bbamcr.2014.10.014.

Tamir, S., Zuris, J.A., Agranat, L., Lipper, C.H., Conlan, A.R., Michaeli, D., Harir, Y., Paddock, M.L., Mittler, R., Cabantchik, Z.I., et al. (2013). Nutrient-deprivation autophagy factor-1 (NAF-1): biochemical properties of a novel cellular target for anti-diabetic drugs. PLoS One *8*, e61202. 10.1371/journal.pone.0061202.

Taylor, C.W., and Tovey, S.C. (2010). IP(3) receptors: toward understanding their activation. Cold Spring Harb Perspect Biol *2*, a004010-a004010. 10.1101/cshperspect.a004010.

Thillaiappan, N.B., Chakraborty, P., Hasan, G., and Taylor, C.W. (2019). IP3 receptors and Ca2+ entry. Biochimica et Biophysica Acta (BBA) - Molecular Cell Research *1866*, 1092-1100. https://doi.org/10.1016/j.bbamcr.2018.11.007.

Thomas, S.A., Storey, K.B., Baynes, J.W., and Frizzell, N. (2012). Tissue distribution of S-(2-succino)cysteine (2SC), a biomarker of mitochondrial stress in obesity and diabetes. Obesity (Silver Spring) *20*, 263-269. 10.1038/oby.2011.340.

Tomar, D., and Elrod, J.W. (2020). Metabolite regulation of the mitochondrial calcium uniporter channel. Cell calcium *92*, 102288-102288. 10.1016/j.ceca.2020.102288.

Tomlinson, I.P., Alam, N.A., Rowan, A.J., Barclay, E., Jaeger, E.E., Kelsell, D., Leigh, I., Gorman, P., Lamlum, H., Rahman, S., et al. (2002). Germline mutations in FH predispose to dominantly inherited uterine fibroids, skin leiomyomata and papillary renal cell cancer. Nat Genet *30*, 406-410. 10.1038/ng849.

Toyoshima, C., Nakasako, M., Nomura, H., and Ogawa, H. (2000). Crystal structure of the calcium pump of sarcoplasmic reticulum at 2.6 Å resolution. Nature *405*, 647-655. 10.1038/35015017.

Toyoshima, C., and Nomura, H. (2002). Structural changes in the calcium pump accompanying the dissociation of calcium. Nature *418*, 605-611. 10.1038/nature00944.

Tsutsui, K., Monfredi, O.J., Sirenko-Tagirova, S.G., Maltseva, L.A., Bychkov, R., Kim, M.S., Ziman, B.D., Tarasov, K.V., Tarasova, Y.S., Zhang, J., et al. (2018). A

coupled-clock system drives the automaticity of human sinoatrial nodal pacemaker cells. Science signaling *11*, eaap7608. 10.1126/scisignal.aap7608.

Tyrakis, P.A., Yurkovich, M.E., Sciacovelli, M., Papachristou, E.K., Bridges, H.R., Gaude, E., Schreiner, A., D'Santos, C., Hirst, J., Hernandez-Fernaud, J., et al. (2017). Fumarate Hydratase Loss Causes Combined Respiratory Chain Defects. Cell Rep *21*, 1036-1047. 10.1016/j.celrep.2017.09.092.

van Goor, M.K.C., Hoenderop, J.G.J., and van der Wijst, J. (2017). TRP channels in calcium homeostasis: from hormonal control to structure-function relationship of TRPV5 and TRPV6. Biochimica et Biophysica Acta (BBA) - Molecular Cell Research *1864*, 883-893. https://doi.org/10.1016/j.bbamcr.2016.11.027.

Vandecaetsbeek, I., Vangheluwe, P., Raeymaekers, L., Wuytack, F., and Vanoevelen, J. (2011). The Ca2+ pumps of the endoplasmic reticulum and Golgi apparatus. Cold Spring Harb Perspect Biol *3*, a004184. 10.1101/cshperspect.a004184.

Wang, C.H., Kao, C.H., Chen, Y.F., Wei, Y.H., and Tsai, T.F. (2014). Cisd2 mediates lifespan: is there an interconnection among Ca^{2+} homeostasis, autophagy, and lifespan? Free Radic Res *48*, 1109-1114. 10.3109/10715762.2014.936431.

Welter, C., Kovacs, G., Seitz, G., and Blin, N. (1989). Alteration of mitochondrial DNA in human oncocytomas. Genes Chromosomes Cancer *1*, 79-82. 10.1002/gcc.2870010112.

Wiley, S.E., Murphy, A.N., Ross, S.A., van der Geer, P., and Dixon, J.E. (2007). MitoNEET is an iron-containing outer mitochondrial membrane protein that regulates oxidative capacity. Proc Natl Acad Sci U S A *104*, 5318-5323. 10.1073/pnas.0701078104.

Wu, H.F., Kao, L.T., Shih, J.H., Kao, H.H., Chou, Y.C., Li, I.H., and Kao, S. (2018). Pioglitazone use and Parkinson's disease: a retrospective cohort study in Taiwan. BMJ Open *8*, e023302. 10.1136/bmjopen-2018-023302.

Wu, Z., and Bowen, W.D. (2008). Role of sigma-1 receptor C-terminal segment in inositol 1,4,5-trisphosphate receptor activation: constitutive enhancement of calcium signaling in MCF-7 tumor cells. The Journal of

biological chemistry *283*, 28198-28215. 10.1074/jbc.M802099200.

Xu, H., and Van Remmen, H. (2021). The SarcoEndoplasmic Reticulum Calcium ATPase (SERCA) pump: a potential target for intervention in aging and skeletal muscle pathologies. Skeletal Muscle *11*, 25. 10.1186/s13395-021-00280-7.

Xu, L., Wang, X., and Tong, C. (2020). Endoplasmic Reticulum-Mitochondria Contact Sites and Neurodegeneration. Front Cell Dev Biol *8*, 428-428. 10.3389/fcell.2020.00428.

Yang, Y., Valera, V., Sourbier, C., Vocke, C.D., Wei, M., Pike, L., Huang, Y., Merino, M.A., Bratslavsky, G., Wu, M., et al. (2012). A novel fumarate hydratase-deficient HLRCC kidney cancer cell line, UOK268: a model of the Warburg effect in cancer. Cancer Genet *205*, 377-390. 10.1016/j.cancergen.2012.05.001.

Yang, Y., Valera, V.A., Padilla-Nash, H.M., Sourbier, C., Vocke, C.D., Vira, M.A., Abu-Asab, M.S., Bratslavsky, G., Tsokos, M., Merino, M.J., et al. (2010). UOK 262 cell line, fumarate hydratase deficient (FH-/FH-) hereditary leiomyomatosis renal cell carcinoma: in vitro and in vivo model of an aberrant energy metabolic pathway in human cancer. Cancer Genet Cytogenet *196*, 45-55. 10.1016/j.cancergencyto.2009.08.018.

Yaniv, Y., Lakatta, E.G., and Maltsev, V.A. (2015). From two competing oscillators to one coupled-clock pacemaker cell system. Front Physiol *6*, 28. 10.3389/fphys.2015.00028.

Ye, L., Zeng, Q., Ling, M., Ma, R., Chen, H., Lin, F., Li, Z., and Pan, L. (2021). Inhibition of IP3R/Ca2+ Dysregulation Protects Mice From Ventilator-Induced Lung Injury via Endoplasmic Reticulum and Mitochondrial Pathways. Frontiers in Immunology *12*. 10.3389/fimmu.2021.729094.

Yuan, M., Gong, M., He, J., Xie, B., Zhang, Z., Meng, L., Tse, G., Zhao, Y., Bao, Q., Zhang, Y., et al. (2022). IP3R1/GRP75/VDAC1 complex mediates endoplasmic reticulum stress-mitochondrial oxidative stress in diabetic atrial remodeling. Redox Biology *52*, 102289. https://doi.org/10.1016/j.redox.2022.102289.

Zhang, X., Huang, R., Zhou, Y., Zhou, W., and Zeng, X. (2020). IP3R Channels in Male Reproduction. Int J Mol Sci *21*. 10.3390/ijms21239179.

Abstract in Korean/국문 초록

세포 내 칼슘 항상성 조절 메커니즘에 관한 연구

칼슘은 세포의 탄생, 발달, 기능 및 궁극적으로 죽음을 포함한 광범위한 생물학적 활동에 관여하는 다양한 신호전달 경로에서 중요한 역할을 하는 이온이다. 칼슘 신호 전달은 이러한 칼슘 의존적 과정이 세포 내에서 적절한 시간과 장소에서 조절되어 활성화되도록 이루어져 있다. 따라서 세포 내에서 항상 적절한 칼슘 항상성을 유지하는 것은 매우 중요하다. 세포 내 칼슘 농도를 조절하기 위해 다양한 운반체와 채널이 사용되기 때문에 칼슘 항상성을 조절하는 여러 칼슘 통로의 활성 기전을 이해하고 규명하는 것은 매우 중요한 연구이다.

1 부에서는 파킨슨병의 원인 유전자인 PINK1 과 Parkin 이 IP_3R 의 활성을 조절하여 소포체의 칼슘 방출을 조절하고, 이러한 칼슘 항상성의 변화로 PINK1 과 Parkin 결손 초파리에서 보이는 파킨슨병 관련 표현형이 나타난다는 것을 발견하였다. 또한

PINK1-Parkin 경로의 하위 단계인 CISD1 은 IP_3R 과 직접적으로 상호작용하며, Parkin 은 정확하게 CISD1 을 ubiquitination 시켜서 분해하는 것을 확인할 수 있었다. 그 결과, CISD knockdown 시 망가진 칼슘 항상성을 회복하며 그에 따라 PINK1 과 Parkin 결손 초파리에서 보이는 파킨슨병 관련 표현형이 모두 회복되는 것도 관찰하였다. 마지막으로, CISD 의 저해제로 알려진 pioglitazone 을 처리하면 IP_3R 과 CISD 의 상호작용을 차단하여 포유류 세포와 초파리 모두에서 PINK1 과 Parkin 결손으로 보이는 파킨슨병 관련 표현형이 완화되는 것을 확인하였고, 이를 파킨슨병 치료 약으로 제안하였다.

2 부에서는 초파리를 이용한 유전학적 스크리닝을 통해 TCA 사이클의 중간 대사물인 fumarate 가 칼슘 항상성을 조절할 수 있다는 것을 찾았다. 또한, fumarate 가 SERCA 의 876 번 시스테인 잔기에 succination 이라는 PTM 을 일으켜 SERCA 의 기능을 억제하는 것을 발견했다. 신기하게도 SERCA 의 876 번 시스테인 잔기를 세린으로 치환하면 포유류 세포나 초파리에서 fumarate 에 의한 SERCA 의 기능 억제가 발생하지 않았다. 이러한 모든 현상은 고 포도당 배지에서 재현되었으며, 이것은 TCA 사이클

활성화로 인한 fumarate 의 증가와 인과 관계가 있다. 다음으로 초파리에 고당 식단을 진행하여 고혈당을 만들어 주었더니 fumarate 에 의해 유발되는 SERCA 억제의 결과로 심장 기능이 빨라지는 빈맥 현상을 관찰하였다.

나의 연구 결과가 파킨슨병 병인에 대한 세포 내 칼슘 조절의 역할을 이해하는데 크게 기여할 것이라고 생각한다. 또한 fumarate 가 세포 내 칼슘 항상성을 조절함을 밝힘으로써, 나의 연구 결과는 대사물과 칼슘 항상성과의 관계에 보다 깊은 이해와 새로운 영감을 제시해 준다.

주요어 : CISD, IP_3R, SERCA, PINK1-Parkin 경로, 파킨슨병, pioglitazone, fumarate, 고혈당증, 빈맥

학번 : 2015-20498